



**MONOTONIC AND FATIGUE LOADING
BEHAVIOR OF AN OXIDE/OXIDE
CERAMIC MATRIX COMPOSITE**

THESIS

Steven G. Steel, Captain, USAF

AFIT/GMS/ENY/00M-02

20000803 136

**DEPARTMENT OF THE AIR FORCE
AIR UNIVERSITY**

AIR FORCE INSTITUTE OF TECHNOLOGY

Wright-Patterson Air Force Base, Ohio

APPROVED FOR PUBLIC RELEASE; DISTRIBUTION UNLIMITED.

DTIC QUALITY INSPECTED 4

The views expressed in this thesis are those of the author and do not reflect the official policy or position of the United States Air Force, Department of Defense or the U.S. Government.

AFIT/GMS/ENY/00M-02

MONOTONIC AND FATIGUE LOADING BEHAVIOR OF AN OXIDE/OXIDE
CERAMIC MATRIX COMPOSITE

THESIS

Presented to the Faculty of the Graduate School of Engineering and Management
Air Force Institute of Technology

Air University

Air Education and Training Command

In Partial Fulfillment of the Requirements for the
Degree of Master of Science in Materials Science and Engineering

Steven G. Steel, B.S.M.E.

Captain, USAF

March 2000

Approved for public release, distribution unlimited

MONOTONIC AND FATIGUE LOADING OF AN OXIDE/OXIDE
CERAMIC MATRIX COMPOSITE

Steven G. Steel, B.S.M.E.
Captain, USAF

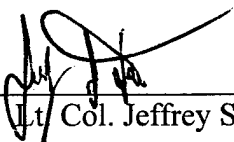
Approved:



Dr. Shankar Mall (Chairman)

3/10/00

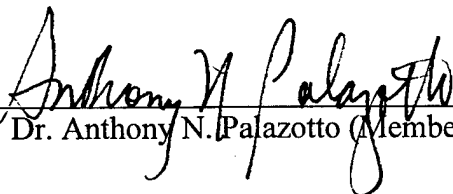
(date)



Lt. Col. Jeffrey S. Turcotte (Member)

10 MAR 2000

(date)



Dr. Anthony N. Palazotto (Member)

10 Mar 2000

(date)

Acknowledgements

I would like to thank the following people for their assistance during the course of my thesis: my faculty advisor, Dr. Shankar Mall, for his guidance and support throughout the course of this work, Larry Zawada, Dr. James Staehler and Dr. Vicki Kramb (AFRL/ML) for sharing their expertise on ceramic matrix composites, Dan Rioux for set-up and assistance with all test equipment, Andy Pitts for trouble-shooting and repair of the furnace, Jay Anderson for timely supply of needed materials, Luanne Piazza (UES) for training on the SEM, Ken Goecke (UDRI) for training on the fog exposure equipment, Debbie Garner (UDRI) for loan of test materials, Brad Ahlers (Wright State University) for assistance with the tedious process of ceramic polishing, fellow student Capt. Brandt Miller for companionship, and most importantly my awesome family, wife Kristin and son Steve II for their love.

Table of Contents

Acknowledgements.....	ii
Table of Contents.....	iii
List of Figures.....	v
List of Tables.....	ix
Abstract.....	x
1 Introduction.....	1-1
2 Background.....	2-1
2.1 Ceramic Matrix Composite Basics.....	2-1
2.1.1 Materials.....	2-1
2.1.1.1 Matrices.....	2-2
2.1.1.2 Fibers.....	2-3
2.1.1.3 Fiber Coatings.....	2-4
2.1.2 Fiber Architecture.....	2-4
2.1.2.1 Unidirectional Fibers.....	2-5
2.1.2.2 Woven Fabrics.....	2-5
2.1.3 Processing.....	2-7
2.1.4 Properties.....	2-8
2.2 Air Force Applications.....	2-11
2.2.1 IHPTET (27).....	2-12
2.2.2 F-16 Afterburner Flaps.....	2-13
2.3 Long Term Durability Concerns.....	2-15
2.3.1 Creep.....	2-15
2.3.2 Environmental Degradation.....	2-16
2.4 Combating Environmental Degradation.....	2-18
2.4.1 Glass-Forming Fillers.....	2-18
2.4.2 Coated BN Coatings.....	2-18
2.4.3 Oxide/Oxide Composites.....	2-19
2.5 Summary of Previous Oxide/Oxide Work.....	2-20
2.5.1 Early Modeling.....	2-20
2.5.2 General Electric's GEN IV.....	2-21
2.5.2.1 Processing and Microstructure.....	2-21
2.5.2.2 Tensile Behavior.....	2-22
2.5.2.3 Fatigue Behavior.....	2-22
2.5.2.4 Salt-Fog Exposure.....	2-23
2.5.2.5 Creep.....	2-24
2.5.3 Nextel 610/mullite and Nextel 720/mullite.....	2-24
2.5.4 Four Oxide/Oxide Composites Evaluated.....	2-26
2.5.5 Composite Optics Inc. Nextel 720/aluminosilicate (N720/AS).....	2-26
2.5.5.1 Materials and Processing.....	2-26

2.5.5.2	Properties	2-27
2.6	Description of Current Material	2-28
3	Experimental Equipment and Procedures.....	3-1
3.1	Equipment.....	3-1
3.1.1	Mechanical Test Apparatus.....	3-1
3.1.2	Environmental Equipment	3-4
3.1.3	Imaging devices	3-7
3.2	Test Procedures.....	3-9
3.2.1	Monotonic Tension	3-9
3.2.2	Cyclic Tension (Fatigue).....	3-10
3.2.3	Moisture Interrupted Fatigue	3-12
3.3	Test Matrix.....	3-13
4	Results and Discussion	4-1
4.1	Microstructure Characterization	4-1
4.2	Monotonic Tensile	4-4
4.2.1	Room Temperature	4-4
4.2.2	1200°C.....	4-14
4.3	Cyclic Tension (Fatigue).....	4-21
4.3.1	Room Temperature	4-21
4.3.2	1200°C Cyclic Tension	4-34
4.4	Moisture Interrupted Fatigue	4-50
5	Conclusions.....	5-1
6	Recommendations.....	6-1
	Appendix A. Grip Failures.....	A-1
	Appendix B. Residual Stress.....	B-1
	Bibliography.....	BIB-1
	Vita	

List of Figures

<u>Figure</u>	<u>Page</u>
2.1 Cross Section of Woven and Cross-ply Laminates.....	2-6
2.2 Two Types of Weave- Plain and Satin.....	2-6
2.3 F-16 with Afterburner Lit.....	2-14
2.4 Fatigue Behavior Nextel 720/AS.....	2-28
2.5 Straight-sided and Dogbone Specimens.....	2-30
3.1 Specimen in Grips with Extensometer Rods.....	3-2
3.2 Furnace Set-up.....	3-4
3.3 Thermocouple Layout on Dummy Specimen.....	3-5
3.4 High Temperature Test in Progress.....	3-6
3.5 Applied Load and Associated Stress-Strain Loop.....	3-10
4.1 Microstructure of N720/A, 50X.....	4-1
4.2 Microstructure of N720/A, 100X.....	4-2
4.3 Matrix Cracks on Specimen Surface, 100X.....	4-3
4.4 Delamination of Plies in Grip Region, 50X.....	4-4
4.5 Typical Room Temperature Stress-strain Curve N720/A.....	4-7
4.6 Typical Stress-strain Curve of CMC with Proportional Limit.....	4-8
4.7 Comparison of Three Room Temperature Stress-strain Curves.....	4-9
4.8 Fracture Surface of Room Temperature Tensile Specimen, 20X.....	4-11
4.9 Fracture Surface of Room Temperature Tensile Specimen, 50X.....	4-12

<u>Figure</u>	<u>Page</u>
4.10 Fracture Surface of Room Temperature Tensile Specimen, 1000X.....	4-13
4.11 Fracture Surface of Room Temperature Tensile Specimen, 3000X.....	4-14
4.12 Typical Stress-strain behavior at 1200°C, N720/A.....	4-17
4.13 Comparison of Tensile Response at Two Temperatures.....	4-17
4.14 Fracture Surface of 1200°C Monotonic Specimen, 20X.....	4-18
4.15 Fracture Surface of 1200°C Monotonic Specimen, 70X.....	4-19
4.16 Fracture Surface of GEN IV After 1200°C Exposure, 20X.....	4-19
4.17 Fracture Surface of GEN IV After 1200°C Exposure, 1800X.....	4-20
4.18 Room Temperature S-N Curve for N720/A.....	4-22
4.19 Normalized Room Temperature S-N Curve for N720/A.....	4-22
4.20 Modulus Degradation During Room Temperature Fatigue.....	4-24
4.21 Trends in Normalized Modulus During Room Temperature Fatigue.....	4-25
4.22 Strain Progression in 70% Stress Level Room Temperature Fatigue.....	4-26
4.23 Strain Progression in 60% Stress Level Room Temperature Fatigue.....	4-27
4.24 Changes in Stress-strain Loops During Room Temperature Fatigue.....	4-27
4.25 Fatigue Damage, 50X.....	4-30
4.26 Fatigue Damage, 100X.....	4-30
4.27 Stress-strain Curves of Room Temperature Fatigue Runout Specimens.....	4-31
4.28 Fracture Surface of Room Temperature Fatigue Specimen After Retained Strength Test, 20X.....	4-32
4.29 Surface of Room Temperature Fatigue Specimen After Retained Strength Test, 140X.....	4-33
4.30 1200°C S-N Curve for N720/A.....	4-35

<u>Figure</u>	<u>Page</u>
4.31 Normalized 1200°C S-N Curve for N720/A.....	4-35
4.32 Modulus Degradation in 1200°C Fatigue Testing.....	4-37
4.33 Normalized Modulus Trends in 1200°C Fatigue Testing.....	4-38
4.34 Strain Accumulation During 70% Stress Level Fatigue Test at 1200°C.....	4-39
4.35 Strain Accumulation During 80% Stress Level Fatigue Test at 1200°C.....	4-39
4.36 Strain Accumulation During 90% Stress Level Fatigue Test at 1200°C.....	4-40
4.37 Maximum Strain Progression in 1200°C Fatigue Tests.....	4-41
4.38 Maximum Strain Progression in 1200°C Fatigue Tests Plotted on Linear Scale.....	4-43
4.39 Steady State Creep Rates for N720 Fiber and N720/A Composite at 1200°C.....	4-43
4.40 Hysteresis Loops at 1200°C, 90% Stress Level.....	4-45
4.41 Fatigue Damage, 50X.....	4-46
4.42 Fatigue Damage, 100X.....	4-47
4.43 Stress-strain Curves for 1200°C Fatigue Runout Specimens.....	4-48
4.44 Fracture Surface of 1200°C Fatigue Specimen After Retained Strength Test, 20X.....	4-49
4.45 Fracture Surface of 1200°C Fatigue Specimen After Retained Strength Test, 360X.....	4-49
4.46 Maximum Strain Comparison, 1200°C Fatigue 90% Stress Level.....	4-52
4.47 Maximum Strain Comparison, 1200°C Fatigue 80% Stress Level.....	4-52

<u>Figure</u>	<u>Page</u>
4.48 Stress-Strain Curves for Retained Strength Tests.....	4-54
4.49 Retained Strength Compared to Original Strength.....	4-55
4.50 Fracture Surface of 1200°C Fatigue Specimen with Moisture Exposure After Retained Strength Test, 10X.....	4-56
A-1 Ideal Specimen Shape vs. Actual Shape.....	A-2

List of Tables

<u>Table</u>	<u>Page</u>
3.1 Strain to Failure for Some Common Materials.....	3-3
3.2 Test Matrix.....	3-13
4.1 Room Temperature Monotonic Test Results.....	4-5
4.2 Comparison of Room Temperature Tensile Properties of N720/AS and N720/A.....	4-6
4.3 Strength Comparison: Common Aerospace Materials and CMCs.....	4-6
4.4 1200°C Monotonic Test Results.....	4-14
4.5 Comparison of Average Properties from Monotonic Tests at Two Temperatures.....	4-15
4.6 Room Temperature Fatigue Results.....	4-21
4.7 Retained Properties of Room Temperature Fatigue Runout Specimens.....	4-31
4.8 1200°C Fatigue Test Results.....	4-34
4.9 Retained Properties of 1200°C Fatigue Runout Specimens.....	4-47
4.10 Cycles to Failure for 1200°C Fatigue Tests.....	4-51
4.11 Retained Properties of Runout Specimens, 1200°C Fatigue, Moisture Exposure.....	4-54

Abstract

The demanding environment in aircraft turbine engines has driven the development of many innovative high temperature materials. This thesis examines one of the latest of these materials, an oxide/oxide ceramic matrix composite (CMC), N720/A. This CMC consists of a porous alumina matrix reinforced by Nextel 720 fibers in a balanced 8-harness satin weave. To characterize this material, monotonic tensile and cyclic fatigue tests were performed at room temperature and at 1200°C. The effects of moisture on fatigue behavior were also investigated at 1200°C. Modulus, maximum and minimum strain and stress-strain hysteresis were monitored during the cycling to characterize fatigue damage mechanisms. Retained strength of all specimens that survived 10^5 cycles was also characterized. Microscopy and fractography were used to examine microstructure, damage mechanisms, and fracture surfaces. N720/A was found to have good room temperature and high temperature properties. At room temperature the ultimate tensile strength was 144 MPa, and fatigue strength was 102 MPa at 10^5 cycles. Fatigue damage involved mainly matrix cracking with no fiber-matrix debonding. At 1200°C the ultimate strength was 140 MPa and fatigue strength was 122 MPa at 10^5 cycles. Fatigue damage at high temperature was similar to that at room temperature with the addition of creep in the fibers. The matrix remained stable and did not sinter at 1200°C. Moisture exposure did not degrade fatigue performance at 1200°C. Based on these results, N720/A appears to be an excellent candidate material for 1200°C applications with exposure to moisture. This is a significant achievement, because no metal can operate for long-term at this temperature.

MONOTONIC AND FATIGUE LOADING BEHAVIOR OF AN OXIDE/OXIDE CERAMIC MATRIX COMPOSITE

1 Introduction

When Orville Wright took to the air for 12 seconds and 120 feet on December 17, 1903, he did so in an aircraft made of wood, cloth, thread and wires. Its internal combustion engine, which weighed 180 pounds and provided twelve horsepower, had a body of cast aluminum, cast iron pistons and a crankshaft chiseled from a block of machine steel (1: 177). In the nearly one hundred years since Kittyhawk the unique demands of powered flight have been the driving force behind many materials innovations. Aircraft structures must be lightweight as well as strong, thus the impetus to develop materials with high strength to weight ratio. The power and efficiency of aircraft turbine engines increases with the combustion temperature of the fuel, hence the drive for materials able to withstand high temperature.

The first nickel-based superalloy, Nimonic 80, was developed around 1940 in response to Whittle's need for a turbine blade material for the first British gas turbine (2:1).

Continuous improvement in superalloys since then has enabled parallel improvements in turbine efficiency and power. Titanium was first used in aircraft structure in 1953 and in turbine engines in the early 1960s (3:7). Today it is the major component of engines

along with the superalloys. Polymer matrix composites (PMCs, plastics reinforced with glass or other fibers) were first used on aircraft in the 1960s but only for non-structural doors and other tertiary structures (4:202). Today carbon fiber reinforced polymer composites make up 10% of the Boeing 777 airframe, including primary structure like the tail assembly (5:59). Metal matrix composites (MMCs) have just recently been used for the first time on aircraft structures. MMCs are metal with reinforcement that is usually ceramic particles or fibers. The actuator piston rods on the exhaust nozzle of the F-22s Pratt and Whitney F119 engine are titanium reinforced with silicon carbide fibers (6:11). The preferred spare for the ventral fin on the F-16 is made of discontinuous reinforced aluminum (DRA), aluminum reinforced with silicon carbide particles.

Ceramic matrix composites (CMCs) are one of the latest in a long line of innovative materials developed for aerospace use. They consist of a ceramic reinforcement embedded in a ceramic matrix. While monolithic ceramics are very brittle and unsuitable for aircraft engine applications, CMCs have a sufficient amount of toughness engineered in to them. Ceramics have better high temperature strength than any other class of materials, and it is hoped they will contribute to the next leap ahead in aircraft performance. In the past decade much research has been devoted to improving the durability of CMCs for the demanding environment of the turbine engine. While much progress has been made, their use is still limited by several factors. An important limiting factor in many CMCs is that they oxidize at high temperatures and subsequently lose their toughness.

There is a class of CMCs called oxide/oxides because both the reinforcement and the matrix are oxide based ceramics. Oxide/oxides are attractive because they are inherently resistant to oxidation. They offer one possible solution to the embrittlement problem. It is hoped that oxide/oxides will maintain their toughness after long-term high temperature exposure. The first oxide/oxide composite was manufactured by General Electric Aircraft Engines in 1988. These materials have evolved since then, with various combinations of matrices and fibers having been tried.

This thesis evaluates one new and promising oxide/oxide ceramic matrix composite. The composite consists of Nextel 720 alumina-mullite fibers (3M) embedded in a porous alumina matrix and was manufactured by Composite Optics Inc of San Diego, CA. In this study the composite's mechanical behavior is characterized at room temperature and at 1200°C (2192°F). The major tests performed are monotonic tensile, cyclic fatigue, and interrupted fatigue to expose to moisture. The key to this material's success will be how well it performs at 1200°C with and without moisture. Some superalloys can operate at 1100°C for short periods of time but no metal can perform at 1200°C. A material that has long-term strength and stability at 1200°C would be an encouraging step forward in the development of CMCs for aerospace systems.

2 Background

This section begins with a broad introduction to the basics of ceramic matrix composites (CMCs) for the reader who may not be familiar with these materials. Following this summary of basic concepts is a sample of CMC applications that are relevant to the United States Air Force (USAF). Next, factors that currently limit the use of CMCs are described including environmental degradation. Ways of combating environmental degradation are then reviewed which leads to discussion of a particular class of CMCs called oxide/oxides. The published (or soon to be published) literature on oxide/oxide CMCs is then reviewed. Finally a description of the material used in this study is given.

2.1 Ceramic Matrix Composite Basics

2.1.1 Materials

Ceramic matrix composites (CMCs) are a class of structural materials consisting of a ceramic reinforcement embedded in a ceramic matrix. Reinforcement may be in the form of particulates, small discontinuous whisker platelets, chopped fibers, or continuous fibers (7:11). In continuous fiber reinforced ceramic composites (CFCCs), the reinforcement consists of long fibers in various configurations. For reasons to be discussed later, CFCCs usually have an interphase, or fiber coating, present between the fiber and the matrix.

2.1.1.1 Matrices

There are several ways to categorize ceramic matrix materials; glass ceramics vs. polycrystalline ceramics is one example. Examples of glass ceramics include lithium aluminosilicate (LAS), calcium aluminosilicate (CAS), and magnesium aluminosilicate (MAS). Glass ceramic matrices have the advantages of easy fabrication and achievement of high matrix densities at low processing temperatures (8:13). High matrix density means low porosity which leads to good mechanical properties. Low processing temperatures means less damage to fibers during composite manufacture. The drawback to glass ceramics is their limited temperature capability compared to the polycrystalline ceramics (8:13). Examples of common polycrystalline ceramic matrices are alumina (Al_2O_3), mullite ($3\text{Al}_2\text{O}_3 \cdot 2\text{SiO}_2$), silicon nitride (Si_3N_4), and silicon carbide (SiC). These materials offer higher temperature capability than the glass ceramics; however, matrix density is not achieved as easily. In the presence of fibers, the processes that lead to sintering and densification of these ceramics are hindered (8:13). Also, polycrystalline matrices generally require higher processing temperatures, which can damage the fibers.

There are other ways to categorize matrices such as oxide vs. non-oxide. Oxide matrices include alumina and mullite; whereas non-oxides include silicon nitride and silicon carbide. An important distinction here is the inherent oxidation resistance of the oxides relative to the non-oxides. The non-oxides rely on the formation of a protective silica (SiO_2) layer to resist further oxidation. Problems arise when this silica layer is attacked by the environment (9:465). In addition, as will be discussed later, the silica layer itself can cause problems when it forms at the fiber matrix interface.

2.1.1.2 Fibers

Ceramic fibers are usually grouped into non-oxide and oxide fibers (10:429). Fibers are produced as either large diameter (100-140 μ m) monofilaments or small diameter (\sim 10 μ m) multi-filament fibers. Monofilaments often have better mechanical properties but they are too large to be woven into fabric. The smaller diameter multi-filaments are easily bundled and woven, a major advantage as will be seen.

The non-oxide fibers are based primarily on SiC (10:429). Nicalon, Hi-Nicalon and Hi-Nicalon S (Nippon Carbon), Tyranno (Ube) and Sylramic (Dow Corning) are common examples of small diameter SiC fibers. Textron produces a large diameter SiC fiber. A non-oxide amorphous Si-B-N-C fiber (Bayer) has recently been introduced and shows considerable promise for high temperature use (10:431). Several companies are also developing silicon nitride fibers (11:60).

The oxide fibers are primarily alumina based, such as Nextel 610 (3M). Nextel 720 (3M) is a composite alumina-mullite fiber. Other oxide fibers, such as polycrystalline yttrium-aluminum garnet or YAG (General Atomics), have been developed but currently are prohibitively expensive (11:60).

Again a key distinction between the oxide and non-oxide based fibers is the inherent oxidation resistance of the oxides.

2.1.1.3 Fiber Coatings

Fiber coating developments have concentrated on non-oxide fibers. To date, carbon and boron nitride (BN) have been the only successful coating materials for these fibers (10:434). Coatings for oxide fibers are a relatively new development. Early research on these coatings has focused on porous alumina and dense lanthanum phosphate (monazite, LaPO_4) (12:53), as well as scheelite (CaWO_4) and erbium tantalite (ErTaO_4) (13:279).

2.1.2 Fiber Architecture

Fiber architecture in CFCCs will affect composite mechanical properties as well as the shape of component that can be made. Four categories of fiber architectures are:

1. Unidirectional (1-D), with fibers straight and parallel.
2. Laminates composed of layers of unidirectional plates bonded together. Each layer may have fibers running in a different direction. An example is a laminate composed of unidirectional laminas with fibers alternating 90° from one lamina to the next. Such an arrangement is called a 0/90 cross-ply laminate (a cross section is shown on the right side of Figure 2-1).
3. Laminates composed of layers of woven fabric reinforced materials. Each layer has 2-D reinforcement rather than 1-D (a cross section is shown on the left side of Figure 2-1).
4. Structures made from woven or braided fiber preforms, which may be 2-D or 3-D (8:16).

In the following section, a few key issues regarding fiber arrangement will be reviewed.

2.1.2.1 Unidirectional Fibers

Larger diameter fibers like the YAG (140 μ m) and some SiC monofilaments (100-140 μ m) are not flexible enough to be woven into fabric. They are therefore limited to use as unidirectional reinforcement. Small diameter ceramic fibers (like the Nicalon and Nextel fibers, 10-12 μ) may be bundled into tows and used as unidirectional reinforcement. Unidirectional fiber arrangement can maximize composite properties, because fibers can be oriented in the direction of applied loads. However unidirectional composites and laminates made from unidirectional plates are severely limited in the shape of components they can produce- namely plates and shells (8:16).

2.1.2.2 Woven Fabrics

The small diameter fibers mentioned above are flexible enough to be woven into fabric. Individual small diameter fibers are difficult to handle so they are furnished in multifilament or tow form with about 500 filaments/tow (14:140). The tows may be woven into many two-dimensional configurations, two of which are shown in Figure 2-2. Individual woven cloth laminas are stacked to form two-dimensional woven laminates. If the individual laminas are cross-linked with fibers, a three-dimensional laminate is formed.

A big advantage of woven fabric composites is that they can assume complex shapes, not just plates and shells. In addition, woven fabric composites offer higher impact resistance and toughness compared to non-woven (unidirectional and cross-ply) composites (15: 2). However woven composites tend to be more porous because of the

waviness of the fiber bundles. The two types of porosity present in a woven composite are illustrated in Figure 2-1. Microporosity ($\sim 10\mu\text{m}$) is present within individual tows, or yarns. Macroporosity ($>100\mu\text{m}$) is present between the yarns (16:222). This macroporosity can reduce composite strength and stiffness. Also, the significant bending of the fibers in woven composites can degrade their properties (8:16).

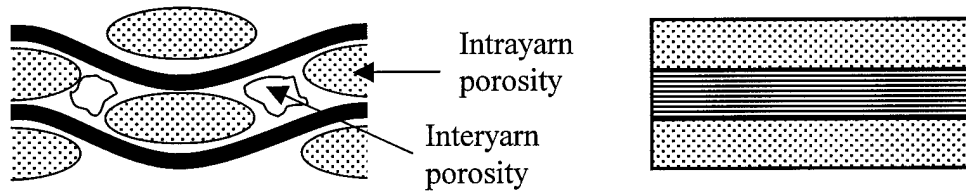


Figure 2-1 Cross section of woven (left) and cross-ply (right) laminates

In a woven fabric, the lengthwise fibers are referred to as the warp yarns, while the transverse fibers are called fill yarns. Figure 2-2 shows the warp and fill directions in two types of weave: plain and satin (17:49).

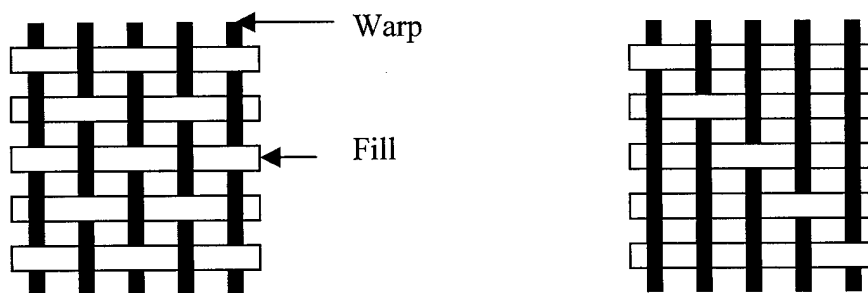


Figure 2-2 Two types of weave: plain and satin

A plain weave has warp ends going alternately over and under a fill yarn. In the satin weave, warp ends weave over a number of fill yarns and then under one fill yarn. For example, a five-harness satin, shown in Figure 2-2, has warp ends going over four fill yarns and under one. Of the two weaves, a satin is more pliable than a plain and can take on more complex shapes and contours. It is also less porous than a plain weave (17:49).

2.1.3 Processing

A wide range of methods have been used for infiltrating the matrix into the fiber architectures, or preforms, but only three basic types are of commercial importance.

These are chemical vapor infiltration (CVI), organic precursor route and liquid infiltration (11:61). The CVI method requires the penetration of vapors into a preform and the production of a solid phase from the chemical reaction of the vapor species to form the matrix of the composite (18:229). Residual porosity of CVI composites is on the order of 10-15% (16:236). This method is used most commonly with silicon carbide and a few other non-oxides. CVI produces the highest quality non-oxide composites but the process is slow and expensive (11:61).

In the organic precursor method, preforms are infiltrated with a liquid silicon polymer, which is then pyrolyzed (decomposed by heat) to leave a SiC or nitride deposit (11:61). The substantial density change from polymer to ceramic leads to high shrinkage, porosity and microcracking (18:218). Porosity content after the first infiltration is about 20-30% (19:287). Porosity is reduced by repeated infiltrations; typically 4-10 reinfiltrations are needed (19:281). The resulting composite properties are generally inferior to CVI due to the higher porosity (11:61).

The third major production option is similar to the organic precursor route in that a liquid ceramic is infiltrated into the preform (11:61). One common form of liquid ceramic is a solution of gels or sol-gel. In the sol-gel method a ceramic precursor is hydrolyzed (reacted with water), polymerized into a gel, then dried and fired to achieve consolidation (20:187). A large amount of shrinkage occurs due to the large amounts of water that must be removed from the solution (20:187). The high shrinkage leads to a microcracked matrix, which can lead to inferior mechanical properties. Properties achieved are inferior to CVI but the process is well established and relatively inexpensive (11:61).

2.1.4 Properties

Properties of ceramics vary greatly according to factors like processing technique and porosity. But in general as a class, ceramics have many properties that make them attractive as engineering materials. Monolithic ceramics (no reinforcement) have low density, high strength, high modulus, high hardness and low thermal expansion. They have high melting points and chemical stability in many hostile environments. But perhaps their most attractive feature for aerospace use is their ability to maintain strength at high temperatures. In this area they exceed any other class of materials. Roughly, polymers can be used up to 150°C, aluminum alloys up to 200°C, titanium up to 600°C, stainless steels up to 850°C and nickel based superalloys up to 1100°C. Refractory metals like tungsten and molybdenum have good strength above 1200°C but they are heavy and oxidize rapidly. Intermetallics, compounds like TiAl and Nb₅Si₃, are a relatively new class of materials being developed for high temperature use. TiAl is

expected to have a maximum operating temperature of about 950°C (46). TiAl recently found its first commercial use on the turbocharger impeller of the Mitsubishi Lancer, but it has not been used on an aerospace component yet (46). Nb₅Si₃ may be able to operate up to 1200-1300°C but it is still in early development (46). Ceramics offer the potential of greater than 1500°C use temperatures.

Ceramics derive their unique combination of properties from very strong chemical bonds, which are a mixture of ionic and covalent. The modulus of elasticity for a given material is an indicator of the strength of its interatomic bonds (21:117). The modulus of alumina is 380 GPa compared to 200 GPa for steel and 70 GPa for aluminum. Melting point is also a good index for atomic bond strength. The melting point of alumina is 2050°C while that of nickel is 1450°C and titanium 1675°C.

The same strong chemical bonds that give ceramics high stiffness and stability also cause them to be brittle. Metals can plastically deform by shear along slip planes to relieve stress. In the presence of a stress riser, a flaw or crack, a metal will plastically deform locally to avoid fracture. When a ceramic is stressed it deforms elastically until sudden catastrophic failure occurs. A ceramic cannot tolerate the high local stresses caused by a flaw. This damage intolerance and low fracture toughness has limited the use of ceramics in structural applications (7:12).

The toughness of ceramics can be greatly improved by adding reinforcement. Toughness of particulate, whisker and discontinuous fiber reinforced ceramics are up to three times

better than monolithic ceramics (22:296). "However only continuous fiber reinforced ceramics can provide non-catastrophic failure CMCs for critical aerospace applications" (22:296).

"High fracture toughness and damage tolerance is engineered into most CFCCs by tailoring properties of the fiber-matrix interface"(23:1). The interface is deliberately made weak to allow fibers to debond and slide within the matrix. The following scenario illustrates how the weak interface promotes toughness and damage tolerance. Suppose a CMC is subjected to a stress high enough to crack the matrix. In a monolithic ceramic there is no mechanism to stop the crack and it will propagate until failure occurs. A crack in the matrix of a CMC will grow until it reaches the fiber-matrix interface. The weak interface allows the fiber to debond from the matrix. Instead of propagating through the fiber, the crack is deflected around the fiber. Once the crack deflects around the fiber it may continue to grow through the matrix while the fiber remains in tact. The fiber then 'bridges' the crack and can still support a load. Under continued stress, frictional sliding occurs between the matrix and the debonded fibers. This frictional sliding is an energy dissipater, like slip in metals, and serves to toughen the CMC. If applied stresses are high enough, the crack will continue to grow. The fibers will eventually fracture and 'pull-out' of the matrix with the expenditure of considerable amounts of energy (24:357). All these mechanisms- debonding, crack deflection, crack bridging, sliding and fiber pull-out - are how CMCs are able to tolerate cracks and overcome the inherent brittleness of ceramics.

The required “weak” interface between the fiber and matrix is often created by coating the fibers before they are incorporated into the matrix (23:1). The usual coating materials, carbon and boron nitride, act as solid lubricants and induce the necessary debonding and sliding mechanisms (23:1). However these materials are susceptible to environmental degradation as will be discussed later.

2.2 Air Force Applications

Why is the Air Force interested in CMCs? One reason is that CMCs may be the enabling technology for many advanced propulsion systems. The principal requirements for a jet engine are high thrust to weight ratio and low fuel consumption. These goals are achievable only by increasing turbine inlet temperatures, which over the years have increased at a rate of ten to fifteen degrees per year from 800°C in 1947 to over 1300°C today (25:151). These high temperatures are possible because of improved materials and cooling methods. For example, in the 1960s Pratt & Whitney developed a process for making polycrystal and single crystal directionally solidified investment cast turbine blades. Turbine blades made of these columnar-grained and single crystal superalloys were introduced into engines during the 1970s and 1980s. These creep resistant alloys enabled an increase of several hundred degrees in engine operating temperature (26:360).

Today single crystal superalloy turbine blades are still the state-of-the-art technology. No further major technology advances have been made. Turbine inlet temperatures have continued to rise but turbine blade temperature has been kept at 1100°C by increased

cooling (through hollowed out passages in the turbine blades). Some further increase in the use temperature of superalloys may still be possible, with such technologies as ceramic thermal barrier coatings (2:22). However, significant improvements are unlikely. If there is to be another substantial increase in engine operating temperature it is likely to come from the use of ceramics.

2.2.1 IHPTET (27)

An example of CMC applications in advanced propulsion systems is the Integrated High Performance Turbine Engine Technology (IHPTET) program started in 1988. The IHPTET team consists of the Army, Navy, Air Force, NASA, DARPA and industry. IHPTET is combining advanced material developments, innovative structural designs and improved thermodynamics to meet engine performance goals. These new technologies are tested on various demonstrator engines such as the Joint Expendable Turbine Engine Concept (JETEC) and the Joint Turbine Advanced Gas Generator (JTAGG). New stronger and more temperature resistant materials- polymer matrix composites, ceramic matrix composites, superalloys and intermetallic composites- are being tested to increase engine thrust to weight ratio. New materials will be transferred to existing systems such as the F-15, F-16, F-18E/F and the F-22, and also applied to newly developed aircraft and missiles. Phase I goals have been demonstrated and provide a 30% increase in propulsion capability. Phase II goals are nearly complete and will provide 60% increase in thrust/weight ratio and a 30% decrease in fuel burn. The Phase III target date is 2003 and the goal is a 100% increase in thrust/weight ratio and a 40% decrease in fuel burn. CMCs are being used in the hottest sections of the demonstrator engines, the turbine and

the combustor. One example is a SiC/SiC composite combustor liner that will enable a 1500°C combustor temperature.

2.2.2 F-16 Afterburner Flaps

CMCs are not solely being looked at for developmental engines. There are possible applications for CMCs in currently fielded engines, in areas where metal components are failing. In one such application, CMCs are being tested in afterburner components of the General Electric F110 turbofan engines that power the F-16. The afterburner is basically a second combustion chamber mounted aft of the turbine engine. It makes use of the fact that the hot gases exiting the turbine have enough oxygen to allow a second combustion if given an injection of fuel (25:176). This reheating of the jet exhaust means it has a higher level of energy available for expansion in the exhaust nozzle. The result is higher exit velocity and more thrust. Combat aircraft use the afterburner to accelerate quickly, for take off on short runways and for supersonic flight (25:176).

The F110 afterburner consists of two main parts; the forward augmentor section and the trailing variable exhaust nozzle. The nozzle consists of 12 divergent flaps and 12 divergent seals, which actuate in unison to change the size of the exhaust opening. During extended afterburner lights, temperatures of the exhaust nozzle components can exceed 1000°C (29:2). Current nozzle flaps and seals are made of Rene' 41, a nickel based superalloy. The combination of high temperature and thermal cycling leads to creep deformation, which eventually results in warping and cracking. "At present a high percentage of the flaps and seals must be removed or repaired after only 1/3 of their

intended design life”(29:3). The advantage of CMCs compared to Rene’ 41 is in creep resistance at temperatures of 1000-1100°C.



Figure 2-3 F-16 with afterburner lit (28)

Zawada and Staehler of the Air Force Research Laboratory (AFRL) ground tested four different CMCs in an F110 engine at General Electric Aircraft Engines in Evandale, OH. The composite flaps accumulated up to 117 hours of engine time or 10% of design life (29:4). Two of the four CMCs showed no degradation while two showed evidence of cracks and wear. The two CMCs that performed best were selected for flight testing. Four flaps were mounted on an F-16 at Hill AFB, Utah and are currently accumulating flight hours.

2.3 Long Term Durability Concerns

While CFCCs continue to show promise for aerospace applications, their long-term durability must be improved. Their durability is currently limited by two factors: creep and rupture of the fibers and environmental degradation of the constituents.

2.3.1 Creep

Creep of ceramic fibers currently limits the maximum use temperature of CMCs. Recent developments in fibers have brought about some improvement in creep behavior. First, developments in the non-oxide fibers will be described. A particular class of SiC based fiber that is polymer derived (i.e. the Nicalon fibers), as opposed to chemical vapor deposited, consists of very small SiC grains along with carbon and an amorphous Si-O-C phase (10:429). Factors affecting creep resistance of this fiber type are grain size and the composition, location and size of the secondary phases (10:429). Creep resistance in these fibers has been improved by increasing the SiC grain size and reducing the oxygen content. For example, the Hi-Nicalon fiber is much more creep resistant than the Nicalon fiber because the Si-O-C secondary phase is essentially replaced with carbon (10:429). The creep resistance of Hi-Nicalon has been further improved (Hi-Nicalon vs. Hi-Nicalon S) by increasing the volume fraction of SiC to near stoichiometry while doubling the grain size (10:31). These fibers are exhibiting useful creep and rupture resistance to nearly 1300°C depending on applied stress (10:436).

The oxide fibers, in general, have poor creep resistance when compared to non-oxide fibers (10:433). Of the oxide fibers Nextel 720 is the most creep resistant fiber currently available (10:433). It was developed as an improvement over Nextel 610 in the area of high temperature performance. Nextel 610 consists of 99% fine-grained alumina and has a maximum use temperature of approximately 950-1000°C. Nextel 720 has both a secondary phase and elongated grains incorporated into its microstructure. The fiber is a composite of mullite (~55 volume %) and alumina (~45 volume %). The mullite is in the form of needles surrounding the alumina grains (10:433). This mixture of mullite and alumina gives improved creep strength and allows for a maximum use temperature in the range of 1075-1125°C (30:328). The better creep performance comes at the expense of strength; with Nextel 610 having a strength of about 3 GPa while the strength of Nextel 720 is about 2 GPa (30:328).

The YAG monofilament mentioned earlier offers superior creep resistance compared to other oxide fibers, as does a single crystal melt-grown sapphire (Saphikon), but these are currently too expensive to use (11:60). New affordable oxide fibers need to be developed in order to substantially improve creep performance.

2.3.2 Environmental Degradation

The second factor limiting long-term durability of CMCs is environmental degradation, especially at the fiber-matrix interface. Environmental degradation results from exposure to the atmosphere, moisture, salt and high temperature. Cracks can form in the matrix material of a CMC at relatively low stresses. Oxygen from the atmosphere travels

through the matrix cracks to the fiber coating. Both the carbon and the boron nitride commonly used as coatings are subjected to oxidation. Carbon coatings can begin oxidizing at 450°C (23:1). Once the carbon is removed, the oxygen reacts with the fiber to form a silica layer (assuming the fiber is SiC based). The silica (SiO_2) layer weakens the fiber and also allows strong bonding to the matrix. The weak interface that CMCs depend on for fiber debonding and sliding is replaced with a strong interface. As a result the CMCs quickly experience a reduction in their fracture toughness and tensile strength (31:2).

Boron nitride is more resistant to oxidation than carbon but still has problems. The BN fiber coating must be applied at relatively low temperatures to minimize damage to the fiber. Deposition at lower temperatures results in an amorphous form of BN that is sensitive to oxidation at temperatures from 650-850°C (31:2). BN forms a protective B_2O_3 layer, which like silica results in a strong fiber-matrix bond (23:1). The strong fiber-matrix bond allows cracks to propagate from the matrix directly through the fiber with no deflection. No crack bridging occurs. Fracture surfaces of these embrittled composites show little fiber pull-out. The toughening mechanisms on which CFCCs rely are greatly reduced by oxidation of the fiber coating. The result of this embrittlement is reduced fatigue life at elevated temperatures.

2.4 Combating Environmental Degradation

There are several approaches to protect CMCs from environmental degradation, three of which will be mentioned here.

2.4.1 Glass-Forming Fillers

One approach is to use glass-forming fillers in the matrix such as BN, SiC and B₄C.

Glassy phases that form in the interior of the CMC during high temperatures act to seal matrix cracks and prevent oxygen from reaching the fiber coating. This approach has contributed to some improvement in elevated temperature fatigue life over earlier generation CMCs (32:1807). "However, in loaded CMCs, continuous damage from matrix cracks facilitates oxygen access and makes sealing difficult particularly at intermediate temperatures where glass formation rates are low and viscosities are high" (23:2). Also the glassy phases that form at high temperature will become brittle as the temperature is reduced under the glass transition temperature and will reduce room temperature residual strength (23:2).

2.4.2 Coated BN Coatings

Another approach is to dope or coat the BN fiber coatings to protect them from oxidation.

"Recently Si-doped BN has been deposited on SiC fibers and shows considerable promise as an oxidation resistant coating that retains desirable mechanical properties" (10:435). This development will likely receive more attention. Layered coatings such as BN/C/BN, BN/C/Si₃N₄, SiC/C/SiC and BN/SiC have also been evaluated in composites

with SiC based fibers. So far the data is not clear whether or not the oxidation problem in these non-oxide composites has been improved (10:435).

2.4.3 Oxide/Oxide Composites

A third approach is to make the composite from an oxide based fiber and oxide based matrix. Such a composite is inherently resistant to oxidation. Oxide/oxide composites are receiving attention for this reason. The development of all oxide composites has followed two distinct design paths (33:2077). The first is based on the same weak interface concept of traditional CFCCs. It uses fugitive layers (layers that disintegrate during processing), porous oxide coatings or dense oxide coatings with suitably low fracture toughness to form the weak interface (33:2077). So far the most promising approach is the dense oxide coatings, and the best of these so far appear to be monazite (LaPO_4) (34:274) and scheelite (CaWO_4) (13:283). These materials are promising but their development is still in the early stages.

In the other approach to flaw tolerant oxide/oxide CMCs, reinforcing fibers are strongly bound to a matrix deliberately made weak by incorporation of high porosity and microcracks (23:2). (Wood gets its toughness from a similar structure.) No fiber coating is necessary so processing is easier (23:2). Porosity is acceptable so an inexpensive processing technique like the sol-gel liquid infiltration method may be used. Instead of crack deflection and sliding at fiber-matrix interfaces, fracture energy is dissipated by diffuse microcracking in the porous matrix (23:2). General Electric Aircraft Engines first produced oxide/oxide CMCs with a porous matrix in 1988 (30:328). An aluminosilicate

matrix material has been commonly used in the past. A range of fibers has been used including Nextel 312, 480, 550, 610 and 720. Nextel 480, 610 and 720 are the only ones suitable for high temperature use (30:328).

2.5 Summary of Previous Work on Oxide/Oxides

Papers on oxide/oxide composites with strong interfaces are so far relatively rare. The following is a summary of those found in the literature. This survey also shows the evolution of oxide/oxide composites over the past few years and will reveal the motivation behind the current material.

2.5.1 Early Modeling

Two articles published in 1996 provide some early modeling of the fracture mechanics of porous matrices strongly bound to fibers (35,36). The models in these articles are based on the concept that when two intrinsically brittle materials are combined, damage tolerance can be achieved whenever cracks are induced to deflect or debond along planes parallel to the loading direction (35:417). Cracks will initiate in and propagate across bundles of fibers but when the crack reaches a matrix-dominated region it will deflect parallel to the load. The crack is thereafter trapped. These models indicate that the matrix regions should be subjected to residual compression and have controlled porosity such that their mode II fracture energy is lower than about half the mode I fracture energy of the fiber bundles (35:423). If these conditions are met, cracks will tend to deflect parallel to the loading and become stable.

2.5.2 General Electric's GEN IV

Perhaps the most extensively characterized oxide/oxide composite is General Electric's GEN IV. Because its behavior has been thoroughly examined, it will serve as a good introduction to all-oxide CMCs with strong interfaces. The sources for this information are two papers, published or soon to be published, by the Materials Directorate of the Air Force Research Laboratory (AFRL/ML) (23,31).

2.5.2.1 Processing and Microstructure

GEN IV uses Nextel 610 fibers in an 8HSW for reinforcement. The fiber cloth is prepregged with a mixture of fine alumina powder and a silica-forming polymer. Twelve individual prepregged cloths are stacked to form the laminate. The laminate is warm molded in an autoclave to produce a dense green state ceramic tile. The tile is pressureless sintered in air at 1000°C to convert the polymer to porous silica.

Because of shrinkage that occurs when the polymer is converted to a ceramic, the matrix is microcracked and porous. The porosity of the material is 17-23%. Approximately half of this is large pores and matrix cracks, the other half is very fine evenly distributed porosity. The matrix is a mechanical mixture of alumina grains cemented together by porous silica. The silica also cements the alumina grains to the Nextel 610 fibers.

2.5.2.2 Tensile Behavior (23)

Tensile response of Gen IV is nearly linear to failure. Deformation is essentially elastic to failure for all temperatures tested. Such linear behavior means that there is little additional matrix cracking during loading and that fiber/matrix debonding is insignificant. Fiber fracture is the dominant damage mode, which is typical for fiber-dominated composites. Average room temperature properties are 205 MPa for ultimate strength, 0.3% strain to failure and a 70 GPa elastic modulus. There are very small changes in properties from room temperature to 1000°C. Ultimate tensile strength decreases from 205 to 173 MPa. The elastic modulus increases from 70 to 77 GPa. The strain to failure decreases from 0.33% to 0.28%. These small changes indicate the system has attractive short-term mechanical properties at 1000°C.

2.5.2.3 Fatigue Behavior

GEN IV performs extremely well in fatigue at both room temperature and at 1000°C. The fatigue, or endurance, limit at room temperature is 170 MPa, which is 85% of room temperature tensile strength. The fatigue limit at 1000°C is 150 MPa also 85% of the tensile strength at that temperature. The room temperature behavior is similar to other CMCs, many of which exhibit fatigue limits within 5-20% of the tensile strength. However fatigue behavior at elevated temperatures is very different. CMCs with a carbon or boron nitride fiber coating typically have fatigue limits of only 75-100 MPa. GEN IV did not degrade at high temperature like other CMCs with these fiber coatings.

Normally CMCs experience cumulative damage during fatigue testing. There are several ways to determine whether fatigue damage is occurring. These include monitoring changes in elastic modulus, stress-strain hysteresis and strain, and testing of retained strength after cycling. Fatigue damage will be indicated by an elastic modulus that degrades over the course of a fatigue test. In the case of GEN IV there was a very slight decrease in elastic modulus up to 100,000 cycles. This indicates that minimal damage occurred and that it was most likely due to slight additional cracking in the matrix. Stress/strain hysteresis will normally increase as a composite accumulates damage. For GEN IV, hysteresis values were very small throughout the test indicating again that very little damage occurred. Maximum and minimum strain values may increase over the course of a test due to a combination of damage and creep. GEN IV had very slight increases in minimum and maximum strain indicating little strain accumulation. In most CMCs exposed to high temperature fatigue testing, degradation of fiber coatings reduces tensile strength in specimens after cycling. GEN IV experienced no loss of tensile strength after fatigue testing. All this data means that oxide/oxides seem to excel in high temperature fatigue environments. Since this is a 'weak spot' for traditional CMCs, these results are highly encouraging.

2.5.2.4 Salt-Fog Exposure

CMCs for turbine engine applications must be able to withstand exposure to the humidity and salt of sea air. Exposure to salt and fog did not decrease the fatigue life of Gen IV at 1000°C. This is another advantage for oxide/oxides. Nicalon fiber based CMCs experience a 30-80% decrease in fatigue life under identical test conditions.

2.5.2.5 Creep

GEN IV was found to be susceptible to creep as the measured creep strains were almost three times larger than Nicalon fiber CMCs at the same stress and temperature. The Nextel 610 fiber is an extremely fine-grained alumina, which makes it susceptible to creep. Consequently GEN IV should not be used at temperatures above 1100°C. Creep performance would likely improve by using the Nextel 720 fiber, which is much more resistant to creep than Nextel 610.

2.5.3 Nextel 610/Mullite and Nextel 720/Mullite

Researchers from University of California, Santa Barbara (UCSB) manufactured and tested two types of oxide-oxide composites. They detailed the processing and performance of Nextel 610 and Nextel 720 reinforcements in porous mullite matrices (33). The reinforcements were in the 8HSW configuration and made up 36 volume percent of the composite. The matrix was actually 80% mullite in the form of relatively large particles (~1µm) and 20% alumina (~200 nm) in the void spaces. The alumina sintered above 800°C to form bridges between the mullite particles as well as between the mullite particles and the fibers. The finished composites had roughly 30% porosity.

The team at UCSB found that the all-oxide composites had the following characteristics:

They were straightforward to manufacture by conventional slurry infiltration methods.

They do not require a fiber coating and use relatively low-cost Nextel fibers. They seem to be an affordable material (33:2086).

Their mechanical performance was comparable to that of other fiber dominated CFCCs, such as SiC/C and C/C. The all-oxide composites represent an oxidation-resistant equivalent to carbon/carbon composites (33:2086).

The composite with the Nextel 720 fibers had very good high-temperature characteristics. The creep strength exhibited at 1200°C makes this composite a serious candidate for applications at this temperature (33:2085).

The porous matrix was effective as a crack deflection medium as evidenced by the fracture surfaces. Fiber tows broke over a wide range of axial locations. Individual fibers within the tows also broke over a wide range of locations. This indicates the cracks did not proceed directly from one fiber through the matrix and then through the next fiber. They were deflected in the porous matrix (33:2081).

Interlaminar shear strength, which is a matrix-dominated property, was low (8-10 MPa) compared to other CMCs. A possible solution is to use three dimensional fiber architectures in the future processing of these materials (33:2084).

2.5.4 Evaluation of Four Oxide/Oxide Composites

Zawada evaluated the longitudinal and transthickness tensile strength of four oxide/oxide composites from different manufacturers (30). Two of these composites were manufactured by General Electric Aircraft Engines, one by 3M and one by Composite Optics Inc. All four composites had aluminosilicate matrices and used either Nextel 610 or Nextel 720 fibers. This study highlighted the conflicting demands placed on the matrix of these materials. The matrix needs to be porous enough to deflect cracks, yet sufficiently dense to provide good compressive and transverse tensile properties. The composites in this study had very low transverse strengths (2.7-7.1 MPa). This is an area that needs improvement in future oxide/oxide development.

2.5.5 Nextel 720/Aluminosilicate (N720/AS) from Composite Optics Inc.

For the past several years Composite Optics Inc. (COI) of San Diego CA has manufactured an all-oxide composite. It combines the promising high temperature fatigue properties of the GEN IV material (as described in Section 2.5.2) with excellent creep resistance.

2.5.5.1 Materials and Processing

The reinforcement in the COI material is Nextel 720 fibers in an 8HSW. The use of Nextel 720 fibers gives N720/AS a substantial increase in creep resistance when compared with GEN IV and its Nextel 610 fibers. As discussed in Section 2.3.1 the Nextel 720 fiber has elongated grains of mullite in its microstructure, which slows creep

deformation. The matrix is a sol-gel derived porous aluminosilicate. COI's process for manufacturing the composite is simple and low cost. The fabrication process does not require repetitive re-infiltration or pyrolyzation steps. The matrix is a viscous slurry that is prepregged into the fabric by hand. Once the slurry is evenly applied to the fabric, the laminates are laid up, bagged and dried under low pressure and temperature. The final step is a pressureless sinter of about 1150°C to sinter the matrix to the appropriate density (37:5).

2.5.5.2 Properties

AFRL/ML has characterized this material. Its room temperature strength is 179 MPa, its modulus is 76.5GPa and its failure strain is 0.3%. The high temperature fatigue behavior is shown in Figure 2-4 below. The material has excellent fatigue properties typical of oxide/oxides to 1100°C. However, as the figure shows, a drop in fatigue strength occurs at 1200°C.

COI believes the degradation in strength at 1200°C is due to sintering of the silica in the aluminosilicate matrix. Sintering is the process by which small particles of a material are bonded together by solid-state diffusion. Particles are coalesced by solid-state diffusion at very high temperatures but below the melting point of the compound being sintered. As the process proceeds larger particles are formed at the expense of smaller ones. As particles get larger, porosity decreases (38:610). So as the silica in the matrix sinters, the porosity of the matrix decreases. Since the composite relies on fine matrix porosity for toughness, toughness decreases along with porosity. So while this composite shows very

promising high temperature performance, for applications at 1200°C a different refractory matrix is required.

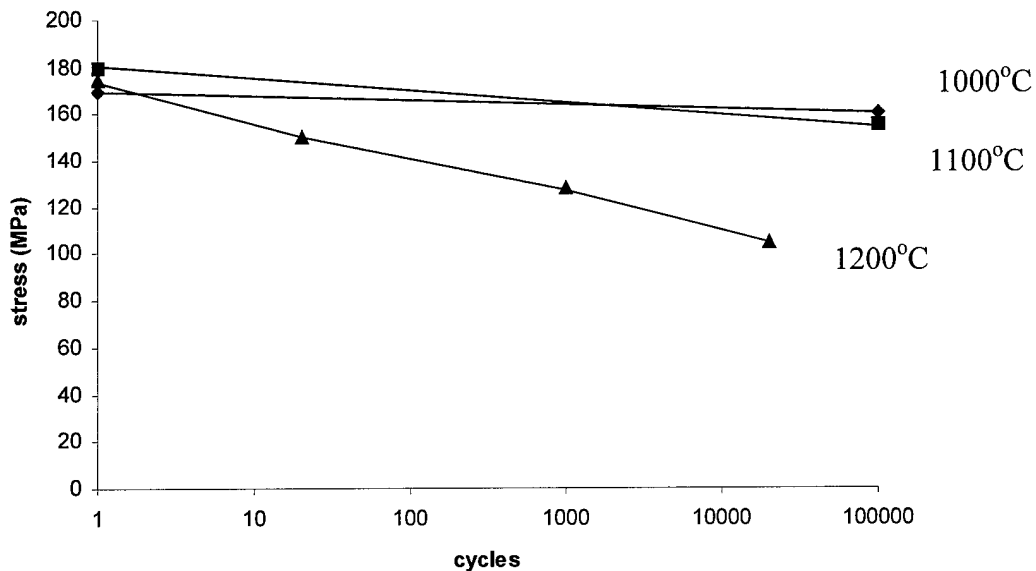


Figure 2-4 Fatigue behavior of Nextel 720/AS (from AFRL/MLLN)

2.6 Description of Current Material

The next step in the evolution of oxide/oxides is to increase their useful temperature from 1100 to 1200°C. Because of COI's experience with oxide/oxide composites they were awarded a Small Business Innovative Research (SBIR) contract to develop an affordable CMC for 1200°C applications.

In Phase I of the SBIR, COI researched various combinations of fibers and matrices. Nextel 720 was selected as the best available oxide fiber. The main problem was to find a substitute for the silica in the aluminosilicate matrix material. A more refractory material that would not sinter or react with the fiber was required. In the end, a pure alumina matrix was chosen.

In Phase II of the SBIR, COI fabricated several sheets of the new Nextel 720/alumina (N720/A) oxide/oxide composite. The new composite is manufactured using the same sol-gel process COI used to manufacture the N720/AS composite. Ten plies of balanced 8HSW Nextel 720 fibers have been used. The matrix has the same porous structure tightly bound to the fibers and no fiber coating. The difference is that the silica has been removed.

Since this is a brand new material, it has yet to be characterized. It has not been determined whether this material has improved upon previous oxide/oxides, nor has it been shown that the new material will be able to operate at 1200°C. This thesis will answer those questions. This thesis will provide the first in-depth study of the new material including its monotonic tensile and fatigue properties as well as its resistance to moisture.

For this testing, COI had the sheets of the new material machined into specimens. Two types of specimens which were used in the testing of this material are shown below in Figure 2-5. The circular inserts are not part of the specimens, but have been drawn to

show the orientation of the fibers. The straight-sided specimens offer the advantage of low machining costs and no stress concentrations. They are generally used for monotonic tensile tests. The dog-bone specimens offer a reduced width gage length to encourage failure within the gage length region. This specimen geometry has a stress concentration factor of about 1.06 (39:37). This means if failure occurs in the transition region at a nominal stress of 140 MPa, the actual strength of the specimen is about 148 MPa. The dog-bone specimens are used for fatigue tests.

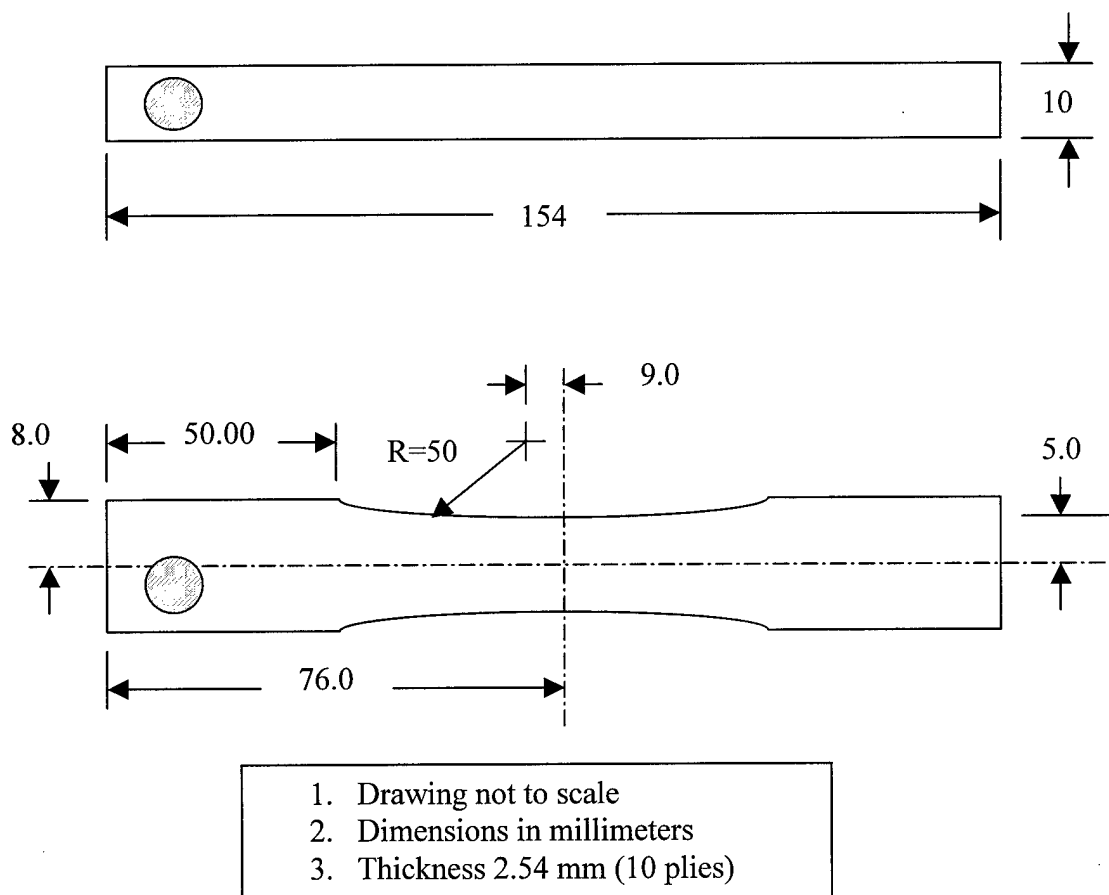


Figure 2-5 Straight-sided and dog-bone specimens (cutouts show fiber orientation)

3 Experimental Equipment and Procedures

This section will describe the equipment used to characterize the N720/A oxide/oxide composite. Pertinent details of all test procedures will be described as well.

3.1 Equipment

The equipment used for testing falls into three major categories: the mechanical test apparatus, the environmental equipment and the imaging devices.

3.1.1 Mechanical Test Apparatus

An MTS (MTS Systems Corporation) horizontal servohydraulic machine with a 25 kN (5500 lb) capacity was used for all tests. (The maximum load reached during any test was approximately 800 lb.) MTS hydraulic wedge type clamping grips were used to grip the specimens. Minimum grip pressure was calculated from a formula in the grip handbook. Grip pressure must be high enough to prevent the specimen from slipping but low enough not to crush the specimen or add excessive out of plane stresses. Minimum calculated grip pressure was about 350 psi. If the specimen slipped in the grips at minimum pressure, pressure was increased. Maximum grip pressure used was about 600 psi. The grips were aligned with a strain gauged alignment fixture to reduce any bending strains on the test specimens. Maximum bending strain was reduced to 60 μ strain, which is about 2-3% of the total strain measured during the tests.

Test control and data acquisition were done by MTS Test-star II software. The Basic Testware feature was used to program simple monotonic tests. The Multi Purpose Testware feature was used to program fatigue cycling with data acquisition at logarithmic intervals (cycles 1,2,5,10,20,50,100,etc.).

Load and extension data were acquired. Load was measured with an MTS 661.20E-01 load cell with a 25 kN capacity. The measured load was divided by specimen cross sectional area to get stress. Specimen extension was measured with an MTS extensometer model number 632.53E-14. The extensometer used two alumina rods, spaced 12.7 mm (0.5 inches) apart, held against the specimen with spring pressure as shown in Figure 3-1.

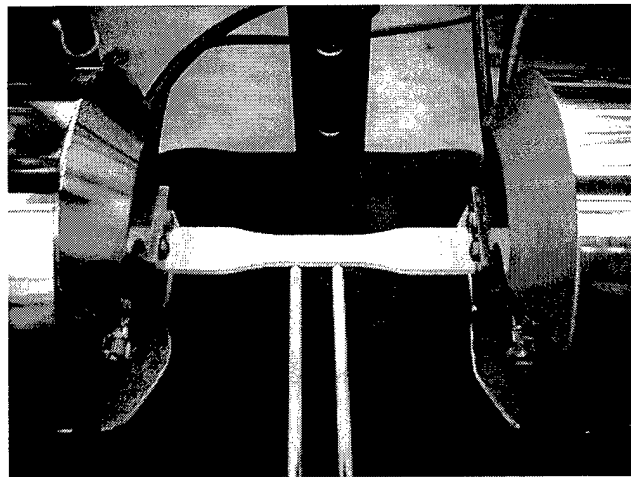


Figure 3-1 Specimen in grips with extensometer rods

When the specimen is stressed the two alumina rods spread apart and track specimen extension. The extension of the specimen was multiplied by an extensometer calibration factor (see below) and divided by the gage length (~12.7 mm) to get strain.

Strains in ceramics are generally very small compared to other materials. Table 3-1 shows a comparison of strain to failure of some common materials.

Table 3-1 Strain to failure for some common materials

Material	ϵ_f (%)
Nylon 6	30-100
Aluminum 2024-T4	20
Ti-6Al-4V annealed	16
AISI 4130 steel	14
A291C-T6 cast magnesium	0.4
Oxide/oxide ceramic composites	0.2-0.3

Because the strains are so small, the extensometer had to be calibrated at its maximum sensitivity. The extensometer was calibrated so that 0.0635 mm (0.0025 inches) extension gave an output of 9.0 volts. 0.0635 mm of extension in a gage length of 12.7 mm is a strain of 0.005 or 0.5%. Strains measured in the monotonic tensile tests ranged from 0.2-0.3 %. The extensometer calibration was periodically checked with MTS calibrator model 650.03 to ensure it did not change over time. The gage length was periodically measured with a Gaertner optical traveling microscope and was generally in the range of 12.77 to 12.85 mm. All data was analyzed and graphed using the Excel spreadsheet application from Microsoft.

3.1.2 Environmental Equipment

1200°C testing was accomplished using a two zone Amteco Hot-Rail Furnace System. The chamber of the furnace is compact, about 5x5x8 cm, so the heat is applied to a very localized area. Figure 3-2 shows the bottom half of the furnace in place beneath the specimen. The furnace chamber has two zones with two silicon carbide heating elements per zone.

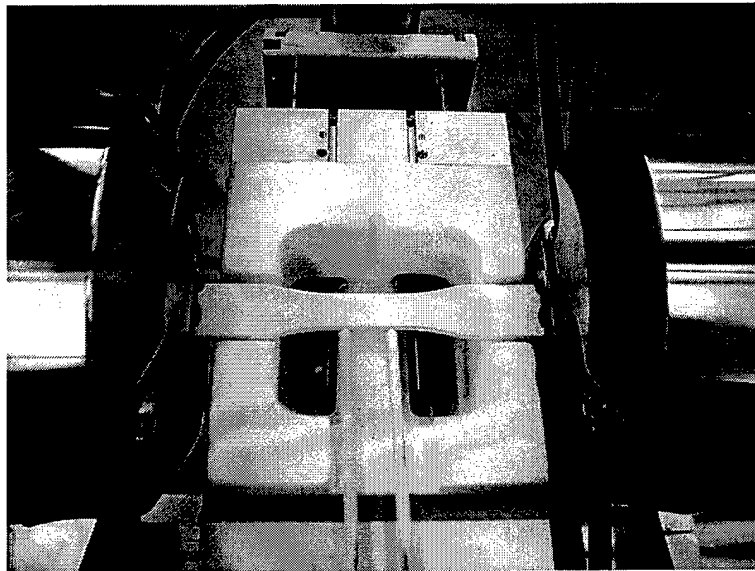


Figure 3-2 Furnace set-up (Bottom half)

The temperature in each zone was controlled by a separate Barber Coleman 560 controller. An S-type thermocouple mounted in each zone sensed the temperature inside the furnace and sent the signal to the Barber Colemans, which supplied power to the heating elements as needed.

To ensure a specimen temperature of 1200°C the following procedure was used. Three S-type thermocouples were bonded to a dummy specimen in the location shown below.

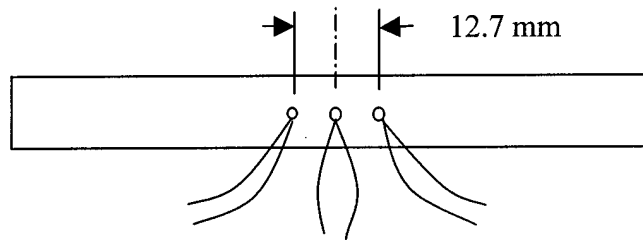


Figure 3-3 Thermocouple layout on dummy specimen

S-type thermocouples have a junction of platinum and rhenium and are especially suited for high temperature testing. The three thermocouples were spaced evenly across the gage length and bonded to the specimen with Zircar ceramic cement.

The furnace was started and the specimen temperature ramped to 1200°C using the Barber Colemans' automatic control. It took approximately 25 minutes to go from room temperature to 1200°C. There was an overshoot in temperature of about 18°C (the temperature peaked at 1218°C then settled at 1200°C). Once at 1200°C the specimen temperature remained essentially constant. The center thermocouple read 1203°C and the two outer ones 1198°C. In order to get this specimen temperature, the two Barber Coleman controllers had to be set at 1080°C and 1093°C. This difference between the furnace thermocouples and the specimen thermocouples (of over 100°C) indicates a fairly steep temperature gradient within the furnace.

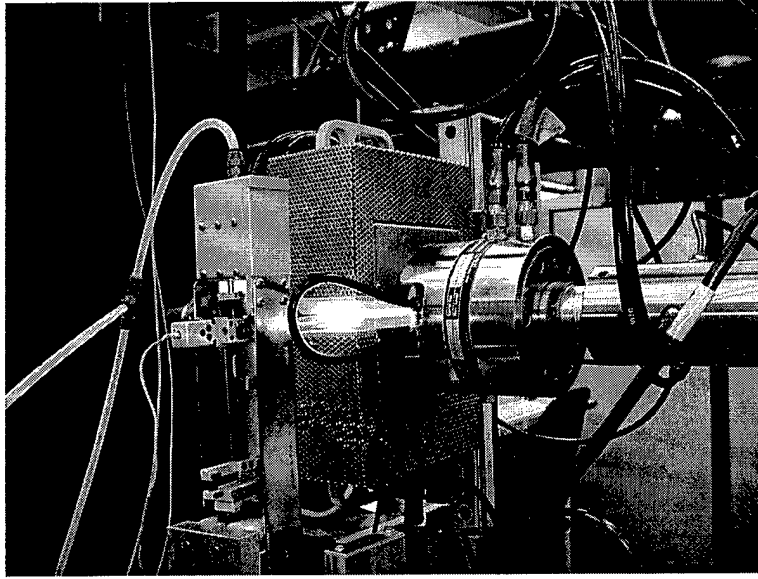


Figure 3-4 High temperature test in progress

These heating procedures were repeated several times with the dummy specimen. After repeatability was demonstrated, the dummy specimen was no longer used. For the actual high temperature tests the Barber Colemans were simply ramped to 1080°C and 1093°C to provide a 1200°C specimen. This meant no thermocouples had to be mounted to actual test specimens. The dummy specimen with thermocouples was reinstalled after every 4-5 tests to recheck furnace calibration. These rechecks verified the repeatability of the furnace set-up and justified the use of such an open loop approach.

During high temperature testing, the grips and load cell were kept cool with a chilled water system. The Neslab system pumped 12°C water through the grips and through a load cell isolation block. The extensometer was fitted with a heat shield and an air-cooling attachment. Room temperature air was forced over the extensometer through a special diffuser.

For the moisture exposure tests, specimens were placed in an Atotech fog chamber. The fog chamber maintains a 95°C cabinet with 100% relative humidity.

3.1.3 Imaging devices

Images of fracture surfaces were obtained with a Leica Cambridge Stereoscan 360 Field Emission Scanning Electron Microscope (SEM). The SEM bombards a specimen with electrons and examines the various electrons knocked off the specimen. The microscope has sensors to detect secondary electrons and backscattered electrons. Images were taken using both types of detectors. Backscattered images are especially good for showing differences in elemental composition. Since the matrix material being studied is alumina and the fiber is 85% alumina and 15% silica this would not appear to offer much advantage. Nevertheless the backscattered images were often more distinct than the secondary.

Ceramics in general are difficult to look at in the SEM, because they are not good conductors of electrons. When ceramics are bombarded with electrons they tend to accumulate charge. This charge distorts SEM images. To help alleviate this problem, specimens are given a thin coating of a conducting material. Two types of coatings were tried in this effort. A carbon coating was used but was not effective in reducing the charging problem. A gold-palladium (Au-Pd) coating was more effective though it did not eliminate the problem. A Hummer X Sputter Coater from Anatech LTD was used to apply the coating. The gold-palladium was sputtered onto the sample by means of a

positively charged argon gas ion plasma. The argon ions strike a Au-Pd target knocking off metal atoms, and then deposit the metal onto the ceramic. Coatings of several nanometers were used. Before coating, the samples were cleaned by soaking for 24 hours in isopropyl alcohol.

A digital optical microscope was used as a non-destructive means to characterize the surface of specimens in as-received condition. The model used was a Nikon Inverted Microscope, EPIPHOT-TME with a Polaroid Digital Microscope Camera attached. Again the oxide/oxide ceramics provided a challenge. Optical microscopes have a very limited depth of focus. They do best on very smooth polished surfaces. The N720/A has a rough surface texture. Therefore the images of the as-received specimens are somewhat fuzzy, but they convey the desired information.

The optical microscope was also used to look for damage in fatigue specimens. To do this the fatigued specimens were sectioned, mounted in phenolic 'hockey pucks' and then polished. Oxide/oxide CMCs are difficult to polish because of their tendency to crumble. The basic polishing technique is summarized as follows: three hours on the Phoenix 4000 Automatic Polisher using six micron diamond grit on a perforated text met polishing pad, one hour on the same automatic polisher but using a one micron diamond grit perforated text met pad, 24 hours in a Buehler Vibramet I vibrating polisher using the one micron diamond grit perforated text met pad.

A digital camera was used for pictures of the test set-up. The model used was a Sony Mavica.

3.2 Test Procedures

3.2.1 Monotonic Tension

All tension tests were done under stroke control mode with a 0.05mm/sec displacement rate. At this rate the tension tests lasted about 10-14 seconds. All specimens were fitted with fiberglass tabs in the grip region to promote even gripping. The tabs were held in place with a drop of superglue.

Monotonic tension tests were run at room temperature and at 1200°C. For the high temperature tests the specimen was heated to 1200°C in 25 minutes. Next the specimen was allowed to stabilize for 15 minutes. Then the test was started and stress was ramped up until failure occurred.

As test specimens were heated from room temperature to 1200°C they underwent thermal expansion. These thermal strains were measured with the extensometer and were used to calculate a coefficient of thermal expansion for the composite. The extensometer was then 'zeroed' at 1200°C so that only mechanical strains were measured during testing at temperature.

A load-displacement data point was taken by the Test-star II software every 0.05 seconds. This gave over 200 data points for a typical tensile test. Load-displacement data were converted to stress-strain. Curves were fit to the data using Microsoft Excel. Second-degree polynomial curves fit the stress-strain data very nicely.

3.2.2 Cyclic Tension (Fatigue)

Cyclic tension tests were done at room temperature and 1200°C. The tests were done in load control with a load ratio of 0.05 ($R = \sigma_{\max}/\sigma_{\min}$). The applied load had a sine wave form as shown in Figure 3-5 and a frequency of one hertz (one cycle per second).

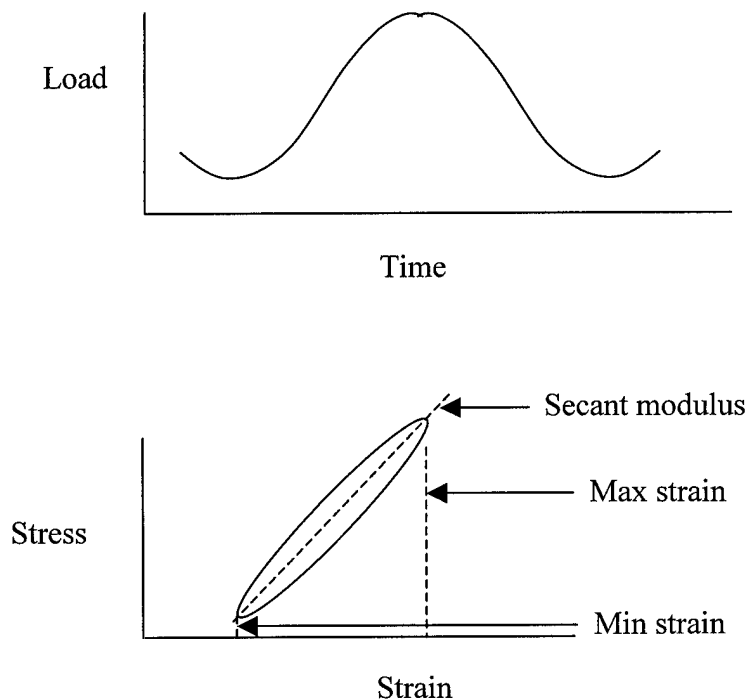


Figure 3-5 Applied fatigue load and associated stress-strain loop

During fatigue testing load-extension data was taken on cycle numbers 1, 2, 5, 10, 20, 50, 100, 200, 500, 1000, 2000, 5000, 10000, 20000, 30000, 40000, 50000, 60000, 70000, 80000, 90000 and 100000. Data points were taken every 0.005 seconds and were taken on the loading and unloading part of the cycle. The load-extension data was converted to stress-strain. Stress-strain data, shown for one fatigue cycle in Figure 3-5, was used to track trends in secant modulus, maximum and minimum strain and hysteresis. All these factors are indicators of damage occurring to the composite during fatigue. The secant modulus was used, as opposed to the tangent modulus used in monotonic tests, for ease of calculation.

Tests were run at maximum cyclic stresses of 60%, 70%, 80% and 90% of ultimate tensile strength and the number of cycles to failure was measured for each stress level. Maximum stress vs. number of cycles to failure data was plotted to create the stress-life plot or S-N curve at each temperature. Although the aerospace industry now uses a fracture mechanics based approach to fatigue life (da/dn vs. ΔK curves), the S-N curve is a useful tool to characterize a material's fatigue performance. One use of the S-N curve is to determine the fatigue limit (also called endurance limit) of a material. The fatigue limit provides a key index for comparing the performance of different materials.

The fatigue limit is the stress level at which the material may be cycled indefinitely without failing. Some materials, like most steels and copper alloys, have true fatigue limits and will not fail when cycled at stresses below that limit. Other materials, like many high strength steels and aluminum alloys, do not exhibit true fatigue limits. For

these materials the allowable stress amplitude continues to decrease with an increasing number of cycles. In this case, the fatigue limit may be defined as the stress level at which the material may be cycled for a given number of times without failing.

Researchers have not yet determined whether CMCs have a true fatigue limit or not. For this effort 100,000 cycles was chosen to define the fatigue limit. 100,000 cycles was considered a reasonable number of stress cycles for the lifetime of an aerospace component. This also limited the maximum length of a fatigue test to about 28 hours (one cycle per second x 100,000 cycles), and test duration was an important consideration. Any specimen that survived for 100,000 cycles without failing was considered a 'runout' specimen.

All specimens that reached 100,000 cycles without failing were then tested for retained strength. Retained strength tests used the same procedures as the monotonic tensile tests described in Section 3.2.1.

3.2.3 Moisture Interrupted Fatigue Tests

In order to investigate the effect of moisture on the fatigue behavior of the present CMC at 1200°C, a few fatigue tests were interrupted and then exposed to moisture. This procedure was continued until either the specimen failed or survived 10^5 cycles. This type of test will be referred to as "Moisture Interrupted Fatigue Tests" in this study.

These tests used the same procedures as the fatigue tests in the previous section.

However, this time the fatigue test was interrupted at cycle numbers 5000, 10000, 15000, 20000, 25000, 50000 and 75000. At each interruption the specimen was removed from

the mechanical test apparatus and placed in the fog chamber. The specimen stayed in the fog chamber overnight (i.e. for 16 hours) to allow complete saturation of the moisture. The specimen was then removed from the fog chamber and placed in a drying oven for 2 hours at 75°C. After drying, the specimen was put back in the mechanical test apparatus, the temperature was ramped to 1200°C and fatigue cycling continued. Just as in the regular fatigue tests, a specimen that reached 100,000 cycles was considered to have runout. The runout specimens were tested for retained strength using the same procedures as a monotonic tensile test.

3.3 Test Matrix

The following table summarizes all tests performed to characterize the oxide/oxide composite:

Table 3-2 Test Matrix

Tensile tests		
Temperature	Number of Tests	Remarks
RT	3	2 dog-bone, 1 straight-sided
1200°C	3	2 dog-bone, 1 straight sided

Fatigue tests		
Temperature	Number of Tests	Stress Level
RT	4	60, 70, 80, 90 (%UTS)
1200°C	3	70, 80, 90 (%UTS)

Moisture interrupted fatigue		
Temperature	Number of Tests	Stress Level
1200°C	2	80, 90 (%UTS)

Retained strength		
Temperature	Number of Tests	Remarks
RT	7	All runout specimens from fatigue tests

4 Results and Discussion

This section will first describe the microstructure of the current CMC, which is important in understanding its mechanical behavior. Next the results of all tests will be detailed and discussed. Characteristics of this CMC are compared and contrasted to typical characteristics of traditional non-oxide CMCs.

4.1 Microstructure Characterization

Before tests, initial investigation was done with the optical microscope to characterize the microstructure of the oxide/oxide, N720/A, in the as-received condition. Figure 4-1 shows a 'through the thickness' view showing the major components of the composite. The 90° fiber tows of the 8HSW are visible as well as the macroporosity and cracks between the tows.

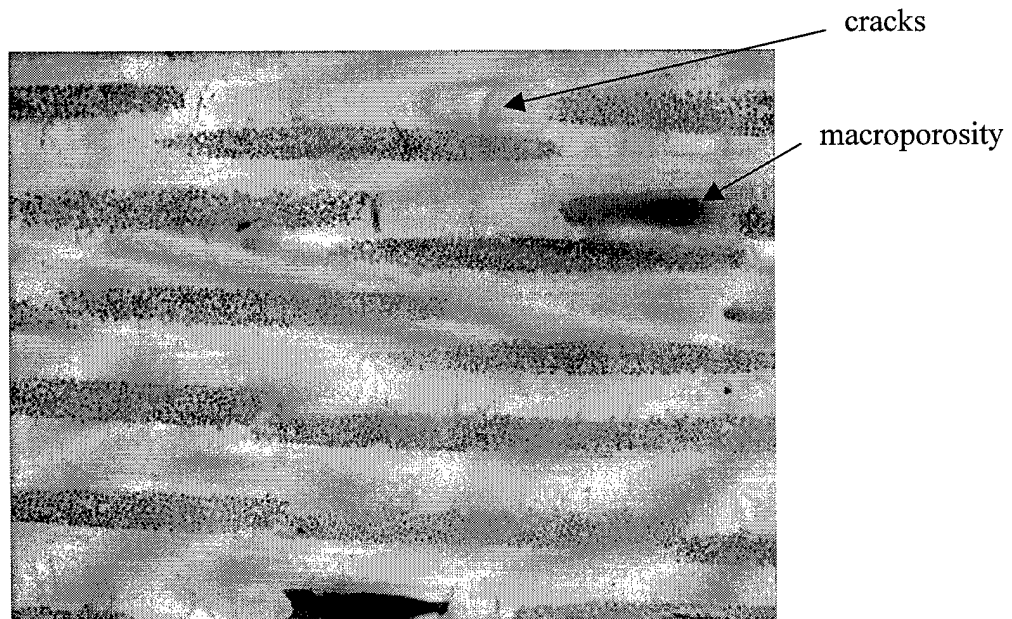


Figure 4-1 Microstructure of N720/A, 50X

Figure 4-2 shows two views of the microstructure at a higher magnification to give a better view of the cracks and pores between the fiber tows. The cracks are due to matrix shrinkage that occurs during the sol-gel processing, as the liquid ceramic precursor solidifies. The large pores are due to the woven fiber architecture. The ceramic precursor has difficulty infiltrating the regions in between the woven fiber tows.

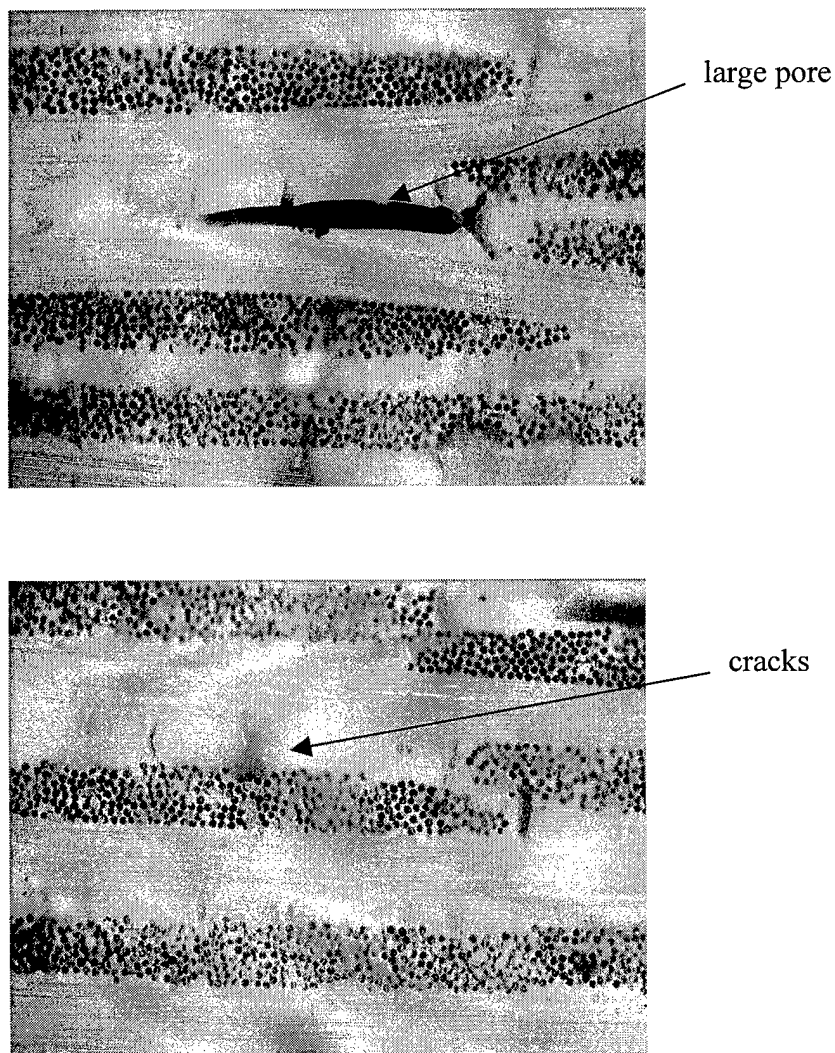


Figure 4-2 Microstructure of N720/A, 100X

Figure 4-3 shows the cracked condition of the matrix on the surface of the specimen. The cracks are again due to the shrinkage that occurs during the sol-gel processing.

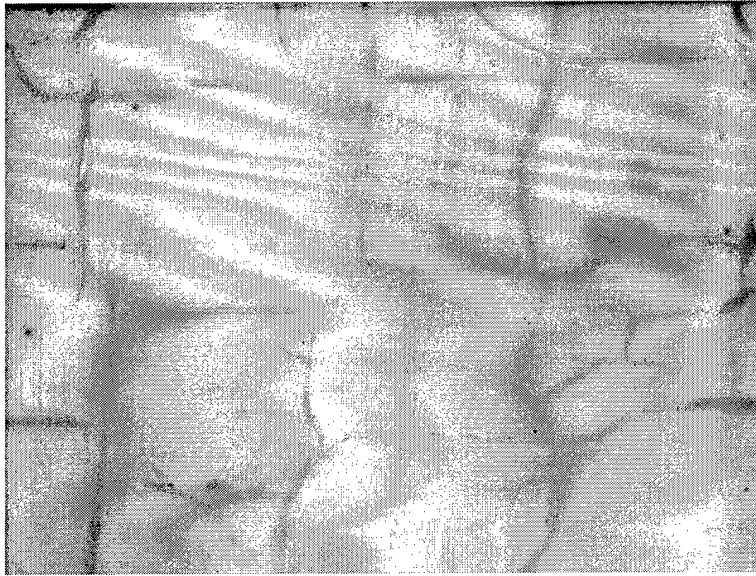


Figure 4-3 Matrix cracks on specimen surface, 100X

These figures show the composite has initial damage when it is manufactured, even before it is subjected to stress. This damage will have an important effect on the mechanical behavior, as will be shown in the next several sections. The damaged condition also makes it difficult to find additional damage that occurs during monotonic or cyclic stresses.

Figure 4-4 shows a delamination, or separation of plies, present at the grip section of a specimen. Such delaminations were present on several specimens. In general, the quality of the composite suffered near the edges of specimens.



Figure 4-4 Delamination of plies in grip region, 50X

In addition to the delaminations, there were regions of poor matrix infiltration and variations in specimen thickness. These quality problems may have contributed to problems with some specimens failing in the grips. These problems are discussed in Appendix A.

4.2 Monotonic Tensile

4.2.1 Room Temperature

Table 4-1 summarizes the results of the three room temperature tensile tests.

Table 4-1 Room temperature monotonic test results

Specimen	UTS (MPa)	E (GPa)	ϵ_f (%)
1 (dog-bone)	147	65	.27
2 (dog-bone)	144	68	.24
3 (straight-sided)	140	75	.21
Average	144	69	.24

At first, the plan was to use straight-sided specimens for all the tensile tests, however these specimens proved difficult to test. With grip pressures of 2.5-3.5 MPa (350-450 psi) the specimens slipped in the grips after reaching stress levels of 85-100 MPa. With higher grip pressures, the specimens failed in the grips. There seemed to be no margin between slipping and failing in the grips. The first two attempts at monotonic tests resulted in specimens failed in the grips at stresses near 120 MPa.

After these problems occurred, dog-bone specimens were used for the next two tests. The dog-bone specimens had no problems with slipping or breaking in the grips even with grip pressures up to 4 MPa (600 psi).

When a straight-sided specimen failed in the grips, usually only about 10mm of material broke off at the end of the specimen. That meant new tabs could be put on and the specimen retested. One of the above specimens was retested in this way. This time the specimen failed just at the edge of the grips at 140MPa. This result agreed much better with results from the dog-bone specimens and so was included in reported data above. The issue of grip failures is further addressed in Appendix A.

Table 4-2 shows the mechanical properties of the current material, N720/A, compared to the previous version of the material, N720/AS. As the table shows, by removing the silica from the matrix some strength has been sacrificed in the hopes of attaining better high temperature performance, as shown later.

Table 4-2 Comparison of room temperature tensile properties of N720/AS and N720/A

Material	UTS (MPa)	E (GPa)	ϵ_f (%)
N720/alumina (present)	144	69	.24
N720/aluminosilicate (previous)	179	76	.30

Table 4-3 compares the ultimate strength of this oxide/oxide with some common aerospace materials and other CMCs. The table shows this composite falls at the lower end of the strength spectrum and would not be suitable for high stress applications. The table also shows that the strength of these CMCs is well below that of aluminum and titanium. Since CMCs are designed for high temperature use, however, strength is not as important at room temperature. Also note that all the CMCs listed here are 2-D woven composites. For higher stress applications, all fibers could be oriented in one direction thus doubling the composite strength in that direction.

Table 4-3 Strength comparison common aerospace materials and CMCs

Material	Description	UTS (MPa)
Ti-4Al-6V	Most commonly used titanium alloy	895
Aluminum 7075-T6	High strength aluminum alloy	538
SiC/SiC	Carbon interface	209
GEN IV	Nextel 610 fibers, oxide/oxide	205
Nicalon/Si-N-C	BN interface	197
N720/A	Oxide/oxide from this study	144
Nextel 312/Blackglass	BN interface	69

Figure 4-5 shows the stress-strain curve for specimen 2. It is typical of the three monotonic tests. A second-degree polynomial curve fit the data very nicely. The stress-strain response is nearly linear at first and then becomes slightly non-linear.

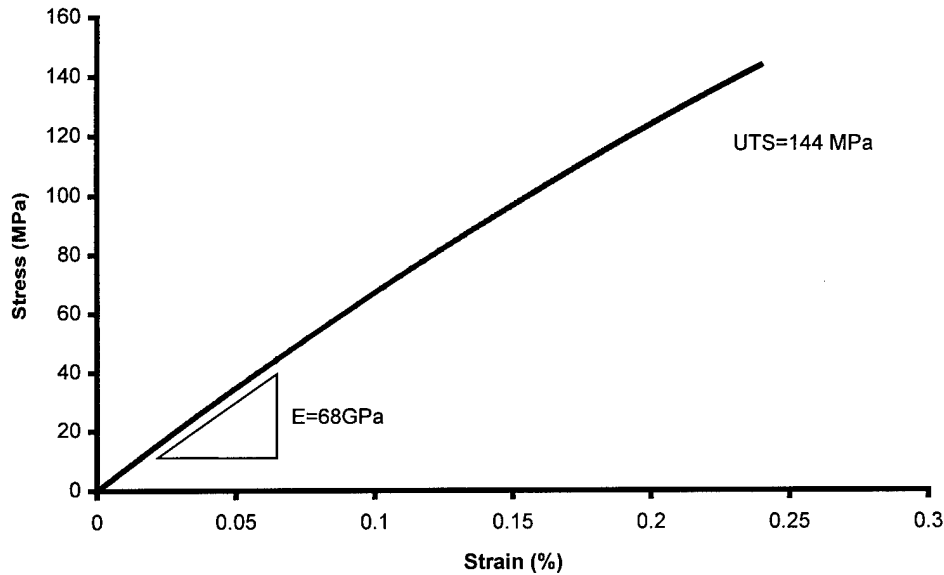


Figure 4-5 Typical room temperature stress-strain curve for N720/A

Compare the stress-strain response of this oxide/oxide with that of a traditional CMC as shown in Figure 4-6. For the traditional CMC, the response is linear until the matrix material begins to crack. In 0/90 cross-ply composites, the first matrix cracks occur in the 90° plies. In woven composites, the first cracks appear at the macroporosity between the warp and fill yarns. The first matrix cracks cause the onset of non-linearity in the stress-strain curve, also called the “knee” or proportional limit. As stress is increased, the number of matrix cracks multiplies and then reaches a level of saturation. Once the

matrix is saturated with cracks the stress strain response becomes linear again and most of the load is carried by 0° fibers.

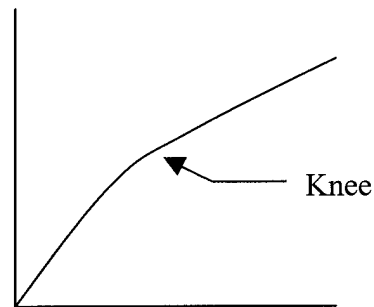


Figure 4-6 Typical stress-strain response of CMC showing proportional limit

The current oxide/oxide composite does not show an obvious knee because its matrix starts out already porous and cracked. Figures 4-1 to 4-4 show the condition of the as received material as viewed under an optical microscope. Note the extensive cracks and pores present. As the material is stressed, some additional matrix cracking occurs which causes the non-linearity in the stress-strain curve. However, the non-linearity is slight and occurs gradually, not over a short duration as with the knee behavior. Given the initial cracked condition of the matrix it was not possible to identify conclusive evidence of the additional matrix cracking.

All three monotonic tests are plotted on the same graph in Figure 4-7.

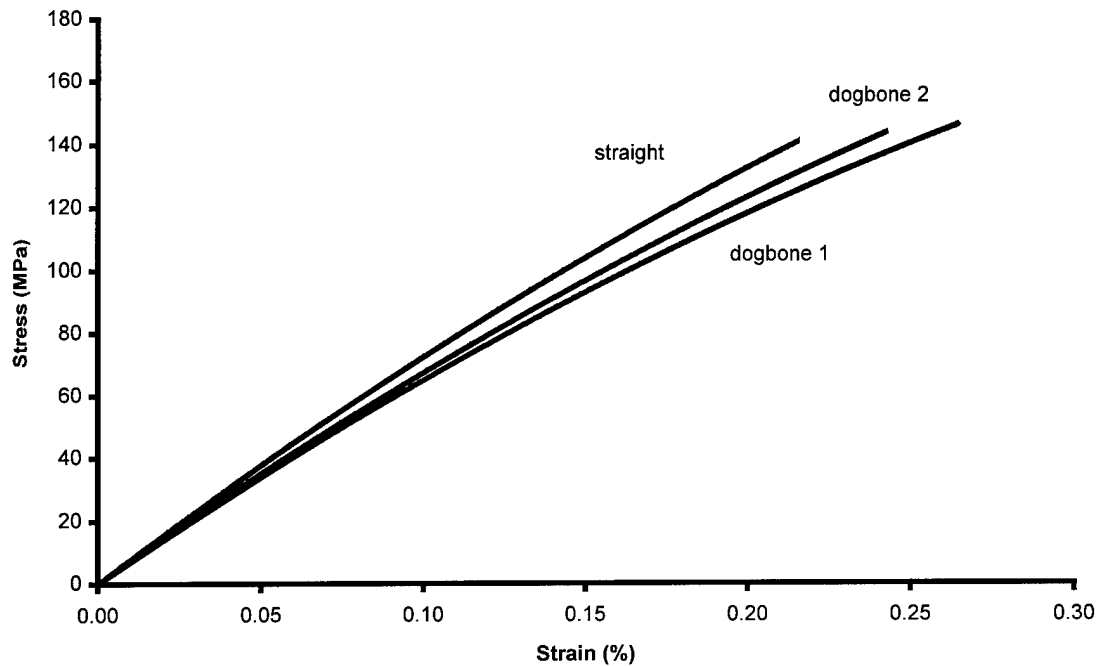


Figure 4-7 Comparison of three room temperature stress-strain curves

The tensile response of two-dimensional woven composites like this one is dominated by the 0° fibers (40:803). Nextel 720 fibers, in an unwoven condition, have a mean filament strength of about 2 GPa. Young's modulus is 260 GPa and mean failure strain is about 0.8% (33:2078). Significant degradation in fiber properties occurs during weaving. Fiber bundles extracted from woven fabric have a strength of ~ 0.9 GPa and a failure strain of 0.3%. The properties of the extracted fibers are the appropriate baseline to analyze the composite's properties (33:2078). Composite strength and failure strain can be estimated fairly well using the properties of the woven fibers. A fiber strength of 0.9 GPa with a fiber volume of 20% in the 0° direction gives an estimated composite strength of 180 MPa (actual results 144 MPa). Composite strain to failure also closely matches

the failure strain of woven Nextel 720 fibers. Average failure strain from the room temperature tensile tests was 0.24% while failure strain of woven Nextel 720 fibers is 0.3%.

The difference in actual strength and strain from estimated values based on fiber properties could be accounted for by residual stresses in the composite, which may be pre-stressing the fibers. The final processing step for this composite is to sinter the matrix at about 1150°C. At that temperature, the composite is stress free. When the composite cools, residual stresses develop due to the thermal expansion mismatch between fibers and matrix. Calculations suggest that the fibers are subjected to a residual tensile stress of around 35 MPa (See Appendix B for calculations).

Most, but not all, of the composite's stiffness is due to the 0° fibers. If the tensile response were entirely due to the 0° fibers, then the composite modulus would be given by the formula:

$$E_c = (V_f/2) \times E_f \quad (1)$$

where E_c is composite modulus, V_f is fiber volume and E_f is fiber modulus. With an estimated fiber volume of 40% and a fiber modulus of 260 GPa, this equation yields a composite modulus of about 52 GPa compared to the actual measured modulus of 69 indicating that the matrix and 90° fibers contribute some stiffness. Using the rule of

mixtures, an effective matrix modulus, with contributions from the matrix and 90° fibers, can be calculated with the following formula:

$$E_m = (E_c - V_f E_f / 2) / (1 - V_f / 2) \quad (2)$$

where E_m is effective matrix modulus. Using this formula, the effective matrix modulus is about 21 GPa.

The following series of SEM photographs show the fracture surface of a tensile specimen at increasing levels of magnification. Figure 4-8 shows the entire fracture surface at a magnification of 20X. The fracture plane is fibrous and rough with fiber tows breaking

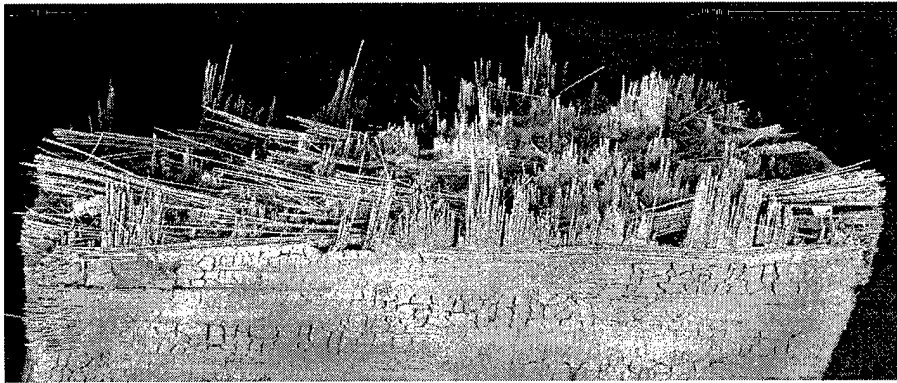


Figure 4-8 Fracture surface of room temperature tensile specimen, 20X

over a wide range of axial locations. Cracks did not propagate directly from one fiber tow to the next but were deflected in the porous matrix.

Figure 4-9 shows the surface at a magnification of 50X. Several zero degree fiber tows are visible in this photograph. Individual fibers within each tow are also broken over a range of axial locations. This indicates the porous matrix is not only effective at crack deflection in between the tows but also between individual fibers within the tows.

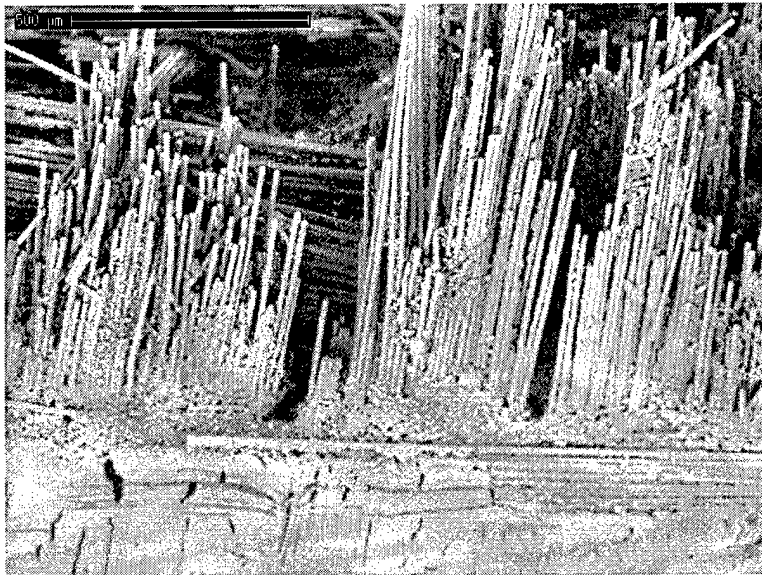


Figure 4-9 Fracture surface of room temperature tensile specimen, 50X

Figure 4-10 shows apparent fiber pullout on the fracture surface at a magnification of 1000X, but this is different than the fiber pullout mechanism of traditional CFCCs. No

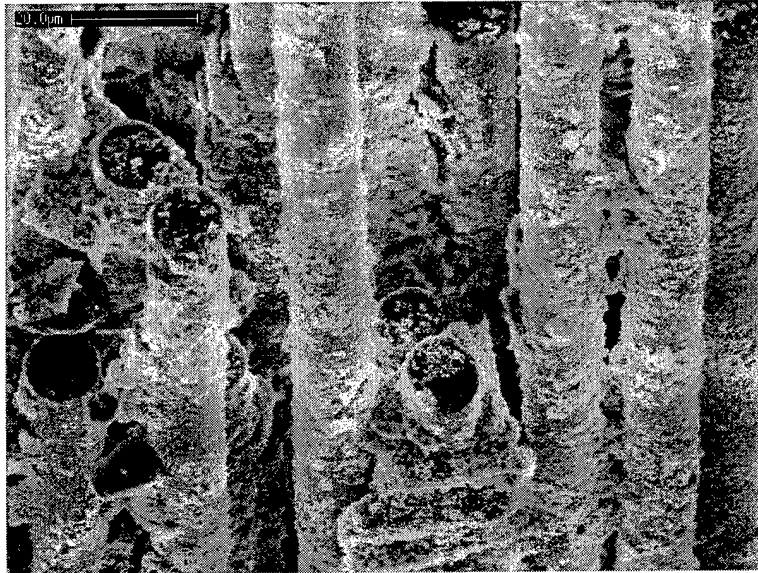


Figure 4-10 Fracture surface of room temperature tensile specimen, 1000X

hollow matrix sockets are visible on the mating fracture surface where the fibers are pulled out (33:2082). Instead, the matrix material fragments and crumbles where the fibers pullout. This composite is tough but not from traditional fiber debonding and pullout.

Figure 4-11 shows fibers at a magnification of 3000X. This image shows the 'strong interface' between matrix and fiber. Even after fracture there is a good amount of matrix material still firmly attached to the fibers. On fracture surfaces of traditional CFCCs, the

fibers appear smooth. Because of the weak fiber coating, they debond and pull out of the matrix material cleanly without the attached matrix material.

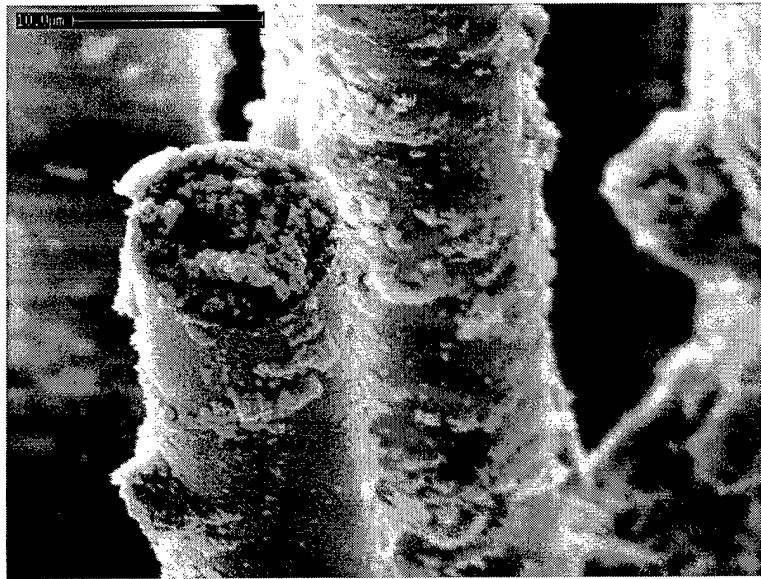


Figure 4-11 Fracture surface of room temperature tensile specimen, 3000X

4.2.2 1200°C

The following tables summarize the results from monotonic tensile tests at 1200°C and compare these results to those obtained at room temperature.

Table 4-4 1200°C monotonic test results

Specimen #	UTS (MPa)	E (GPa)	ϵ_f (%)
4 (dog-bone)	137+	54	.29
5 (dog-bone)	137+	52	.30
6 (straight-sided)	145+	59	.30
Average	140	55	.30

Note: For explanation of “+” see text.

Table 4-5 Comparison of average properties from monotonic tensile tests at two temperatures

Temperature (°C)	UTS (MPa)	E (GPa)	ϵ_f (%)
23	144	69	.24
1200	140	55	.30

Several observations can be made from the data in these tables. First, this material loses very little strength at high temperature. Average strength dropped only about 3% at high temperature. This value is somewhat misleading. All three specimens tested at 1200°C broke outside the furnace- two at the grips and one in the transition zone between the furnace and ambient air. These specimens have a '+' next to their ultimate strength in Table 4-3 to indicate that they are at least this strong. Grip failures have already been discussed and are further addressed in Appendix A. Thermal stresses in the furnace transition zone are also addressed in Appendix A.

A key factor in this material's ability to maintain strength at high temperatures is the stability of the Nextel 720 fiber at 1200°C. Wilson and coworkers tensile tested single Nextel 720 fibers at room temperature and 1200°C (41:1009). They found that the fibers maintained 88% of their room temperature strength at 1200°C. This composite does even better than the fibers alone; it loses at most 3% of its strength at 1200°C. This indicates the matrix is also maintaining tensile strength at high temperatures.

A second observation is that though temperature had little effect on strength, it did have an effect on the elastic modulus. The average modulus value dropped about 20% at high temperature. This is most likely due to the 0° Nextel 720 fibers becoming less stiff since

they are the dominant factor in the composite's overall modulus. Values for the modulus of Nextel 720 fibers at 1200°C were not found in the literature.

Thirdly, temperature also had an effect on strain to failure. Average strain to failure increased from 0.24% at room temperature to 0.3% at high temperature. This value (0.3%) is equal to the failure strain of Nextel 720 fibers extracted from woven tows. This increase in failure strain is possibly due to the relief of residual stresses. As mentioned in the previous section, this composite is processed at about 1150°C. As the composite cools, residual stresses develop and remain present during room temperature testing. When the composite is heated to 1200°C for high temperature testing, it is very close to the processing temperature where there are no residual stresses. With no residual stresses or strains on the fibers, they can strain a full 0.3% under loading before failing.

Overall, this material has very good monotonic tensile properties at 1200°C. Figure 4-12 shows a typical stress-strain curve obtained at 1200°C (specimen #5). It has the same characteristics as the room temperature tests, linear at low stress and then slightly non-linear at higher stress as the matrix cracks. Figure 4-13 shows a comparison of stress-strain curves at the two different temperatures. The difference in modulus and strain to failure is evident.

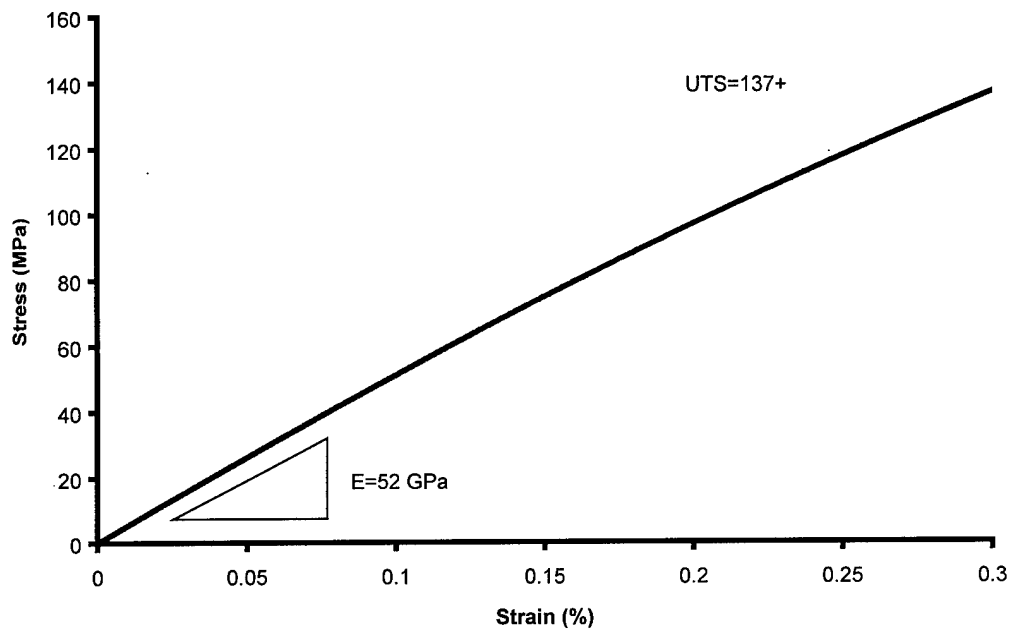


Figure 4-12 Typical stress-strain behavior at high temperature

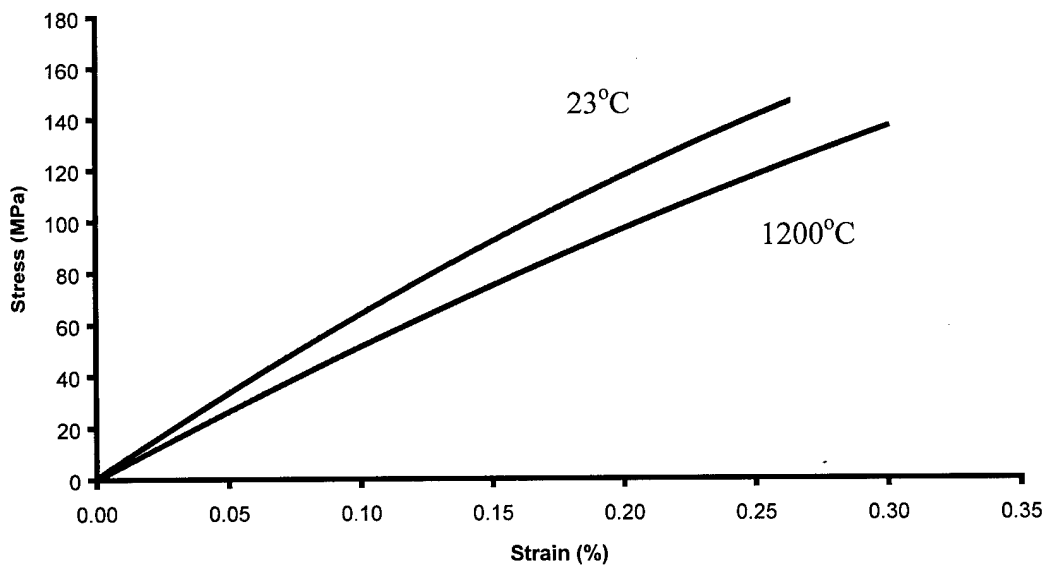


Figure 4-13 Comparison of tensile response at two temperatures

Figure 4-14 is an SEM image of the fracture surface of a high temperature monotonic specimen at a magnification of 20X.

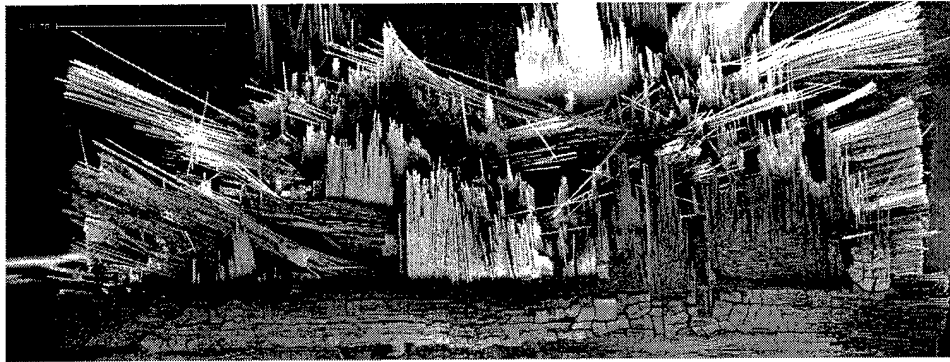


Figure 4-14 Fracture surface of 1200°C monotonic specimen, 20X

This fracture surface looks essentially the same as the fracture surface at room temperature, very rough. This indicates that the composite is stable during short-term exposure at 1200°C. Apparently no sintering of the matrix or of the matrix to the fibers has occurred. Figure 4-15 shows part of the fracture surface at a magnification of 700X. The fibers within a single tow are broken over a wide range of axial locations indicating that the matrix has not sintered to the fibers and is still serving as a crack deflecting medium.

To compare these images with those of a composite that has become brittle at high temperatures, the following are images taken of a GEN IV oxide/oxide specimen. This specimen was used as a dummy specimen to calibrate the furnace (see Figure 3-3). In



**Figure 4-15 Fracture surface of 1200°C monotonic specimen,
700X**

this role it was subjected to temperatures of 1200°C for several hours total. It was then accidentally dropped on the floor and it suffered a brittle fracture. The following figures illustrate the improvement in high temperature performance of N720/Alumina over GEN IV (N610/Aluminosilicate).



Figure 4-16 Fracture surface of GEN IV after 1200°C exposure, 20X

As Figure 4-16 shows, the fracture surface of GEN IV is much smoother than the Nextel 720/Alumina composite. There are no fibers of various lengths protruding from the surface. The crack penetrated straight through the composite without much deflection at all. (Granted the type of loading was different- impact vs. monotonic.)

Figure 4-17 shows how the matrix has sintered to the fibers and consequently the crack travels directly from the matrix through the fiber with no deflection. This is in contrast with the irregular fracture surface shown in Figure 4-15.

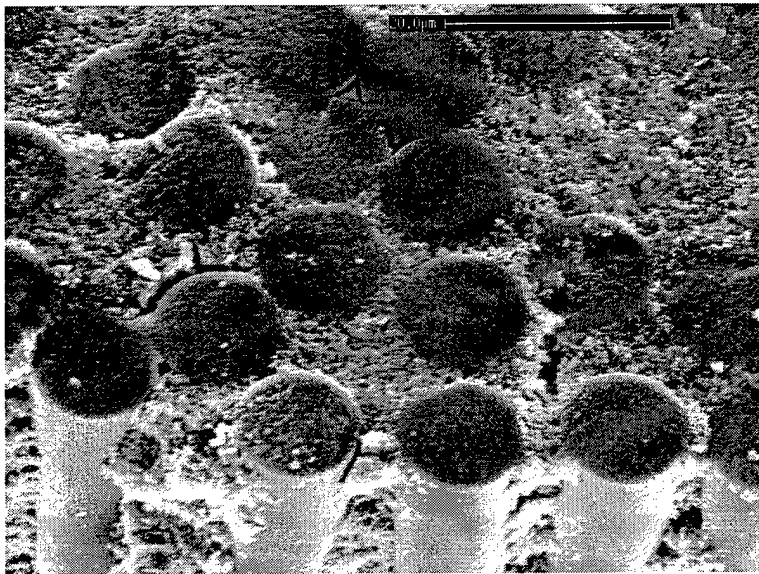


Figure 4-17 Fracture surface of GEN IV, 1800X

As mentioned in Section 3.2.1, when the test specimens were heated from room temperature to 1200°C they experienced thermal strains. These thermal strains were measured with the extensometer and used to calculate a coefficient of thermal expansion

(CTE) for the composite. The calculated CTE for the composite was $6.1 \mu\text{strain}/^{\circ}\text{C}$, which very nearly matches the CTE of the Nextel 720 fiber as given in Reference 41 ($6.01 \mu\text{strain}/^{\circ}\text{C}$).

4.3 Cyclic Tension (Fatigue)

4.3.1 Room Temperature

Cyclic tension tests were carried out at stress levels of 60, 70, 80 and 90% of room temperature ultimate strength. Results are summarized in Table 4-6.

Table 4-6 Room temperature fatigue results

Specimen	Maximum stress level (MPa)	Maximum stress level (%UTS)	Cycles to failure
7	130	90	74
8	116	80	130
9	102	70	100,000 (no failure)
10	87	60	100,000 (no failure)

Maximum stress level vs. number of cycles to failure data are plotted in Figures 4-18 and 4-19. Figure 4-18 shows maximum stress level on the y-axis while Figure 4-19 shows stress as a percentage of ultimate tensile strength. The fatigue limit for 10^5 cycles was approximately 102 MPa or 70% of room temperature tensile strength. This is lower than the previous oxide/oxide GEN IV, which had the corresponding fatigue limit of 85% of its room temperature tensile strength (23:10). The S-N curve is similar to Gen IV in that

it is nearly horizontal. Specimens tested at 90 and 80% stress levels failed after only 70 and 130 cycles.

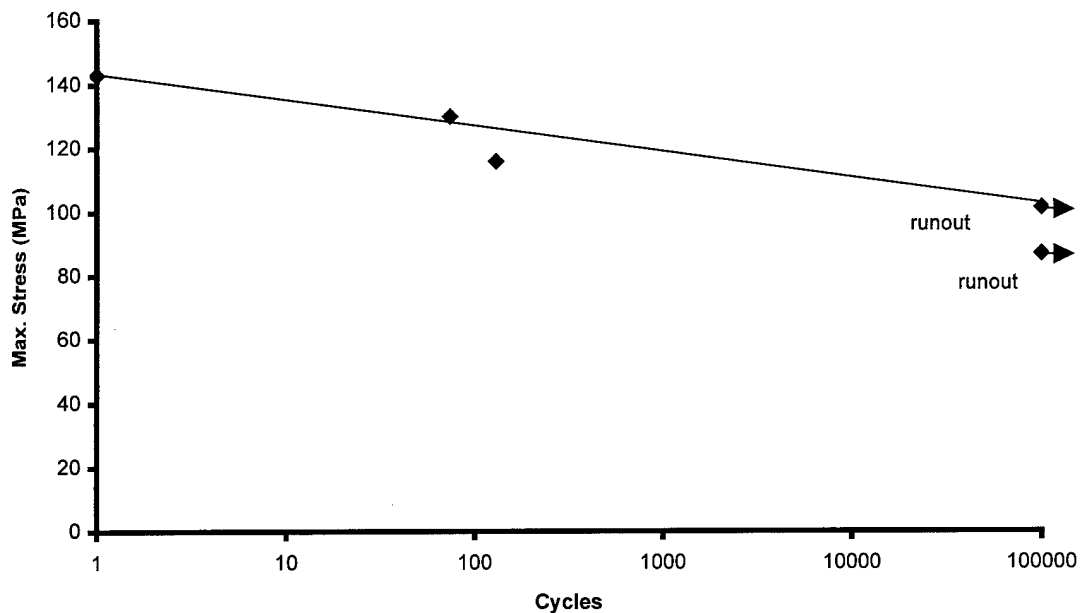


Figure 4-18 Room temperature S-N curve for N720/A

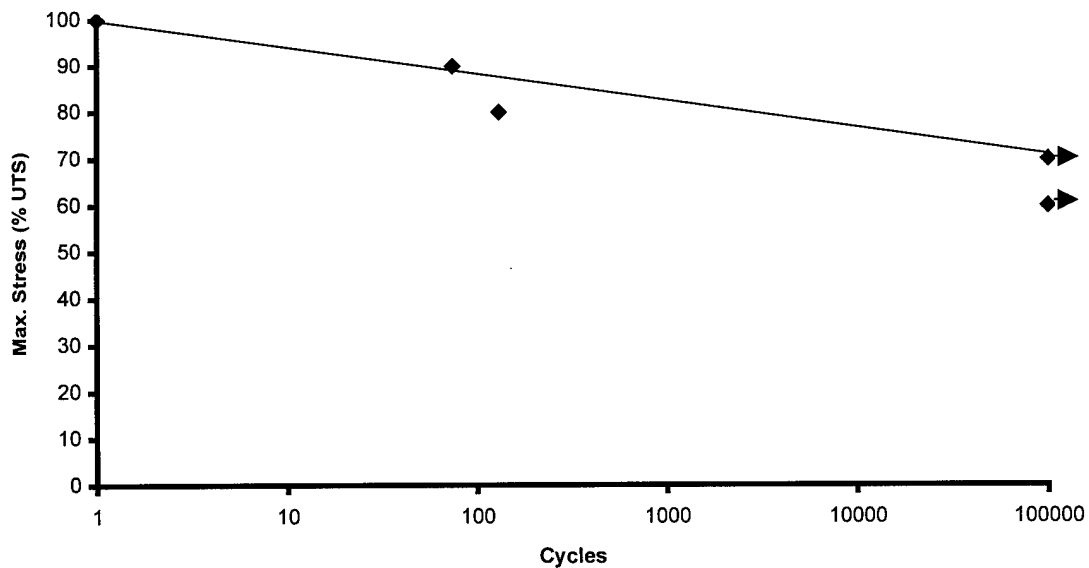


Figure 4-19 Normalized room temperature S-N curve for N720/A

respectively. Specimens tested at 60 and 70% stress levels ran out up to 100,000 cycles. There is a very steep reduction in life when going from a 70 to 80% stress level (102 to 116 MPa). The fatigue limit lies somewhere in this range but is conservatively estimated to be at the lower end.

Before proceeding with further analysis of the fatigue behavior of N720/A, a brief overview of fatigue mechanisms in CMCs with weak interfaces will be given for comparison. If a CMC is cycled at stresses lower than the proportional limit, there will be no matrix cracking and no fatigue should occur. If the CMC is cycled at stresses higher than the proportional limit, the matrix will crack. It will become saturated with cracks rapidly, possibly after the first stress cycle. Matrix cracking will cause a decrease in composite modulus as well as permanent strain due to the relief of residual stresses. As the matrix cracks open and close during further cycling, fibers will debond from the matrix at the site of those cracks. Once fibers debond, frictional sliding occurs between the fibers and matrix. This frictional sliding causes the composite's temperature to rise as demonstrated by Holmes and coworkers (42). Holmes showed that the faster a CMC was cycled, the more heat was generated by friction and this heat could be detrimental to fatigue life. The sliding between fiber and matrix wears and degrades the interface. Increased wear at the interface is evidenced by increased stress-strain hysteresis, decreased secant modulus and permanent strain accumulation. Some fatigue models state that these degraded interfaces lead directly to composite failure (43), while others claim that the interfacial sliding degrades the fibers, which leads to failure (44).

In the next several pages, fatigue behavior of N720/A will be analyzed using some of the concepts just mentioned. Trends in modulus, strain and stress-strain hysteresis will be examined to detect damage mechanisms. The retained strength of runout specimens will be another tool used to detect fatigue damage.

Figure 4-20 shows the modulus behavior for the four room temperature fatigue tests. For convenience the modulus used here is the secant modulus. Because the stress-strain behavior is close to linear, there is very little difference between the secant modulus and the tangent modulus calculated in the monotonic tests. As Figure 4-20 shows, there is a definite decreasing trend in the modulus behavior with cycling.

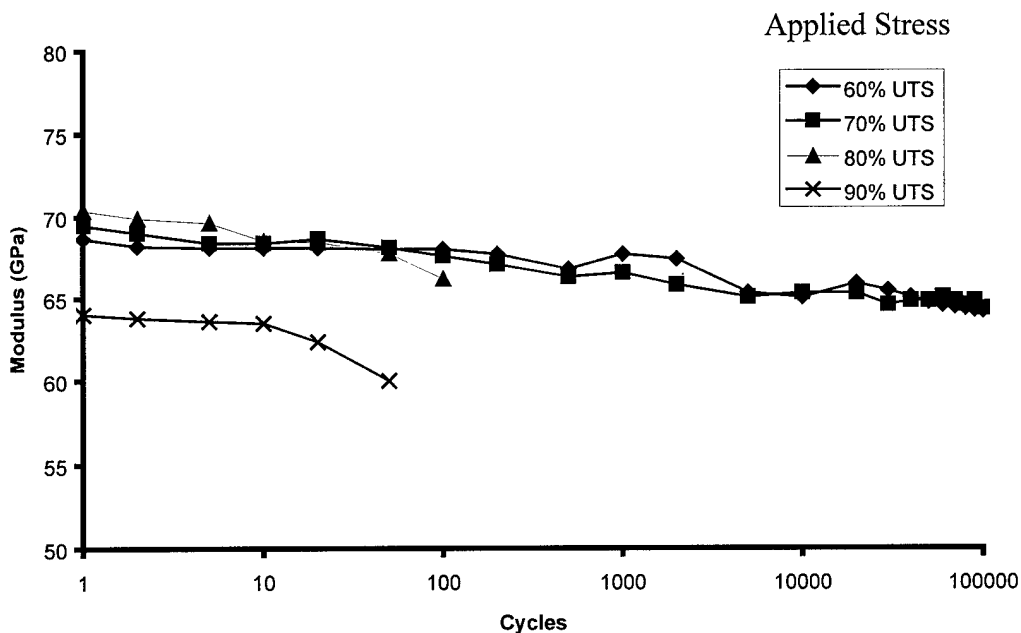


Figure 4-20 Modulus degradation during room temperature fatigue

Figure 4-21 shows the same data but with normalized moduli. Here moduli are normalized by dividing by the initial modulus measured in the first stress cycle. This figure shows the same trend as Figure 4-20. However it also shows that even after 100,000 cycles in the 60 and 70% tests the modulus maintains 92-93% of its initial value. So the degradation in composite stiffness is relatively small. This slight degradation is likely due to additional matrix cracking, beyond the initial cracked condition. Another possible explanation for the decreasing modulus is that the fraction of broken fibers may increase with the number of cycles, especially at the higher stress levels. The data also appears to show that the higher the stress level the more the modulus degrades.

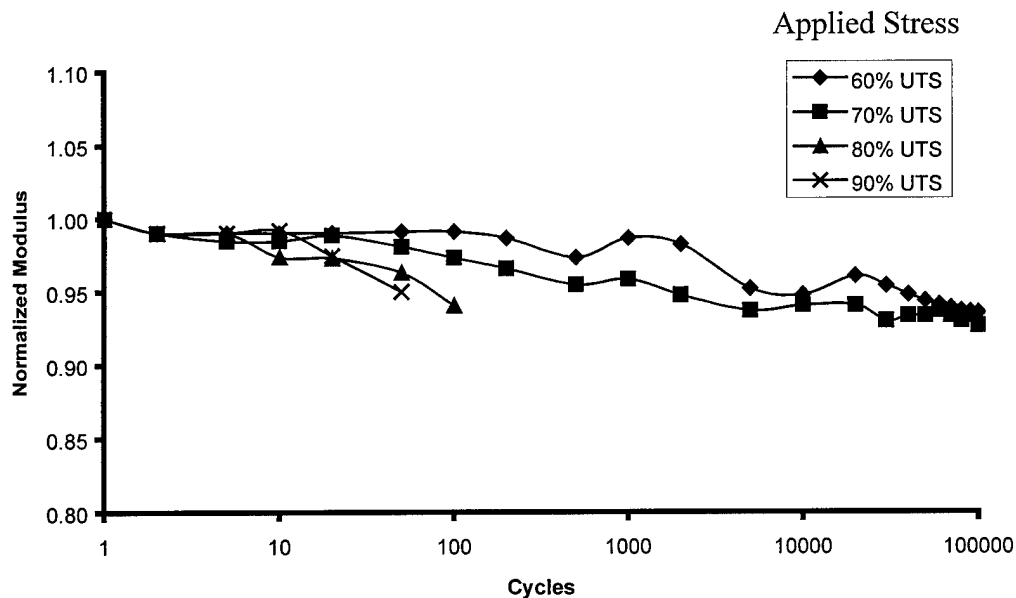


Figure 4-21 Trends in normalized modulus during room temperature fatigue

Strain progression is the second way to monitor damage during fatigue. Figure 4-22 shows the maximum and minimum strain during the 70% test and Figure 4-23 for the

60% test. The data shows that there is very little strain accumulation during the course of the fatigue tests. The maximum strain increases slightly due to the decreasing modulus. If both the maximum and minimum strain increase over the course of a test, this would indicate permanent strain accumulation by mechanisms such as interfacial wear (strain ratcheting). But this is not the case here. There is little or no debonding and sliding between the fibers and matrix. The apparent strain decrease over the last 30,000 cycles in Figure 4-22 is most likely due to a slipping extensometer.

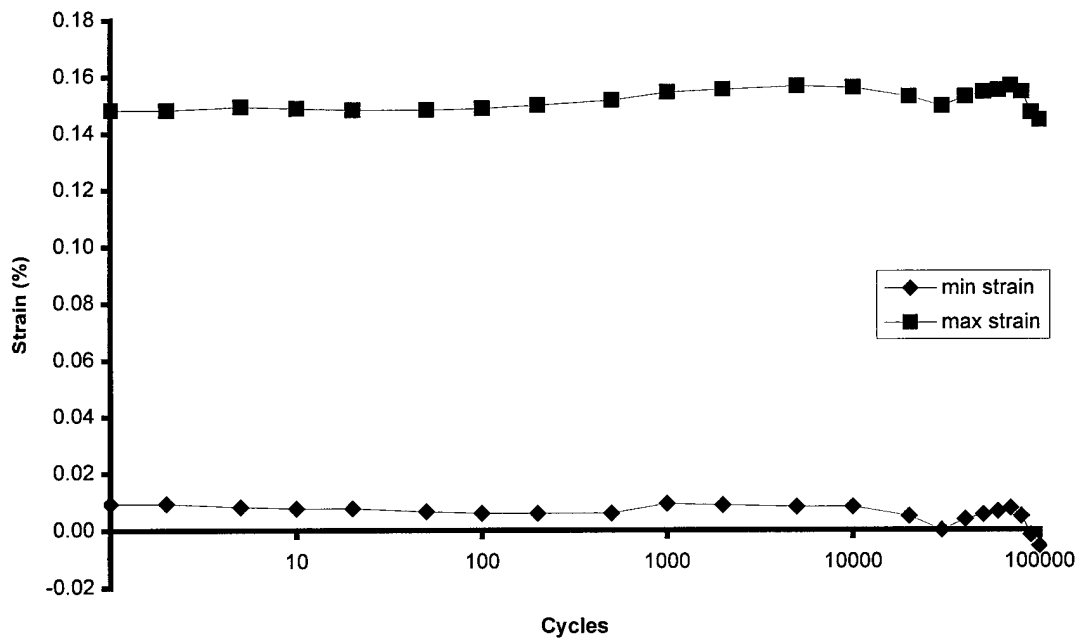


Figure 4-22 Strain progression in 70% stress level, room temperature fatigue test

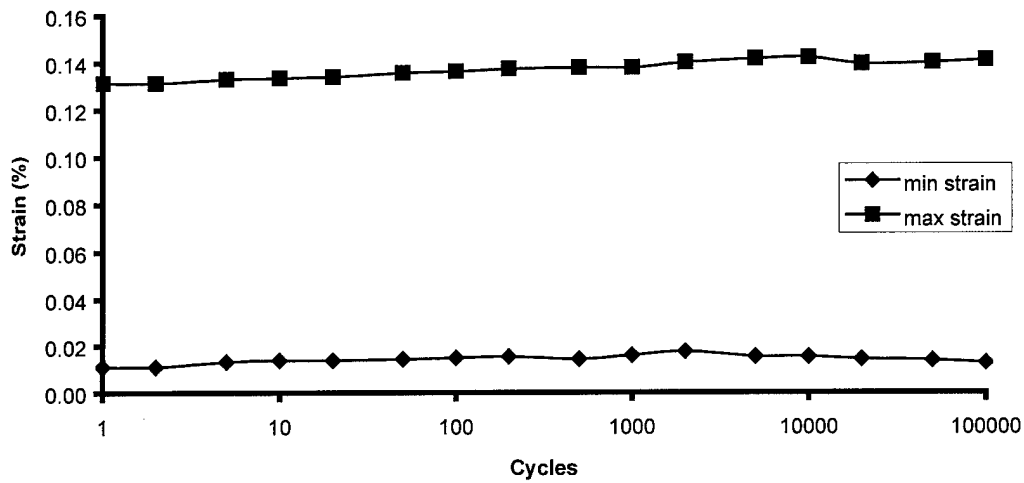


Figure 4-23 Strain progression in 60% stress level, room temperature fatigue test

Stress-strain loop plots are a third way to track damage occurring during fatigue. Figure 4-24 shows stress-strain loops for the first and last cycles of the 70% stress level test.

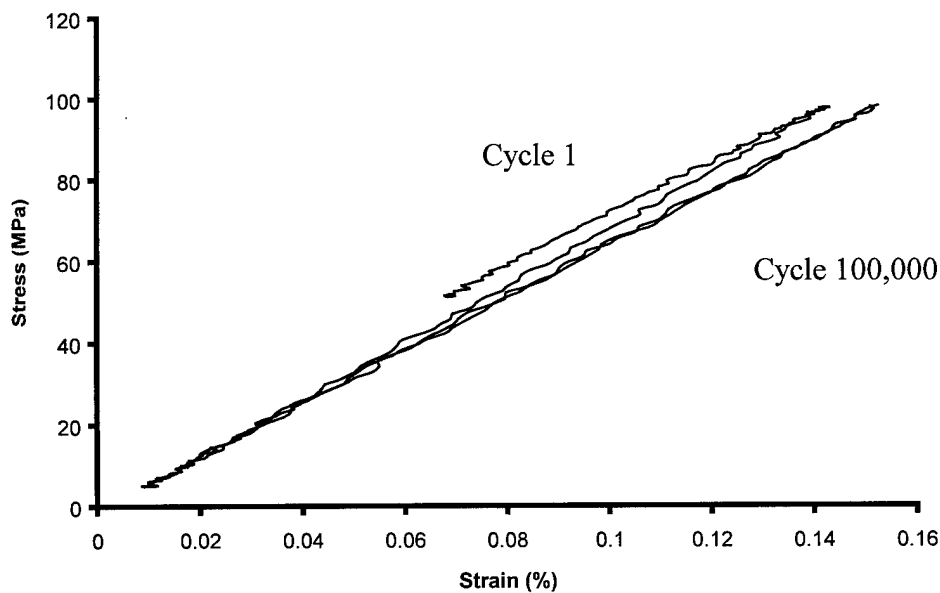


Figure 4-24 Changes in stress-strain loops during room temperature fatigue (70%)

As Figure 4-24 shows there is some hysteresis during the first fatigue cycle. This is most likely due to matrix cracking, which occurs during the first stress cycle. However, after the first cycle there is no discernable hysteresis in any further cycles. After the first cycle, the loops close and appear as shown in the cycle 100,000 plot in Figure 4-24.

There may be some additional matrix cracking occurring after the first stress cycle (as the modulus trends of Figure 4-21 indicate) but it cannot be discerned from the shape of the stress-strain loops. Loading and unloading portions during cycling are essentially elastic.

In many traditional CMCs there is a gradual widening of the stress-strain loops due to interfacial wear as the fibers debond and slide within the matrix. The width of the loops then stabilizes after 10,000 cycles or so. In this oxide/oxide with strong interfaces, the fibers do not debond from the matrix and there is no trend of increasing hysteresis.

Figure 4-24 also shows the change in slope of the stress-strain loops that occurs as the modulus decreases from cycle 1 to cycle 100,000. There is no permanent strain accumulation shown. If there were permanent strain, the cycle 100,000 plot would be displaced to the right along the x-axis.

An attempt was made to see evidence of fatigue damage. Fatigue specimens were sectioned through the gage length and polished as described in Section 3.1.3. Then they were examined under the digital optical microscope. Figures 4-25 and 4-26 show two images of fatigue specimens at magnifications of 50X and 100X. The views are toward the longitudinal or 0° direction unlike Figures 4-1 and 4-2, which are toward the transverse or 90° direction. When compared with the untested specimens of Figures 4-1

and 4-2, it appears that the matrix crack density may be higher in the fatigued specimens as expected. Figure 4-26 also appears to show a crack that has extended around the edge of a fiber tow. However, there are so many cracks in both the as-received specimens and the fatigued specimens that it is difficult to tell which cracks were there from the start and which ones are damage. Also the fatigued specimens have been sectioned and polished, which makes the cracks show up much more vividly. This material was too expensive to sacrifice an untested specimen for sectioning and polishing, which would have given a better comparison.

The fourth way to study fatigue damage is to test the strength of specimens that survived 100,000 fatigue cycles. If any damage occurred during fatigue, the retained strength of these specimens will be lower than the strength of specimens not subjected to fatigue. The results from the retained strength tests are plotted in Figure 4-27 and summarized in Table 4-7.

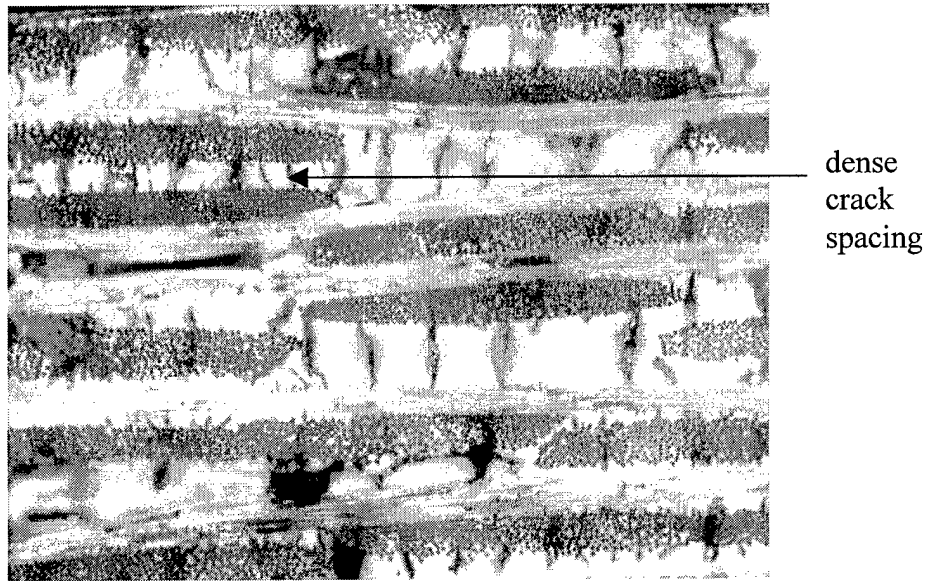


Figure 4-25 Possible fatigue damage, 50X

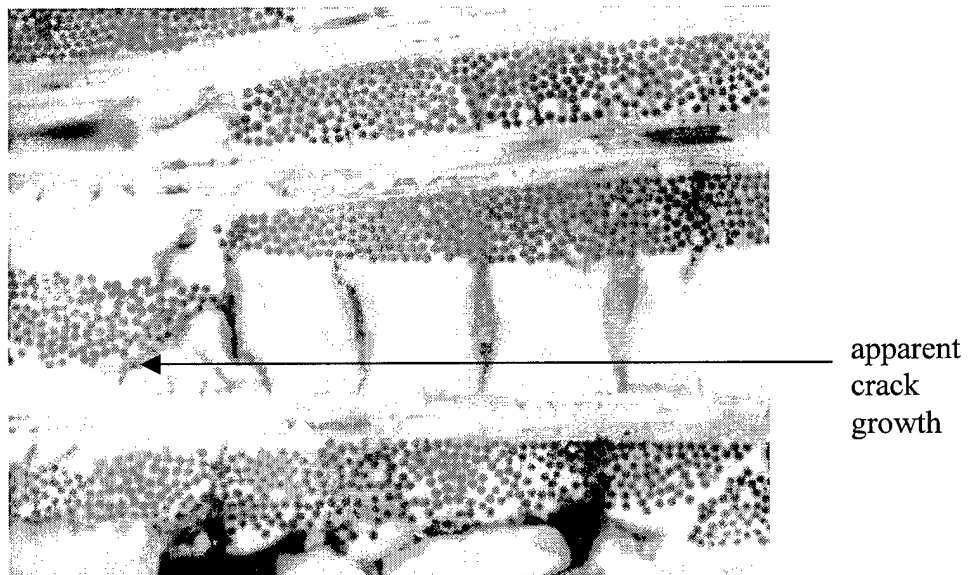


Figure 4-26 Possible fatigue damage, 100x

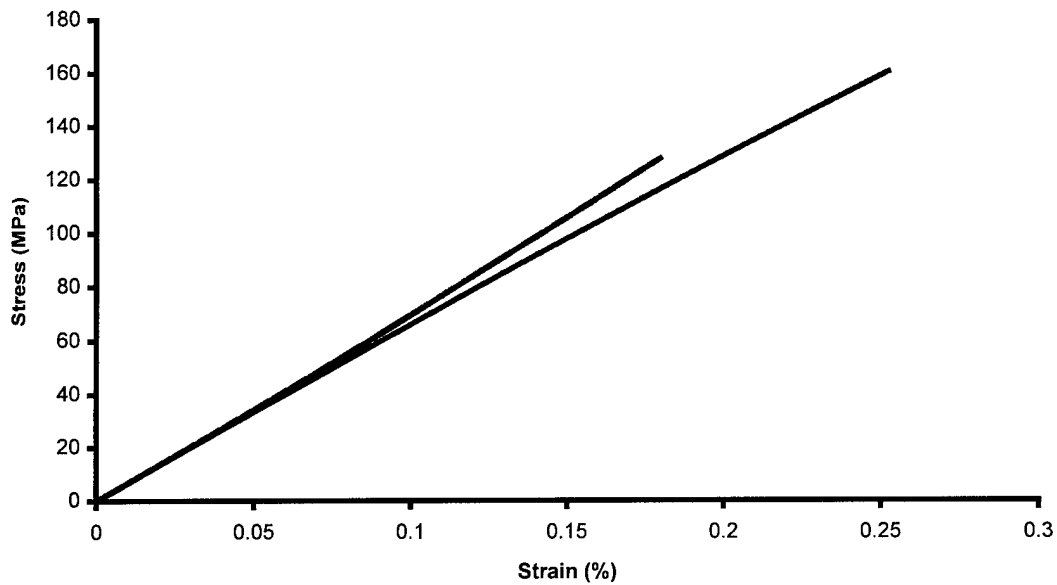


Figure 4-27 Stress-strain curves of room temperature fatigue runout specimens

Table 4-7 Retained properties of room temperature fatigue runout specimens

Specimen	Max fatigue stress (%UTS)	Retained strength (MPa)	Modulus (GPa)	ϵ_f (%)
9	70	157	64	.25
10	60	131	70	.18

Results from the two retained strength tests varied greatly. For the specimen cycled at 60% UTS retained strength was 131 MPa or about 8% below the average room temperature strength of 143 MPa obtained for this material. The specimen cycled at 70% UTS had a retained strength of 157 MPa or almost 10% above the average room temperature strength of this material. A possible explanation for this increase in strength after fatigue is variability in the processing technique, which gives a rather wide variation in mechanical properties. Another possibility is that cycling at high enough stresses

cracks the matrix and relieves some residual stresses. In any case, retained properties appear very good which again indicates that little damage occurs to this material when exposed to cyclic stresses up to 70% of its ultimate strength. Also note the linearity of the stress-strain curves. The matrix has been sufficiently cracked during fatigue cycling to remove most of the non-linear behavior.

The following pictures show the fracture surface of the specimen which was fatigued for 100,000 at 70% UTS then tested for retained strength. Figure 4-28 shows the fracture surface magnified to 20X. The surface appears much like the surface shown in Figure 4-8 for the room temperature tensile tests. Subjecting the specimen to 100,000 stress cycles did not change the fracture behavior. This is a good composite failure exhibiting a very fibrous and rough texture. This figure also shows the charging phenomenon mentioned in Section 3.1.3. The tops of long fibers are especially susceptible to charging by electrons from the SEM.

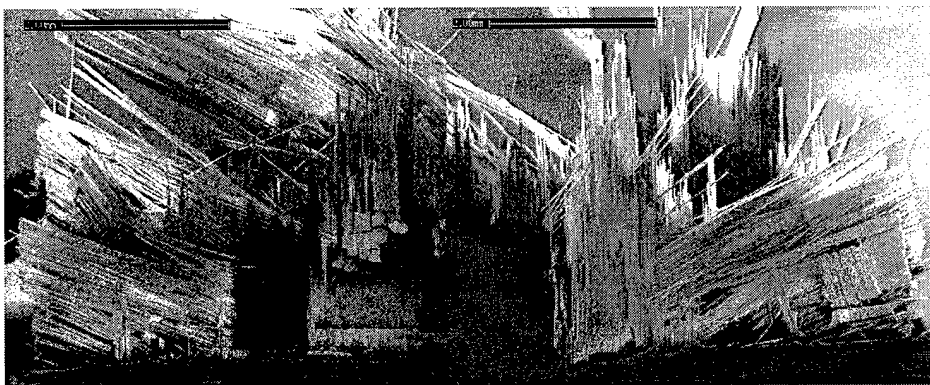


Figure 4-28 Fracture surface of room temperature fatigue specimen after retained strength test, 20X

Figure 4-29 shows the cracked condition of the matrix on the specimen surface. The matrix is so cracked in the as received condition that it is impossible to tell which of these cracks if any occurred during fatigue. But the data in this section shows the composite is damaged slightly during fatigue and a likely source of this damage is cracking of the matrix beyond the original cracked condition.



Figure 4-29 Surface of room temperature fatigue specimen after retained strength test, 140X

Here is the summary of the room temperature fatigue behavior of N720/A. If this material is subjected to fatigue loads of greater than 102 MPa, it fails rapidly. Failure is likely due to fiber fracture. A percentage of fibers fail with each stress cycle until a critical number is reached and the composite fails. If the composite is cycled at a stress lower than 102 MPa, it experiences some slight matrix cracking but little other damage.

The composite will not fail before 100,000 cycles. The fatigue behavior is probably better described by a 'go - no go' stress level than a traditional S-N curve.

4.3.2 1200°C Cyclic Tension

It is with 1200°C fatigue testing where this material shows its real potential. Table 4-8 summarizes the results of the three 1200°C fatigue tests.

Table 4-8 1200°C Fatigue results

Specimen	Maximum stress level (MPa)	Maximum stress level (% UTS)	Cycles to failure
11	122	90	100,000 (no failure)
12	108	80	100,000 (no failure)
13	95	70	100,000 (no failure)

Figures 4-30 and 4-31 show the results in graphical form. The two figures show the same data but Figure 4-30 plots the nominal maximum cyclic stress on the y-axis while Figure 4-31 has this stress as a percentage of the ultimate tensile strength at 1200°C. The average of the three 1200°C monotonic tensile tests was used for the ultimate tensile strength. The S-N curves are very close to horizontal. If a component made of this material would be subjected to cyclic loads of 140 MPa, it would fail on the first cycle. If the stress were reduced slightly to 122 MPa the component would last for 100,000 cycles. The fatigue limit is actually somewhere between 140 and 122 MPa, but the conservative value of 122 MPa is used.

In traditional CMCs, the fatigue limit at high temperatures is often at or below the proportional limit. One such example is a woven SiC/SiC composite with a carbon interface tested by Minuzo and others (45). This composite had a fatigue limit of only 75

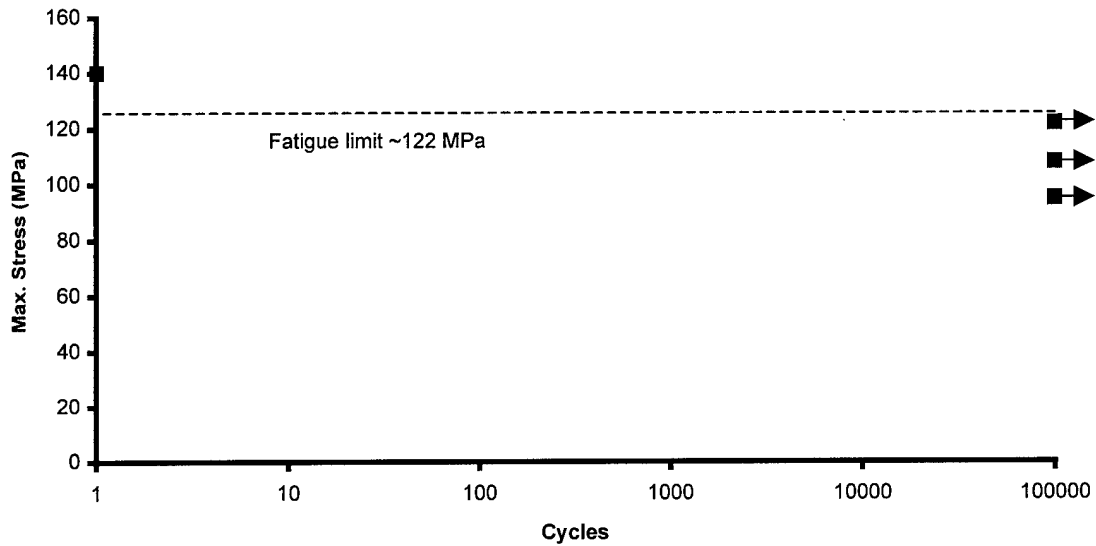


Figure 4-30 1200°C S-N curve for N720/A

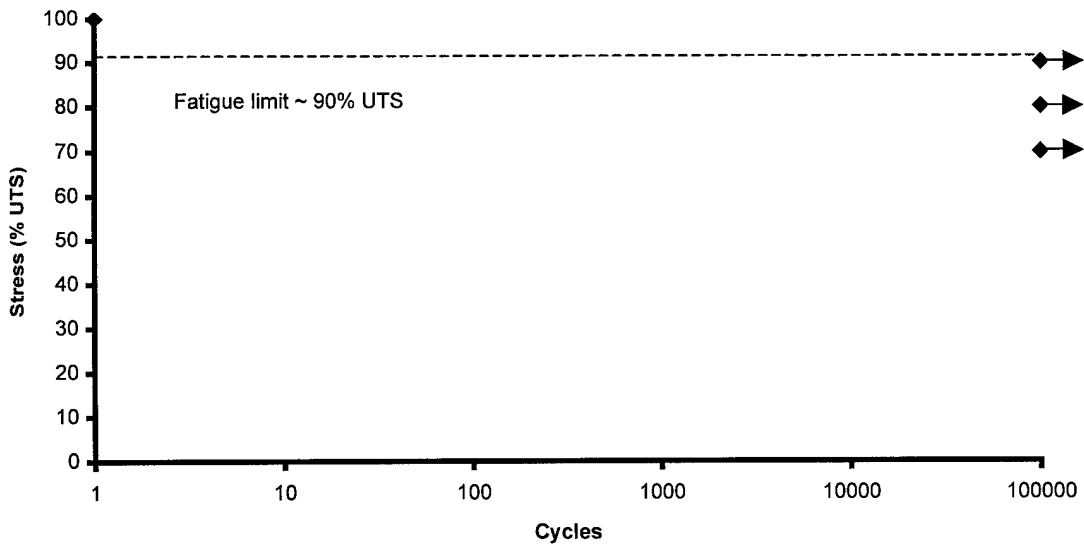


Figure 4-31 Normalized 1200°C S-N curve for N720/A

MPa at 1000°C (its proportional limit was 100 MPa). The reason for this is that once the matrix cracks, oxygen can penetrate to the fiber coating and react with it. The weak interface is transformed by oxidation to a strong interface and the composite becomes brittle. Some newer CMCs have improved upon this. A woven Nicalon/Si-N-C composite tested by Lee and others had a fatigue limit of 110 MPa at 1000°C, which was 35 MPa above the proportional limit (32:1807). This improvement was attributed to several factors including glass forming matrix fillers, which act to seal matrix cracks, and a BN fiber coating, which oxidizes slower than a carbon coating (32:1807). Despite these improvements to non-oxide CMCs, the N720/A is far superior with a fatigue limit of 122 MPa at 1200°C.

Fatigue behavior will now be analyzed using the same four tools as in the room temperature case. First is modulus degradation. The next two figures show how the secant modulus of the composite changes with the number of stress cycles. Figure 4-32 has the secant modulus plotted on the y-axis. Figure 4-33 shows the same data on a normalized scale.

The data is not as clear-cut as the room temperature modulus data, however the overall trend is the same. The data shows a gradual decrease in modulus through the duration of a fatigue test. The modulus decrease may be due to additional matrix cracking and/or an increasing fraction of broken fibers. In all three tests the modulus never drops below 0.88 of its original value, which means damage is slight even after 100,000 cycles. The

bumps in the data are likely caused by thermal currents from the furnace. The thermal currents cause small fluctuations in the extension measured by the extensometer. Most of the extension measured at 1200°C is actually due to the specimen being stressed, but a small part is the expansion and contraction of the specimen due to thermal currents.

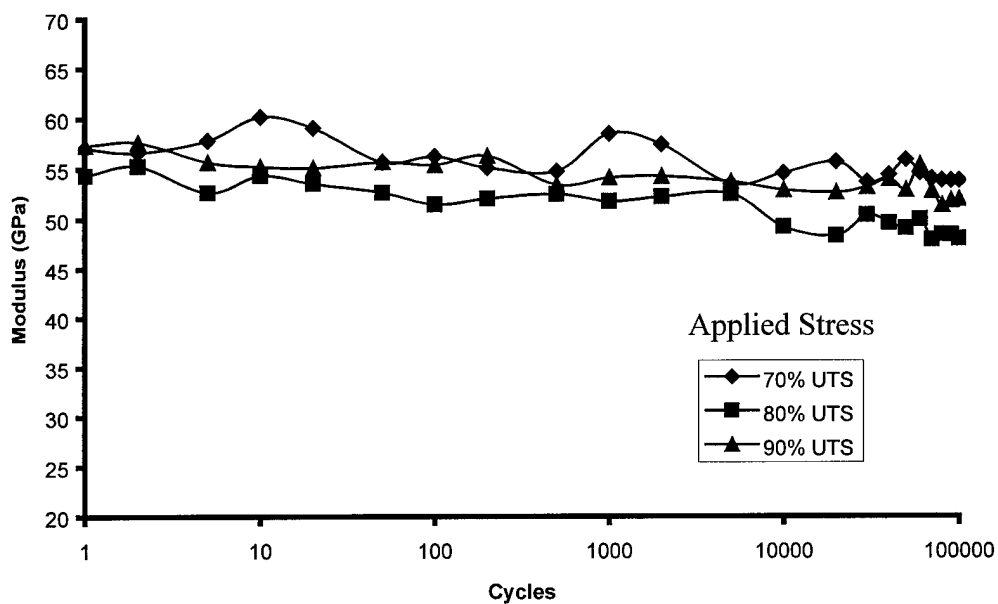


Figure 4-32 Modulus degradation in 1200°C fatigue testing

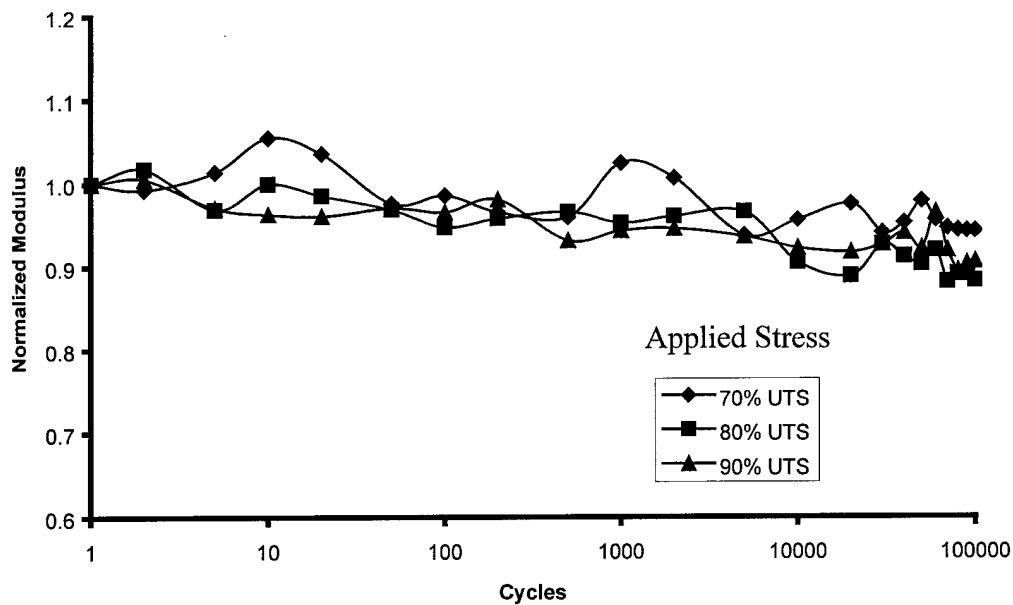


Figure 4-33 Normalized modulus trends in 1200°C fatigue testing

Strain data is the next indicator of damage during fatigue. The next three figures show maximum strain and minimum strain vs. number of stress cycles for each of the three high temperature fatigue tests (at 70, 80 and 90% stress levels). These graphs are very different from the room temperature graphs. At room temperature the minimum strain stayed about the same while the maximum strain drifted higher due to the decrease in composite modulus. There was no permanent strain that remained even after stress was removed. In all three high temperature tests both the maximum and minimum strains drift higher and reach much greater levels than at room temperature. There are two things going on here. Some of the increase in maximum strain is due to the decrease in composite modulus demonstrated in Figures 4-32 and 4-33. As the composite becomes less stiff the maximum strain increases. In addition, there is a permanent strain causing

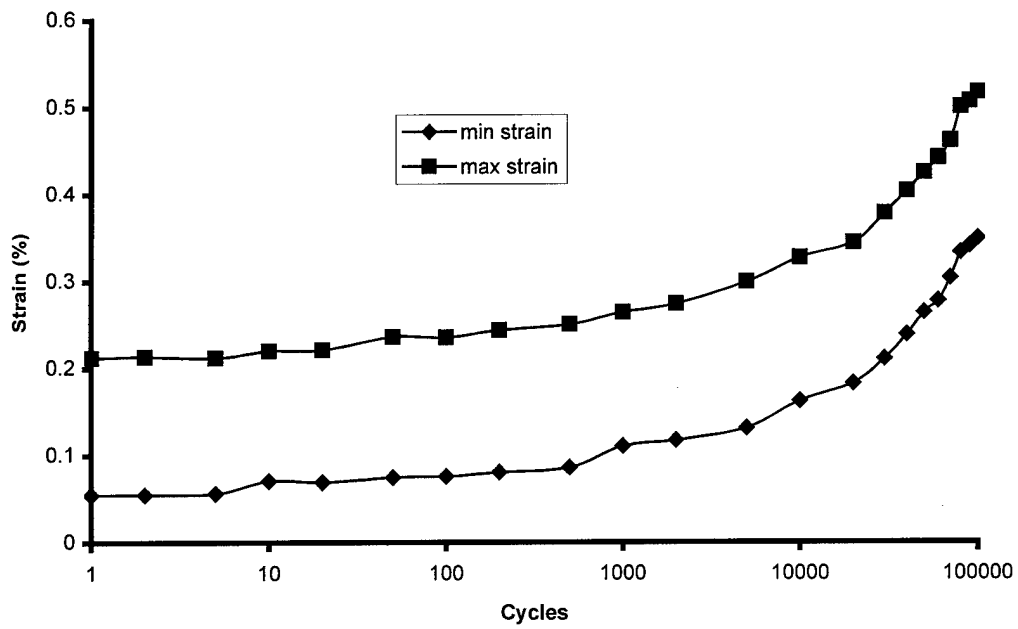


Figure 4-34 Strain accumulation during 70% stress level fatigue test at 1200°C

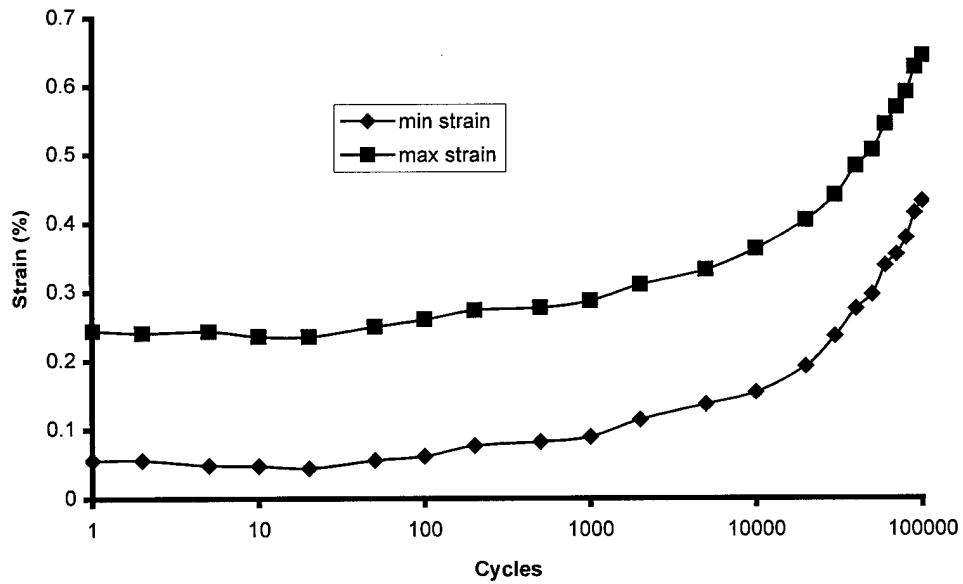


Figure 4-35 Strain accumulation during 80% stress level fatigue test at 1200°C

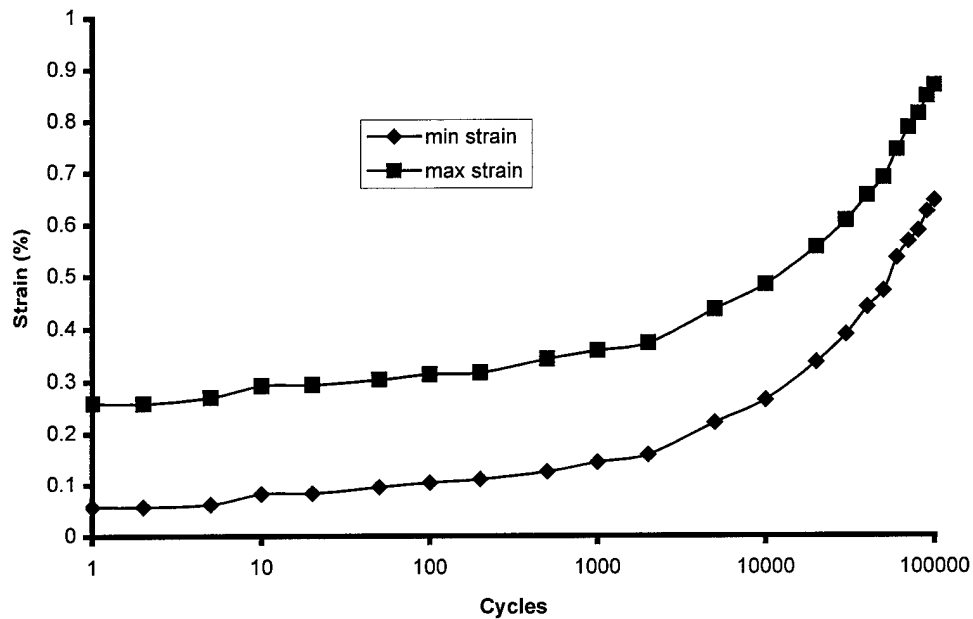


Figure 4-36 Strain accumulation during 90% stress level fatigue test at 1200°C

both the maximum and minimum strains to increase. This permanent strain is creep.

Creep is the slow deformation that occurs under sustained loads at high temperatures.

Figure 4-37 shows the maximum strains from all three tests plotted on the same graph.

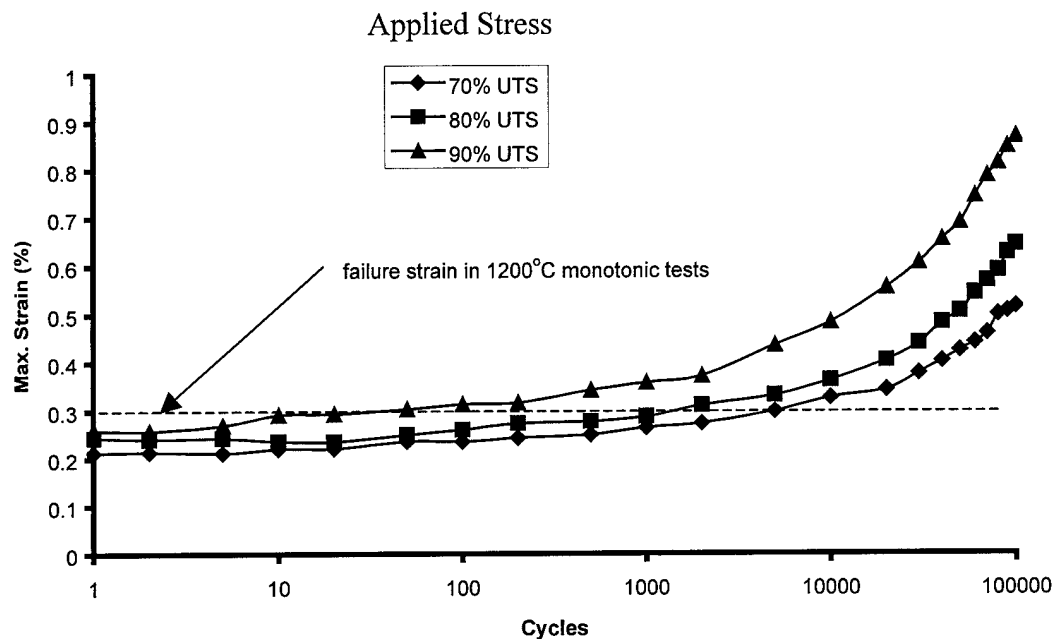


Figure 4-37 Maximum strain progression in 1200°C fatigue tests

The maximum strains represent the sum of permanent strain due to creep and mechanical strain due to the applied stress. As the figure shows, the higher the stress the more the composite creeps. This is expected, since creep is dependent on both stress and temperature. The figure also shows that the material reaches much greater strain levels than those reached during monotonic tests. In monotonic tests at high temperature the composite failed at strains of 0.3%. In fatigue testing the composite reached strains of up to 0.9% without failing. Based on these results the creep behavior of this material at 1200°C is excellent. "It is generally accepted that over the service life of a component, only small stress induced dimensional changes can be tolerated, typically less than 1%" (14:159). This material endured 100,000 stress cycles (122MPa) at 1200°C and

accumulated a creep strain of about 0.6% and a maximum strain (creep plus mechanical) of 0.9%. These are well within the acceptable range.

Figure 4-38 shows the same data as 4-37 but plotted on a linear scale instead of logarithmic. The data is plotted on a linear scale to show how the composite creeps very rapidly in the beginning of the tests. The creep rate then slows and reaches a constant value. In general, the creep behavior of this composite mirrors the creep behavior of Nextel 720 fibers as described by Wilson. He found that the fibers experienced transient creep behavior in the early stages of testing followed by a period of slow steady state creep. The steady state creep continued until failure. There was no period of increased creep rate (tertiary creep) just before the fiber failed (41:1010).

Creep of this composite appears to be controlled by the creep of the fibers. Figure 4-39 compares the steady state creep rate of Nextel 720 fibers at 1200°C with that of the N720/A composite. The creep rate of single Nextel filaments was measured by Wilson and coworkers. In that case creep occurred under a constant applied stress. The creep of the composite in this effort occurred under a cyclic stress so an exact comparison is not possible. In Figure 4-39 the stress plotted for the composite is the mean cyclic fatigue stress. The steady state creep rate of the composite was found by measuring the slope of the linear portion of the plots in Figure 4-38. When this creep rate is plotted against

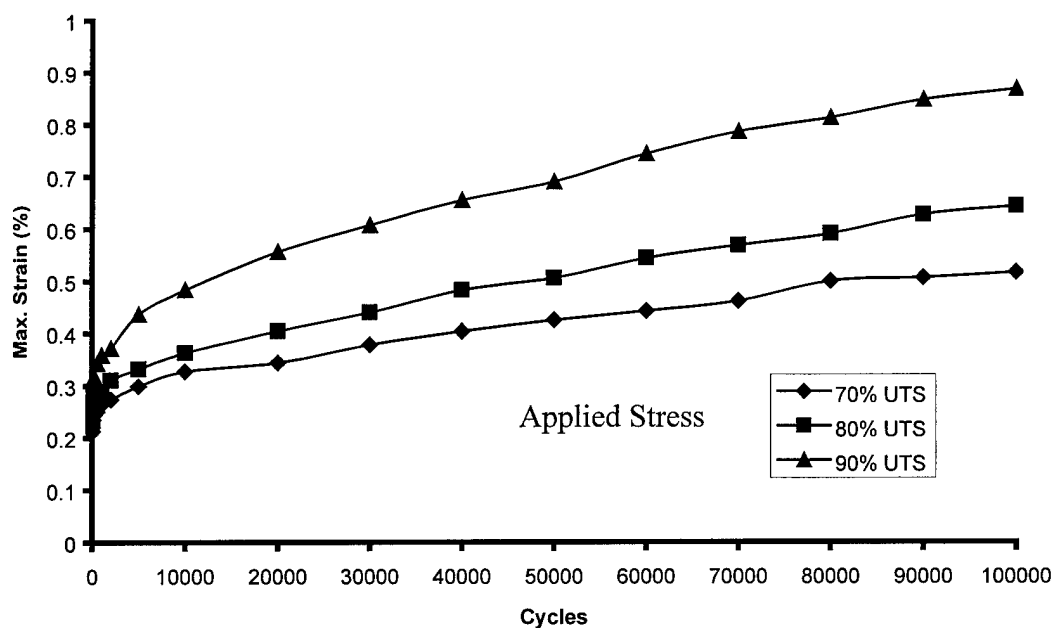


Figure 4-38 Maximum strain in 1200°C fatigue tests plotted on linear scale

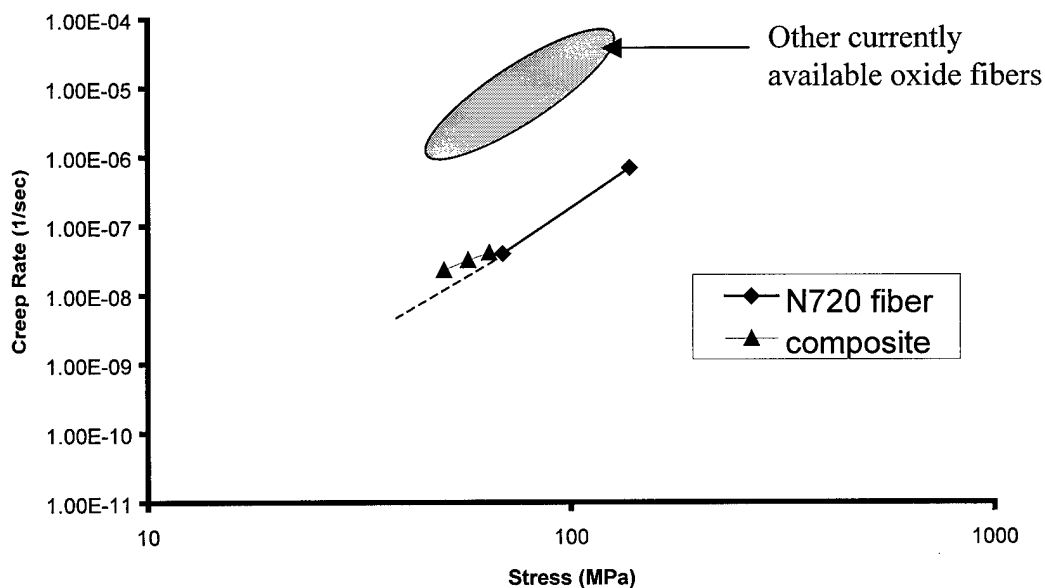


Figure 4-39 Steady state creep rates for N720 fiber (41) and N720/A composite at 1200°C

mean cyclic stress, the results fall closely in line with the fiber creep data. The composite creep rate is slightly above that expected for the fibers alone. This probably is a result of trying to compare a constant load in one case to the mean of a cyclic load in the other case.

Creep in ceramics is due to several mechanisms. There is dislocation creep, where deformation occurs by the generation and movement of dislocations. In ceramics, however, dislocations do not move easily because of the strong interatomic bonds so this type of creep would only occur at very high stresses. Diffusional creep occurs at lower stresses and is due to the flow of vacancy defects. At high temperatures, vacancies will flow through the crystal lattice structure. This is called Nabarro-Herring creep. At lower temperatures, vacancies can flow along grain boundaries. This is called Coble creep. Another creep mechanism in ceramics is grain boundary sliding.

In fine-grained polycrystalline ceramics like the Nextel 720 fiber, grain boundary phenomena like Coble creep and grain boundary sliding control the creep behavior (41:1012). Wilson found that a major factor for the excellent creep behavior of Nextel 720 was the shape of the grains. The grains were elongated and globular shaped, which inhibited grain boundary sliding (41:1012). Creep behavior was also improved by the addition of the secondary mullite phase, which is inherently more creep resistant than alumina.

For further insight into fatigue behavior, stress-strain loops are examined next. Stress-strain loops are plotted for the 90% stress level test in Figure 4-40.

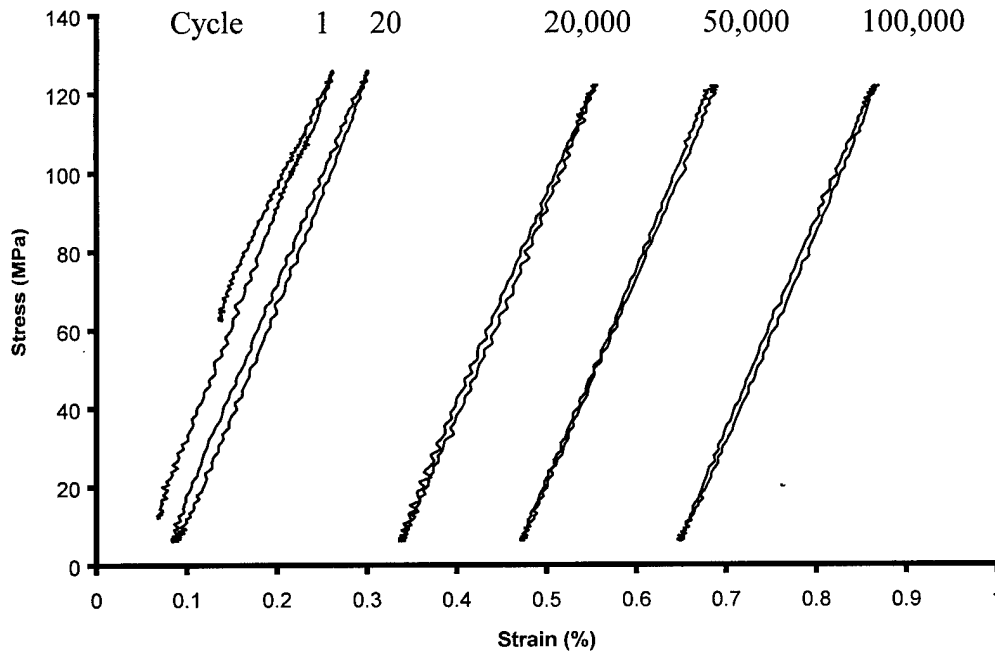


Figure 4-40 Hysteresis loops at 1200°C, 90% stress level

Similar to room temperature behavior, there is obvious hysteresis in the first stress-strain loop, again due to matrix cracking. Also like the room temperature fatigue case, the width of the stress-strain loops narrows after the first cycle. However, at 1200°C, hysteresis loops remain visible, if very slender, whereas at room temperature the loops collapsed completely. The narrow hysteresis loops could be due to a slight creeping of the fibers during each cycle. There is very little change in loop width after the first cycle. There is no apparent trend that would indicate frictional wear at the fiber-matrix interface. Even at 1200°C there is no debonding and sliding of the fibers. The loops shift

towards the right with increasing cycles due to creep strain. The slope of the loops decreases slightly due to the decrease in modulus.

As in the room temperature case, an attempt was made to see evidence of fatigue damage. Specimens were sectioned, polished and viewed under the digital optical microscope. The following two figures are images of the polished surfaces at magnifications of 50X and 100X. The view is in the longitudinal direction. Figure 4-41 shows a crack extending through a fiber tow and Figure 4-42 shows what appear to be multiple cracks emanating from a large matrix pore. This could be the matrix cracking that is indicated by the modulus data in Figures 4-32 and 33. However because of the initial cracked condition of the matrix it cannot be concluded that these cracks are definitely fatigue damage.



Figure 4-41 Possible fatigue damage, 50X

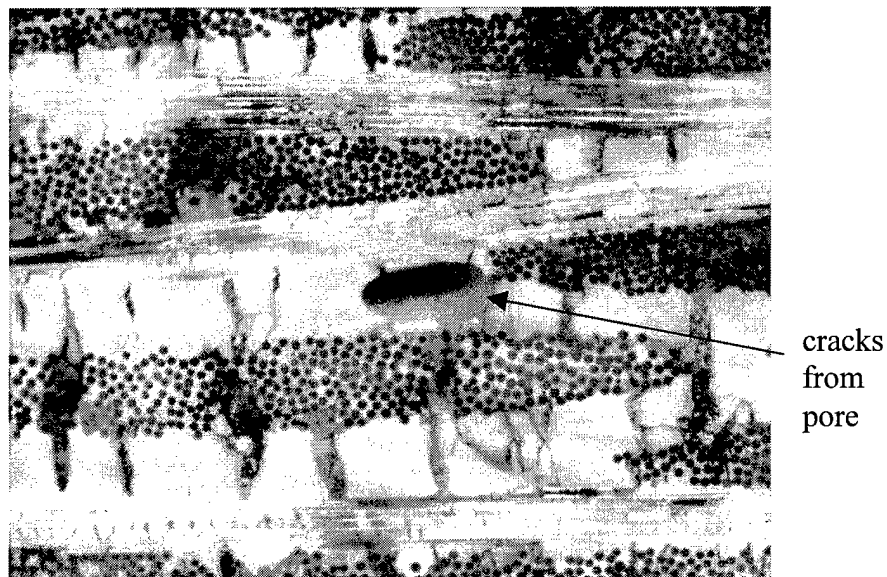


Figure 4-42 Possible fatigue damage, 100X

As a final check for damage, the three run-out specimens were tested for retained strength. The results are summarized in Table 4-9 and plotted in Figure 4-43.

Table 4-9 Retained properties of 1200°C fatigue runout specimens

Specimen	Fatigue stress level (%UTS)	Retained strength (MPa)	Modulus (GPa)	ϵ_f (%)
11	90	152	64	.27
12	80	143	66	.22
13	70	143	63	.24

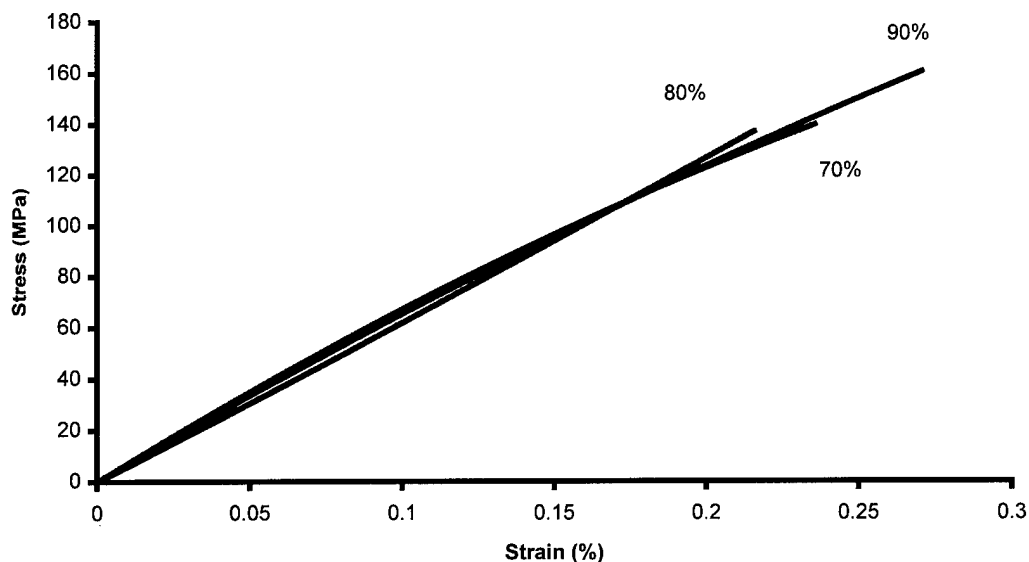
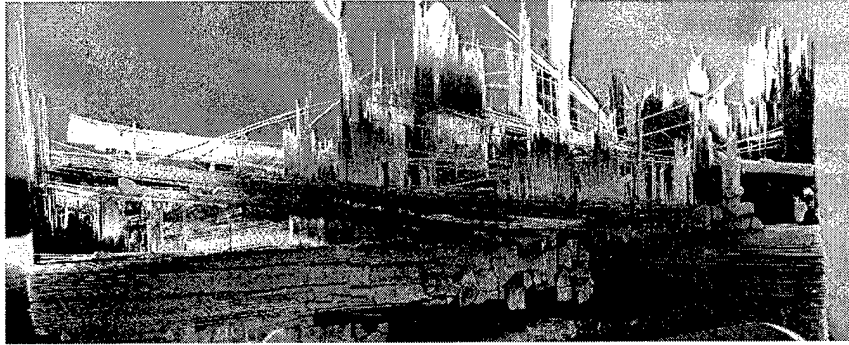


Figure 4-43 Stress-strain curves for 1200°C fatigue run-out specimens

As the table and figure show, retained properties are very good even after 100,000 cycles at 1200°C. All mechanical properties, including strength, modulus and strain to failure, are about the same as specimens that were not subjected to fatigue. The one exception is the retained strength of the 90% specimen, which is 152 MPa. This value represents a 6% increase over the average room temperature strength of this material (144 MPa). This scatter may be due to naturally occurring variations in composite quality. More likely, fatigue cycling at high stress cracks the matrix and relieves some of the composite's residual stress. Again, the shapes of the curves are almost linear. The major source of non-linearity, cracking of the matrix, was removed during fatigue cycling.

The following SEM images show the fracture surface of the 90% stress level fatigue specimen after the retained strength test.



**Figure 4-44 Fracture surface of 1200°C fatigue specimen
after retained strength test, 20X**

As Figure 4-44 shows, the fracture surface is still very fibrous and rough even after 100,000 cycles (27.8 hours) at 1200°C. Figure 4-45 shows there was no excessive sintering of the matrix to the fibers that would have caused the failure to be brittle.

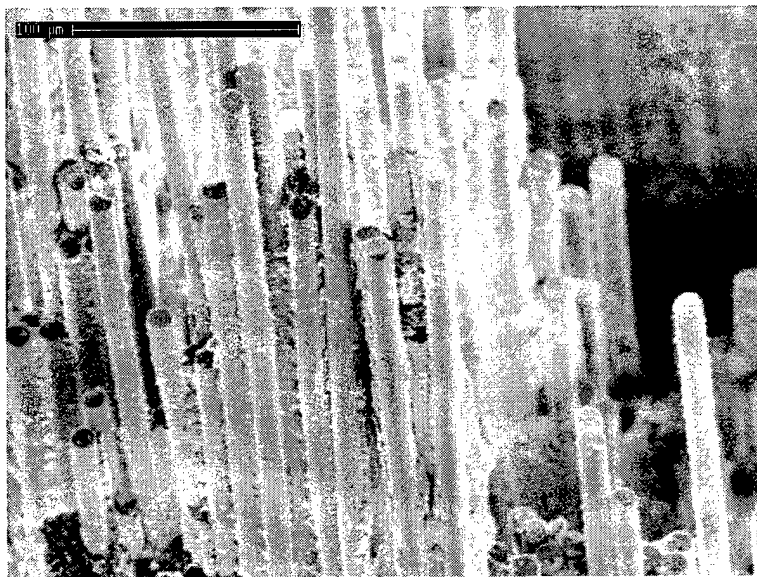


**Figure 4-45 Fracture surface of 1200°C fatigue specimen after
retained strength test, 360X**

Here is the summary of the fatigue behavior of N720/A at 1200°C. Fatigue at 1200°C is very similar to fatigue at room temperature. It could be described by a 'go – no go' stress instead of an S-N curve. Not only is there no degradation in fatigue life at high temperature, performance actually improves. The fatigue limit at room temperature is 102 MPa, at 1200°C its 122 MPa. The improvement may again be due to lower residual stresses at 1200°C. At room temperature, with fibers under residual stress, it takes less applied stress for fibers to reach their failure strain. At high temperature with no residual stress, a much higher stress must be applied to strain the fibers to failure. When the composite is cycled at 122 MPa or less, very little damage accumulates just as at room temperature. Creep does occur but it stays steady state and does not cause rupture before 100,000 cycles.

4.4 Moisture Interrupted Fatigue

Fatigue tests at 1200°C with intermittent moisture exposure were performed as described in Section 3.2.3. The purpose of these tests was to see if moisture would degrade the high temperature fatigue performance of the material. This is important for applications, like the afterburner flaps and seals, where components are exposed to rain and humidity. The moisture interrupted fatigue tests were run at two stress levels, 122 MPa and 108 MPa, to coincide with the previous fatigue tests without moisture. Table 4-10 summarizes the results.

Table 4-10 Cycles to failure for 1200°C fatigue tests

Test	122 MPa (90%)	108 MPa (80%)	95 MPa (70%)
Moisture Interrupted	100,000 Runout	100,000 Runout	N/A
No Moisture	100,000 Runout	100,000 Runout	100,000 Runout

The results show that moisture exposure had no effect on fatigue life. At both stress levels, the moisture-exposed specimens lasted 100,000 cycles. The S-N curve is identical to the no moisture tests and could be represented as a straight horizontal line as shown in Figure 4-30. Again the fatigue strength is conservatively estimated to be 122 MPa.

This moisture resistance is expected and is a significant advantage of the oxide/oxide class of CMCs. Non-oxide CMCs often do not perform well in moisture environments. In one instance, the fatigue life of a NicalonTM/Si-N-C composite was reduced 85% after exposure to a salt fog environment (32:1809).

In both moisture tests, the composite showed the familiar creep behavior exhibited in the no moisture tests. However, as the following figures show, more creep strain occurred in the moisture-exposed specimens. A possible explanation for this phenomenon follows the figures.

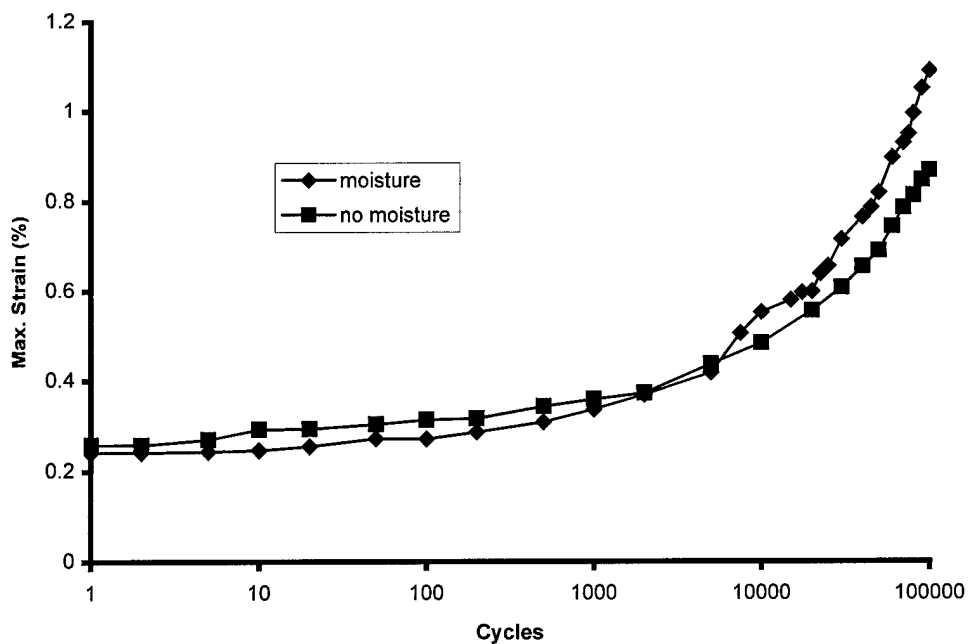


Figure 4-46 Maximum strain comparison, 1200°C fatigue, 90% stress level

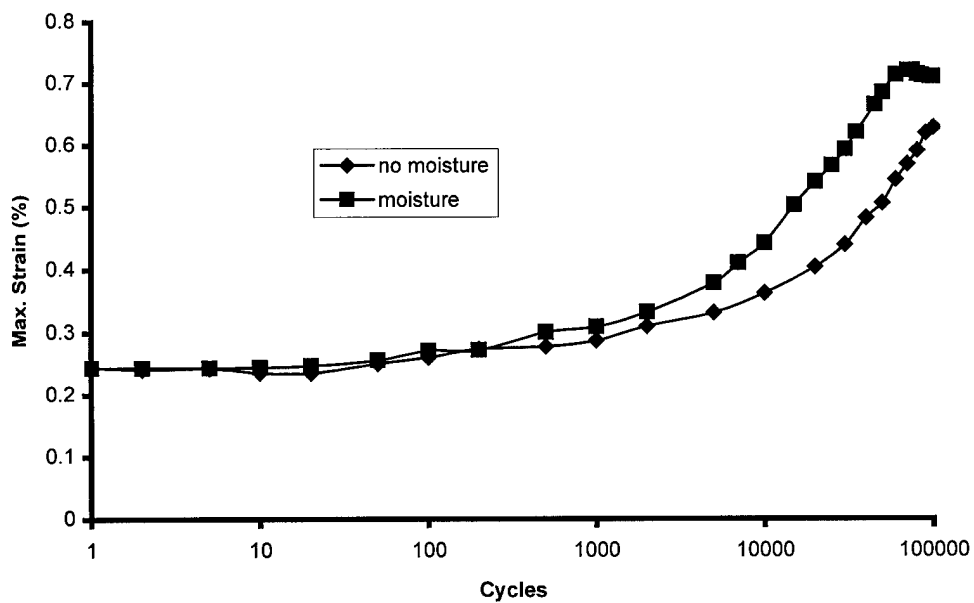


Figure 4-47 Maximum strain comparison, 1200°C fatigue, 80% stress level

(Some extensometer slippage apparently occurred at the end of the 80% stress level moisture test.)

The maximum strain plotted in these graphs is the sum of the creep strain and the mechanical strain from the maximum applied stress. The higher creep strains are not necessarily due to the moisture exposure. The moisture fatigue tests were interrupted at intervals of 5000 or 25000 cycles. These interruptions may have prevented the specimen from reaching a steady state creep rate. This would keep the specimen in the more rapid primary creep realm. So it is more likely that the increased creep strains were due to the test interruptions than the moisture exposure.

Retained strength of both moisture specimens was tested, and results are summarized in the table and figure below. This data shows that moisture exposure did not degrade composite properties in the least. In fact, the retained strength of specimen 15 (174 MPa) exceeds the strength of any other specimen tested in this study. There may be a strain hardening effect occurring during high temperature fatigue. However, the most likely explanation is that cycling at high temperature and high stress relieves some of the residual stresses within the composite. With reduced residual stress, the composite can handle a higher applied load before failing. With the limited number of tests, it is difficult to say for sure. However, the retained strength of the high temperature fatigue specimens has been consistently equal to or greater than the room temperature strength of this material.

Table 4-11 Retained properties of runout specimens, 1200°C fatigue, moisture exposure

Specimen	Fatigue Stress Level (MPa, %UTS)	UTS (MPa)	Modulus (GPa)	ϵ_f (%)
14	108, 80	148	62	.25
15	122, 90	174	62	.28

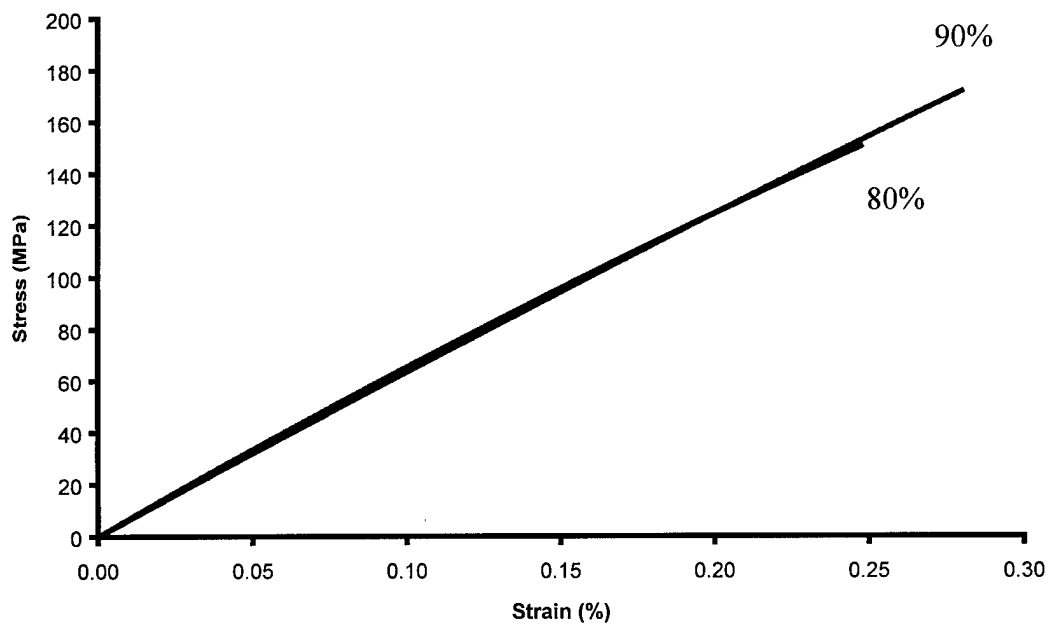


Figure 4-48 Stress-strain curves for retained strength tests

The following graph compares the average retained strengths of specimens from different tests.

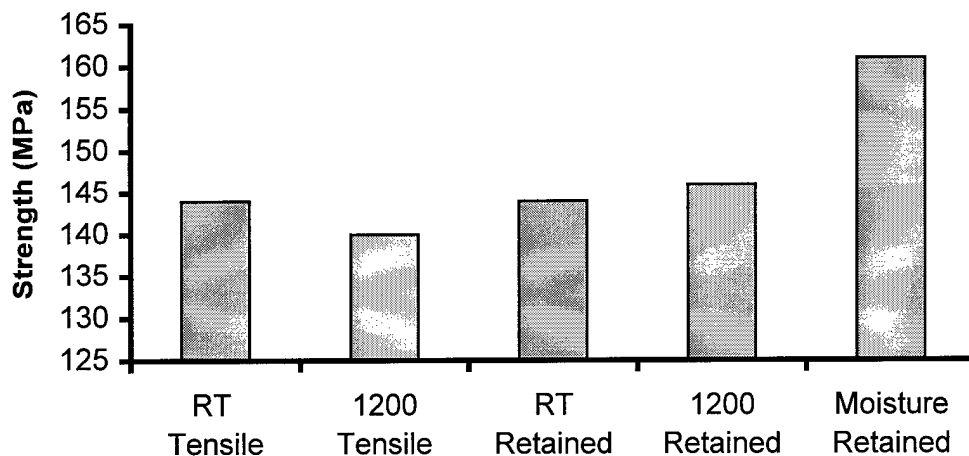


Figure 4-49 Retained strength compared to original strength

This graph shows the excellent retained strength of the high temperature fatigue specimens in the last two columns. The variations in strength could still be attributed to variations in material quality. But, as stated earlier, it appears that cycling at 1200°C actually strengthens the composite by relieving residual stresses.

The following figure shows an SEM image of the fracture surface of the moisture-exposed specimen after the retained strength test. The surface shows the familiar fibrous texture common to all fracture surfaces in this study. In all, this specimen was subjected

to 100,000 stress cycles at 1200°C and exposed to extreme humidity for about 112 hours.

Through this the matrix remained stable as shown by the rough fracture surface.

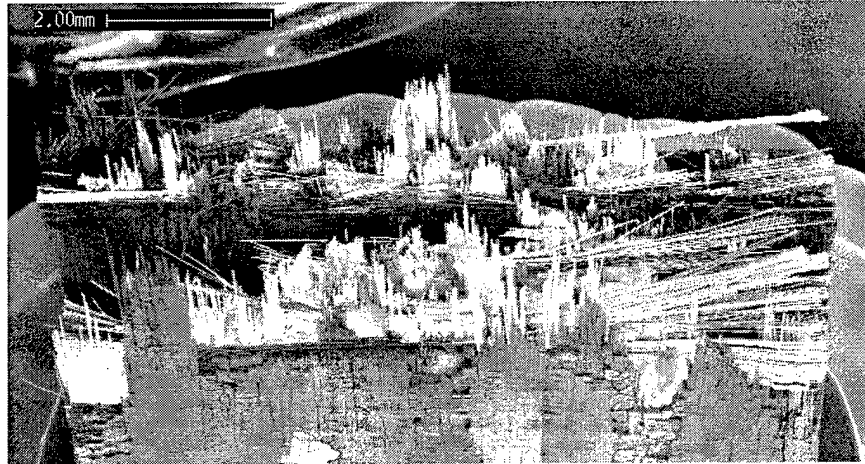


Figure 4-50 Fracture surface of 1200°C fatigue with moisture exposure after retained strength test, 10X

Overall, this material shows excellent resistance to moisture as well as high temperatures and is a good candidate for applications in wet environments also.

5 Conclusions

The most important conclusion drawn from this study is that the N720/A oxide/oxide composite manufactured by Composite Optics Inc. is suitable for applications requiring long-term exposure to temperatures of 1200°C. It appears that this material has advanced the state-of-the-art for oxide-oxide composites. No other oxide/oxide has performed so well at such high temperature. Perhaps, for that matter, no other ceramic matrix composite, oxide or non-oxide, has such high fatigue strength (122 MPa) at 1200°C. This material is also suitable for 1200°C applications with moisture exposure and cyclic stresses of up to 122 MPa. Such applications may include combustion chamber liners in aerospace and land-based turbine engines, stationary vanes in turbine engines and afterburner nozzle flaps and seals.

The N720/A oxide/oxide composite has room temperature tensile strength of 144 MPa and fatigue strength at 10^5 cycles of 102 MPa. There are many other CMCs that can exceed this performance. Even previous oxide/oxide composites like GEN IV, which had a tensile strength of 205 MPa and fatigue strength of 170 MPa, outperform N720/A at room temperature.

Room temperature stress-strain curve starts out linear then becomes slightly non-linear. The slight non-linearity is due to matrix cracking and possibly fiber fracture. There is no obvious 'knee' in the curve as is the case for traditional CMCs.

Data monitored during room temperature fatigue cycling, including modulus, strain and stress-strain loops, indicates that when N720/A is cycled at stresses below 102 MPa only slight damage occurs. The damage is not due to interfacial wear but due to matrix cracking. Retained strength tests show that the damage does not have much affect on strength. Rapid failure occurs when the material is cycled at stresses above 102 MPa. At these higher stresses fiber fractures accompany matrix cracking and a rapid failure is the result.

What makes this material special is its performance at 1200°C, where it has a tensile strength of 140 MPa and fatigue strength for 10^5 cycles of 122 MPa. It owes its high temperature performance to a porous alumina matrix that remains stable at 1200°C. Microscopic examination of specimens tested at temperature show no evidence of matrix sintering. The porous matrix remains an effective crack deflection medium even after long-term high temperature exposure. There were no signs of this composite becoming embrittled at any time during this effort. In using a pure alumina matrix instead of an aluminosilicate, the temperature capability of the tested oxide/oxide extended from 1100 to 1200°C.

High temperature stress-strain response is basically the same as room temperature response, almost linear. Failure strains at temperature increase (0.24 to 0.30%) while modulus decreases (69 to 55 GPa).

High temperature fatigue mechanisms are basically the same as room temperature; slight damage from matrix cracking and fiber fracture. However, at high temperature, creep strain is superimposed on the other damage mechanisms. The maximum creep strain measured during any fatigue test was about 0.8%, well within expected limit of 1.0%.

The higher fatigue strength at 1200°C compared to room temperature (122 vs. 102 MPa) may be due to relief of residual stresses. When cycled at room temperature, the composite is subjected to mechanical stresses superimposed on residual stresses. When cycled at 1200°C, which is very near its processing temperature, the composite is subjected to mechanical stresses only. Calculations indicate residual tensile stresses of roughly 35 MPa on the fibers.

Fatigue runout specimens often had higher tensile strength than un-fatigued specimens. This effect may also be explained by residual stresses. The specimens that had the highest retained strength were those that cycled at the highest stresses. Cycling at high stress cracks the matrix enough to relieve some residual stress. With residual stress reduced, the specimen can then endure a higher applied load before failing. Temperature may also have an effect. The strongest specimen of all was one that cycled 100,000 times at 1200°C (with moisture). Cycling at high temperatures and stress may relieve even more of the residual stress.

The properties of the composite are largely dictated by the properties of the Nextel 720 fibers. The coefficient of thermal expansion, strength, failure strain and creep rate of the

fibers and the composite match very closely. Rule of mixture calculations for the composite modulus indicate the 0° fibers provide most of the stiffness with a contribution from the matrix.

6 Recommendations

Obviously much more testing is needed than the limited amount performed in this effort. Additional testing is particularly important given the possible variability in this material's properties. More monotonic and fatigue tests would give a better picture of the scatter in properties.

Variability is especially evident in retained strength tests. In three cases, retained strength of fatigued specimens was well above that of the as received specimens. Additional tests should help reveal if variability in composite properties from specimen to specimen is a factor, or whether the entire effect is due to relief of residual stress.

Previous oxide/oxides have had very low interlaminar strength. Interlaminar strength of this composite should be measured to see if any improvement has been made. If there is no improvement, then perhaps a three dimensional fiber architecture should be considered in future versions of this material.

Previous oxide/oxide have also had poor resistance to wear. Wear resistance is critical in the afterburner flap and seal application. This composite will probably suffer from the same poor wear resistance. Perhaps some wear resistant particles could be incorporated into the matrix. However, the particles must not react with the matrix or sinter at high temperatures.

In this effort, creep performance was estimated indirectly from creep effects that occurred during fatigue tests. Actual creep rupture tests should be performed for a better comparison with existing data on other materials.

It would be interesting to see how this material performs at temperatures other than 1200°C. Fatigue testing in the 1000 to 1300°C temperature range may give valuable information. 1200°C may be the optimum temperature to use this material. What if it is exposed to temperatures other than 1200°C? It may have lower fatigue strengths at these other temperatures. Maybe this material could be used at temperatures up to 1250 or 1300°C. These questions should be examined.

Measurements should be made to determine residual stresses in the composite. In this effort it is hypothesized that the residual stresses are responsible for the lower fatigue strength at room temperature. When the composite is fatigued at 1200°C, very close to its processing temperature, the residual stresses are relieved and the fatigue strength increases. It is also hypothesized that the residual stresses explain 1) the lower strain to failure of room temperature tensile specimens compared to that in the specimens tested at temperature and 2) (by the relief of residual stress) the increase in the strength of fatigued specimens.

The quality of this material was inconsistent. Delamination of plies occurred at the ends of several specimens. The area of the delaminations corresponds to the edge of the plate from which the specimens were machined. The manufacturer should pay particular

attention to this area in the future and ensure that the matrix material is distributed evenly all the way to the edge of the plate. If delaminations continue to be a problem, the ends of the plates could be cut off and not used.

A truly successful high temperature tensile test was not achieved during this study. In the first attempts grip failures occurred. Grip failures were eventually eliminated but then failures occurred in the transition zone between furnace and ambient air. To achieve a successful high temperature test with this material, a new furnace set-up may be required. The entire specimen must be heated in order to eliminate the thermal gradient on the specimen and the accompanying thermal stresses. Quartz lamps may be more effective at heating the entire specimen.

Appendix A. Grip Failures

Grip failures were a problem at various times throughout testing. Grip failures mainly occurred in the monotonic testing, but also one time during fatigue testing. At first, the common causes of grip failures were suspected- grip misalignment and grip pressure too high. To correct any misalignment the grips were removed, new mounting hardware was installed and the grips were reinstalled. The alignment fixture was again used to align grips and bending strains were reduced to 2-3%. Grip pressure was reduced to a minimum, just above the amount required to prevent slipping. These actions did not resolve the grip failures. Finally, after a grip failure during a moisture exposure test and consultations with Larry Zawada, a potential problem with the specimen geometry was found. Figure A-1 shows the ideal shape of a specimen through the thickness compared to the actual shape of the specimen that failed in the grips.

The ends of the specimen were flared out so that they were thicker than the rest of the specimen. The figure exaggerates the effect. Even with the fiberglass tabs glued on, the ends of the specimen flared out slightly wider than the rest of the specimen. This was part of the inconsistent quality of the composite material. The ends of the specimens not only flared out but in some cases delaminations occurred between plies.

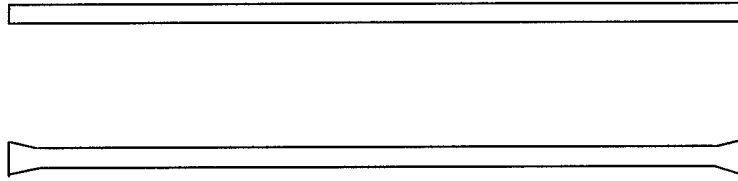


Figure A-1 Ideal specimen shape (top) vs. actual shape (bottom)

It was suspected that only the thickest part of the specimen was being gripped causing a region of high stress. After this finding, the thickness of all specimens was checked before testing. Some specimens flared out as much as 0.016 inches in the grip region. The flared out areas of the specimens were ground down with a diamond wheel until specimen thickness was uniform. No further grip failures occurred.

Another action was taken that may have helped reduce grip failures. At first only one drop of superglue was being used to hold tabs in place. While this amount is adequate for a smooth surfaced material it may not be adequate for a porous material like this oxide/oxide composite. The amount of glue was increased to five drops per tab.

Once grip failures were eliminated another problem surfaced in the high temperature monotonic tests. One high temperature tensile specimen failed in the transition region between the hot furnace air and the cooler ambient air. Thermal stresses in the transition region were most likely a factor.

The following equation gives a rough approximation of the thermal stresses induced on a material by a temperature gradient:

$$\sigma_{TH} = (\alpha) \Delta T (E) / 2 \quad (3)$$

where σ_{TH} is thermal stress, α is the coefficient of thermal expansion, ΔT is the temperature gradient, and E is the modulus. Alumina is particularly vulnerable to thermal stresses because of its high modulus, low tensile strength, and relatively high thermal expansion. The problem of failure due to the thermal gradient was not resolved during this study. A different furnace system may be required to reduce the thermal gradient as discussed in the Recommendations section.

As a result of the problems with grip failures and thermal stresses, the true high temperature strength of this material is not known. 140 MPa represents a minimum value but the composite may be as strong as 180 MPa at high temperatures (see Appendix B).

Appendix B. Residual Stress

The final processing step for this composite is to sinter the matrix at about 1150°C. At that temperature, the composite is stress free. When the composite cools, residual strains and stresses develop due to the thermal expansion mismatch between fibers and matrix. Residual strains and stresses in the composite were estimated using the following equations:

$$\epsilon_R = \Delta T(\text{CTE}_{\text{fiber}} - \text{CTE}_{\text{matrix}})/2 \quad (4)$$

$$\sigma_R = (E)\epsilon_R \quad (5)$$

where ϵ_R is residual strain, ΔT is the difference between processing temperature (1150°C) and test temperature, $\text{CTE}_{\text{fiber}}$ is the coefficient of thermal expansion for the fiber, $\text{CTE}_{\text{matrix}}$ is the coefficient of thermal expansion for the matrix, σ_R is residual stress and E is composite modulus. $\text{CTE}_{\text{fiber}}$ is given in Reference 41 as 6.01 $\mu\text{strain}/^\circ\text{C}$. $\text{CTE}_{\text{matrix}}$ is not known. The CTE for a porous alumina was found in a database (48). This value of 5.1 $\mu\text{strain}/^\circ\text{C}$ was used as an approximation for the $\text{CTE}_{\text{matrix}}$. Using these values and a test temperature of 23 °C the residual strain on the fibers is .00051 and the residual tensile stress is 35 MPa.

This existence of residual stress and strain would help to explain several things. First, the average failure strain of this composite at room temperature is 0.24%, while the reported failure strain of the N720 fiber is 0.30%. The difference is due to the residual strain of 0.0005 or 0.05% on the fibers.

Second, the calculated theoretical strength of this material was 180 MPa, while actual strength at room temperature was 144 MPa. The difference is 36 MPa, which is close to the value for residual stress calculated above. The composite could not reach its full theoretical strength at room temperature because the fibers are already stressed at 35 MPa before any load is applied. This would indicate that the strength of the material at 1200°C, where residual stresses are relieved, should approach the theoretical strength of 180 MPa. The strength of the material inside the furnace may have in fact been 180 MPa but failures occurred outside the furnace or in the transition region at lower stresses.

Residual stress would also help to explain two other phenomena. First, the fatigue strength at 1200°C, where residual stresses are near zero, was at least 20 MPa greater than at room temperature (122 vs. 102 MPa). Second, the retained strength of some of the specimens was very high. One specimen approached the theoretical strength with an UTS of 174 MPa. This could happen if fatigue cycling removed some of the residual stresses through matrix cracking.

Bibliography

1. Combs, Harry. Kill Devil Hill, Discovering the Secrets of the Wright Brothers. Boston: Houghton Mifflin Company, 1979.
2. McLean, M. "Nickel-based Superalloys: Current Status and Potential," in High Temperature Structural Materials. Ed. R.W. Cahn and others. London: Chapman and Hall, 1996.
3. Lippert, T.W. "Titanium in the U.S.A.," in The Science, Technology and Application of Titanium. Ed. R.I. Jaffee and N.E. Promisel. Oxford: Pergamon Press, 1966.
4. Marks, N. "Polymer Based Composite Materials," in High Performance Materials in Aerospace. Ed. Harvey M. Flower. London: Chapman and Hall, 1995.
5. Birtles, Philip. Boeing 777: Jetliner for a New Century. U.S.A: MBI Publishing Company, 1998.
6. Mall, S., Fecke, T. and Foringer, M.A. "Chapter 1: Introduction," in Titanium Matrix Composites. Ed. Shankar Mall and Theodore Nicholas. Lancaster, PA, U.S.A.: Techomic Publishing Co. Inc., 1998.
7. Schwartz, Mel M. Composite Materials: Vol. 1, Properties, Non-Destructive Testing and Repair. Upper Saddle River, NJ: Prentice Hall, 1997.
8. Lewis, David III. "Continuous Fiber-Reinforced Ceramic Matrix Composites: An Historical Overview," in Handbook on Continuous Fiber-Reinforced Ceramic Matrix Composites. Ed. Richard L. Lehman and others. West Lafayette, IN, U.S.A.: Purdue Research Foundation, 1995.
9. Wu Xin, Holmes John W. and Hilmas Greg E. "Environmental Properties of Ceramic Matrix Composites," in Handbook on Continuous Fiber-Reinforced Ceramic Matrix Composites. Ed. Richard L. Lehman and others. West Lafayette, IN, U.S.A.: Purdue Research Foundation, 1995.
10. Tressler, Richard E. "Recent Developments in Fibers and Interphases for High Temperature Ceramic Matrix Composites," Composites Part A, 30:429-437(1999).
11. Van de Voorde, M.H. "Developments of Continuous Fibre Reinforced Ceramic Matrix Composites(CFCC) in Europe," Silicates Industriels, 63 [5-6]:59-67(1998).

12. Boakye, E., Petry, M.D. and Hay, R.S. "Porous Aluminum oxide and Lanthanum Phosphate Fiber Coatings," Ceramic Engineering and Science Proceedings, 17 [4-5]: 53-57(1996).
13. Goettler, R., Sambasivan, S. and Dravid, V.P. "Isotropic Complex Oxides as Fiber Coatings for Oxide-Oxide CFCC," Ceramic Engineering and Science Proceedings, 18 [3]: 279-283(1997).
14. DiCarlo, James A. and Dutta, Sunil. "Continuous Ceramic Fibers for Ceramic Matrix Composites," in Handbook on Continuous Fiber-Reinforced Ceramic Matrix Composites. Ed. Richard L. Lehman and others. West Lafayette, IN, U.S.A.: Purdue Research Foundation, 1995.
15. Naik, Niranjan K. Woven Fabric Composites. Lancaster, PA: Techomic Publishing, 1994.
16. Lowden, Richard A., Stinton, David P. and Besmann, Theodore M. "Ceramic Matrix Composite Fabrication and Processing: Chemical Vapor Infiltration," in Handbook on Continuous Fiber-Reinforced Ceramic Matrix Composites. Ed. Richard L. Lehman and others. West Lafayette, IN, U.S.A.: Purdue Research Foundation, 1995.
17. Chawla, K.K. Ceramic Matrix Composites. London: Chapman and Hall, 1993.
18. Schwartz, Mel M. Composite Materials: Vol. 2, Processing, Fabrication and Applications. Upper Saddle River, NJ: Prentice Hall, 1997.
19. French, James E. "Ceramic Matrix Composite Fabrication and Processing: Polymer Pyrolysis," in Handbook on Continuous Fiber-Reinforced Ceramic Matrix Composites. Ed. Richard L. Lehman and others. West Lafayette, IN, U.S.A.: Purdue Research Foundation, 1995.
20. Cullum, Gail H. "Ceramic Matrix Composite Fabrication and Processing: Sol-Gel Infiltration," in Handbook on Continuous Fiber-Reinforced Ceramic Matrix Composites. Ed. Richard L. Lehman and others. West Lafayette, IN, U.S.A.: Purdue Research Foundation, 1995.
21. Van Vlack, Lawrence H. Physical Ceramics for Engineers. Reading, MA: Addison Wesley Publishing Company, 1964.
22. Belithus, David. "CMC Components for Advanced Propulsion Systems," in Flight Vehicle Materials, Structures and Dynamics- Assessment and Future Directions, Volume 1, New and Projected Aeronautical and Space Systems. Ed Noor, A.K. and Venneri, S.L. New York: The American Society of Mechanical Engineers, 1994.

23. Lee, S.S., Zawada, L.P., Hay, R.S. and Staehler, J. "High Temperature Mechanical Behavior and Characterization of an Oxide/Oxide Composite," Journal of the American Ceramic Society, Submitted for Publication (1998).
24. Hertzberg, Richard W. Deformation and Fracture Mechanics of Engineering Materials, 3rd Edition. New York: John Wiley and Sons, 1989.
25. Huenecke, Klaus. Jet Engines: Fundamentals of Theory, Design and Operation. Osceola, WI, USA: Motorbooks International Publishers and Wholesalers, 1997.
26. Freeman, William Jr. and Norris, L. Frederick. "Single Crystal Superalloys for Gas Turbine Engine Applications," in Flight Vehicle Materials, Structures and Dynamics- Assessment and Future Directions, Volume 1, New and Projected Aeronautical and Space Systems. Ed Noor, A.K. and Venneri, S.L. New York: The American Society of Mechanical Engineers, 1994.
27. "IHPTET: Air Dominance Through Propulsion Superiority," Excerpt from brochure, n. pag. <http://www.pr.af.mil/divisions/prt/ihptet/brochure>. 10 May 1999.
28. U.S. Air Force Photo from <http://www.af.mil/photos/Jul1999/990402-6afterburner.html>
29. Staehler, J.M. and Zawada, L.P. "The Performance of Four Ceramic Matrix Composite Divergent Flaps Following Ground Testing on an F110 Turbofan Engine," Journal of the American Ceramic Society, Submitted for Publication (1998).
30. Zawada, L.P. "Longitudinal and Transthickness Tensile Behavior of Several Oxide/Oxide Composites," Ceramic Engineering and Science Proceedings, Submitted for Publication (1998).
31. Zawada, L.P. and Lee, S.S. "The Effect of Hold Times on the Fatigue Behavior of an Oxide/Oxide Ceramic Matrix Composite," in Thermal and Mechanical Test Methods and Behavior of Continuous-Fiber Ceramic Matrix Composites, ASTM 1309. Ed. Jenkins, M.G. and others, American Society for Testing and Materials, Philadelphia, PA, 1996.
32. Lee, S.S., Zawada, L.P., Staehler, J.M and Folsom, C.A. "Mechanical Behavior and High-Temperature Performance of a Woven NicalonTM/Si-N-C Ceramic Matrix Composite," Journal of the American Ceramic Society, 81 [7]: 1797-1811(1998).
33. Levi, Carlos G. and others. "Processing and Performance of an All-Oxide Ceramic Matrix Composite," Journal of the American Ceramic Society, 81 [8]: 2077-86 (1998).

34. Cazzato, A. and others. "Monazite Interface Coatings in Polymer and Sol-Gel Derived Ceramic Matrix Composites," Ceramic Engineering and Science Proceedings, 18 [3]: 269-277 (1997).
35. Tu, Wen-Chiang and others. "Concept for a Damage Tolerant Ceramic Composite with Strong Interfaces," Journal of the American Ceramic Society, 79 [2]: 417-24 (1996).
36. Lu, T.J. "Crack Branching in All-Oxide Ceramic Composites," Journal of the American Ceramic Society, 79 [1]: 266-74 (1996).
37. Jurf, R.A. and Butner, S.C. "Advances in Oxide-Oxide CMCs," Unpublished Article, Composite Optics Inc., San Diego CA, 1998.
38. Smith, William F. Principles of Materials Science and Engineering, 3rd Edition. New York: McGraw-Hill Inc., 1996.
39. Peterson, R.E. Stress Concentration Factors. New York: John Wiley and Sons, 1974.
40. Evans, A.G. and others. "Structural Performance of Ceramic Matrix Composites," in Fracture: A Topical Encyclopedia of Current Knowledge. Ed. Cherepanov, G.P. Malabar, FL: Krieger Publishing Company, 1998.
41. Wilson, D.M. and others. "Microstructure and High-Temperature Properties of Nextel 720 Fibers," Ceramic Engineering and Science Proceedings, 16 [5]: 1005-1013 (1995).
42. Holmes, John.W and others. "Frequency Dependence of Fatigue Life and Internal Heating of a Fiber-Reinforced Ceramic Matrix Composite," Journal of the American Ceramic Society, 77 [12]: 3284-86 (1994).
43. Evans, A.G. and others. "Fatigue of Ceramic Matrix Composites," Acta Metallurgica, 43 [3]: 859-875 (1995).
44. Reynaud, P. "Cyclic Fatigue of Ceramic-Matrix Composites at Ambient and Elevated Temperatures," Composites Science and Technology, 56: 809-814 (1996).
45. Minuzo, M. and others. "Cyclic Fatigue of SiC/SiC Composites at Room and High Temperature," Journal of the American Ceramic Society, 79, [12]: 3065-77 (1996).

46. Dimiduk, Dennis. Class lecture, MAT 685, Materials Selection and Processing. School of Engineering, Air Force Institute of Technology, Wright-Patterson AFB OH, January 2000.
47. Al-Hussein, Musa. Monotonic and Fatigue Behavior of 2-D Woven Ceramic Matrix Composite at Room and Elevated Temperatures (Blackglas/Nextel 312). MS thesis, AFIT/GAE/ENY/98S-01. School of Engineering, Air Force Institute of Technology (AU), Wright-Patterson AFB OH, August 1998.
48. Material Properties of Porous Alumina from <http://www.matweb.com>.

Vita

Captain Steven G. Steel was born on 12 July 1963 in Detroit, Michigan. He graduated from Valparaiso High School in Valparaiso, Indiana in June 1981. He enlisted in the Air Force in October 1983 and served for seven years as a refrigeration and air conditioning technician, reaching the rank of Staff Sergeant. He was then accepted into the Airman's Education and Commissioning Program. Through this program he received his Bachelor of Science in Mechanical Engineering degree from Ohio State University. In January 1994, he was commissioned through Officer Training School at Maxwell AFB where he was recognized as a Distinguished Graduate.

His first assignment as an officer was in the Air Force Research Laboratory at Wright-Patterson AFB where he was a materials test engineer. In September of 1995 he was assigned to Warner Robins Air Logistics Center at Robins AFB in support of aircraft armament systems. In September 1998, he entered the Material Science and Engineering program, School of Engineering, Air Force Institute of Technology. Upon graduation he will be assigned to the Materials Directorate of AFRL.

Permanent Address:	2630 Oak Park Ave Kettering, OH 45419
--------------------	--

REPORT DOCUMENTATION PAGE			Form Approved OMB No. 0704-0188	
Public reporting burden for this collection of information is estimated to average 1 hour per response, including the time for reviewing instructions, searching existing data sources, gathering and maintaining the data needed, and completing and reviewing the collection of information. Send comments regarding this burden estimate or any other aspect of this collection of information, including suggestions for reducing this burden, to Washington Headquarters Services, Directorate for Information Operations and Reports, 1215 Jefferson Davis Highway, Suite 1204, Arlington, VA 22202-4302, and to the Office of Management and Budget, Paperwork Reduction Project (0704-0188), Washington, DC 20503.				
1. AGENCY USE ONLY (Leave blank)		2. REPORT DATE March 2000		3. REPORT TYPE AND DATES COVERED Master's Thesis
4. TITLE AND SUBTITLE MONOTONIC AND FATIGUE LOADING BEHAVIOR OF AN OXIDE /OXIDE CERAMIC MATRIX COMPOSITE			5. FUNDING NUMBERS	
6. AUTHOR(S) Steven G. Steel, Captain, USAF				
7. PERFORMING ORGANIZATION NAME(S) AND ADDRESS(ES) Air Force Institute of Technology Graduate School of Engineering and Management (AFIT/EN) 2950 P Street, Building 640 WPAFB OH 45433-7765			8. PERFORMING ORGANIZATION REPORT NUMBER AFIT/GMS/ENY/00M-02	
9. SPONSORING/MONITORING AGENCY NAME(S) AND ADDRESS(ES) AFRL/MLLN Attn: Larry Zawada Building 655 WPAFB OH 45433 DSN: 785-1352			10. SPONSORING/MONITORING AGENCY REPORT NUMBER	
11. SUPPLEMENTARY NOTES Advisor: Dr. Shankar Mall, ENY, DSN: 785-3636x4587, Email: shankar.mall@wpafb.af.mil				
12a. DISTRIBUTION AVAILABILITY STATEMENT APPROVED FOR PUBLIC RELEASE; DISTRIBUTION UNLIMITED.			12b. DISTRIBUTION CODE	
13. ABSTRACT (Maximum 200 words) <p>This thesis evaluates an oxide/oxide ceramic matrix composite, N720/A, for high temperature aerospace applications. The composite consists of a porous alumina matrix reinforced by ten plies of Nextel 720 fibers in a balanced 8 harness satin weave. Monotonic tensile and fatigue tests were performed at room temperature and 1200C. The effect of moisture on 1200C fatigue life was also examined. Modulus, maximum and minimum strain, and stress-strain hysteresis were monitored to characterize fatigue damage. Retained strength of all specimens that survived 100000 fatigue cycles was tested. Microscopy and fractography were used to examine damage and fracture surfaces.</p> <p>N720/A was found to have good room temperature and high temperature properties. At room temperature the ultimate tensile strength was 144 MPa and fatigue strength was 102 MPa. Fatigue damage involved mainly matrix cracking with no fiber-matrix debonding. At 1200C the ultimate strength was 140 MPa and fatigue strength was 122 MPa. Fatigue damage was similar to room temperature with the addition of creep in the fibers. Exposure to moisture did not degrade fatigue performance. N720/A appears to be an excellent candidate for 1200C applications with exposure to moisture.</p>				
14. SUBJECT TERMS Ceramic Matrix Composites, High Temperature, Mechanical Properties, Tensile Properties, Fatigue, Creep, Aerospace Craft, Ceramic Fibers, Materials			15. NUMBER OF PAGES 132	
			16. PRICE CODE	
17. SECURITY CLASSIFICATION OF REPORT UNCLASSIFIED	18. SECURITY CLASSIFICATION OF THIS PAGE UNCLASSIFIED	19. SECURITY CLASSIFICATION OF ABSTRACT UNCLASSIFIED	20. LIMITATION OF ABSTRACT UL	